

https://dspace.org/

Thermodynamic and parametric modeling in the refining of high carbon ferrochromium alloys using manually operated AODs

Mukuku, Kelvin

2017

https://hdl.handle.net/10539/24239

Mukuku, Kelvin (2017) Thermodynamic and parametric modeling in the refining of high carbon ferrochromium alloys using manually operated AODs, University of the Witwatersrand, <https://hdl.handle.net/10539/24239>

Downloaded from a DSpace repository. https://dspace.org/



Thermodynamic and parametric modeling in the refining of high carbon ferrochromium alloys using manually operated AODs.

MSc (50/50) RESEARCH PROJECT

Prepared by

Kelvin Mukuku (782232)

Submitted to

School of Chemical and Metallurgical Engineering, Faculty of Engineering and the Built Environment, University of the Witwatersrand, Johannesburg, South Africa

Supervisor: Dr. E. Matinde

18 July 2017

DECLARATION

I declare that this report is my own unaided work. I am submitting it in partial fulfilment of the requirements of Master of Science in Metallurgical Engineering at the University of Witwatersrand, Johannesburg.

It has not been submitted before for any degree or examination to any other university.

…….

(Signature of Candidate)

DEDICATION

I dedicate this work to my family; they were patient with me whilst I dedicated more time to my school work.

ACKNOWLEDGEMENTS

I would like to extend my thanks to the following people;

1. My Supervisor Dr. E. Matinde whose guidance was the source of my strength even when I thought I could not go on.
2. Mr. Jacques Beylefeld of XRAM Technologies who took his time to explain to me some complicated thermodynamic principles.
3. Mr. Mark Verwayen, a friend and brother who introduced me to AOD technology.

ABSTRACT

This study and the work done involves investigating the effects of different parameters on the decarburization process of high carbon ferrochromium melts to produce medium carbon ferrochrome, and takes into account the manipulation of the different parameters and thermodynamic models based on actual plant data. Process plant data was collected from a typical plant producing medium carbon ferrochrome alloys using AODs. The molten alloy was tapped from the EAF and charged into the AOD for decarburization using oxygen and nitrogen gas mixtures. The gases were blown into the converter through the bottom tuyeres. Metal and slag samples and temperature measurements were taken throughout the duration of each heat. The decarburization process was split into two main intervals namely first stage blow (where carbon content in the metal bath is between 2-8 wt. % C) and second stage blow (carbon mass% below 2 wt. %). The first and second blow stages were differentiated by the gas flow rates whereby the first stage was signified by gas flow ratio of 2:1 (O_2:N_2), whilst the stage blow had 1:1 ratio of oxygen and nitrogen respectively.

The effect of Cr mass% on carbon activity and how it relates to rate of decarburization was investigated, and the results indicated that an increase in Cr 66.54 – 70.5 wt. % reduced carbon activity in the metal bath from 0.336 – 0.511 for the first blowing stage. For the second blowing stage, the increase in Cr mass % of 67.22 – 71.65 wt. % resulted in an increase in C activity from 0.336 – 0.57. The trend showed that an increase in chromium composition resulted in a decrease in carbon activity and the same increase in Cr mass% resulted in reduced carbon solubility.

Based on the plant data, it was observed that the rate of decarburization was time dependent, that is, the longer the decarburization time interval, the better the carbon removal from the metal bath. An interesting observation was that the change in carbon mass percent from the initial composition to the final (Δ%C) decreased from 10.18 – 8.37 wt. % with the increase in Cr/C ratio from 8.37 – 10.18. This effect was attributed to the chromium affinity for carbon and the fact that an increase in chromium content in the bath was seen to reduce activity of carbon. It was also observed that the effect of the Cr/C ratio was more significant in the first stage of the blowing process compared to the second blowing stage. A mass and energy balance model was constructed for the process under study to predict composition of the metal bath at any time interval under specified plant conditions and parameters. The model was used to predict the outcome of the process by manipulating certain parameters to achieve a set target. By keeping

the gas flow rates, blowing times, gas ratios and initial metal bath temperature unchanged, the effect of initial temperature on decarburization in the converter was investigated. The results showed that the carbon end point with these parameters fixed decreased with increasing initial temperature, and this was supported by literature. The partial pressure of oxygen was observed to increase with decrease in C mass % between the first and second blow stages. For the second stage blow the partial pressure changed from $5.52*10^{-12}$ – $2.1*10^{-10}$ and carbon mass % increased from 0.754 – 2.99 wt. %. A carbon mass % of 7.87 had an oxygen partial pressure of $4.51*10^{-13}$ whilst a lower carbon content of 1.53 wt. % had an oxygen partial pressure of $8.06*10^{-11}$. The CO partial pressure however increased with increase in carbon composition in the metal bath.

When the oxygen flow rate increased, a corresponding increase in the carbon removed (Δ%C) was observed. For the first stage of the blowing process, an increase in oxygen flow rate from 388.67 – 666.5Nm^3 resulted in an increase in carbon removed from 5.06 – 7.28 wt. %. The second blowing stage had lower oxygen flow rates because of the carbon levels remaining in the metal bath were around +/- 2 wt. %. In this stage oxygen flow rates increased from 125 – 286.67 Nm^3 and carbon removed (Δ%C) from 0.16 – 2.093 wt. %. The slag showed that an increase in basicity resulted in an increase in Cr_2O_3 in the slag. As the basicity increased from 0.478 – 1.281, this resulted in an increase in Cr_2O_3 increase from 0.26 – 0.68. Nitrogen solubility in the metal bath was investigated and it was observed that it increased with increasing Cr mass %. The increase in nitrogen solubility with increasing Cr mass % was independent of the nitrogen partial pressures.

TABLE OF CONTENTS

DECLARATION.....**i**

DEDICATION.....**ii**

ACKNOWLEDGEMENTS.....**iii**

ABSTRACT.....**iv**

ABBREVIATION NOTATION AND NOMANCLATURE.....**xii**

1. INTRODUCTION.....**1**

2. LITERATURE REVIEW.....**6**

2.1. Introduction.....6

2.2 High Carbon Ferrochrome production.....6

2.3 Production of Low and Medium Carbon Ferrochrome alloys.....9

2.3.1 Unit processes in the production of low and medium carbon ferrochromium alloys.....9

2.4. Refining process of High carbon Ferrochromium alloys.....10

2.4.1 Refining of ferrochrome by chromium ore.....11

2.4.2 Metallothermic Reduction.....11

2.4.3 Converter Refining.....13

2.5 Reactions & thermodynamic considerations in the converter refining process.....16

2.5.1 AOD decarburization process.....18

2.5.2 Thermodynamic considerations for metal & slag in ferrochrome refining.....20

2.5.3 Activities of Cr and C in ferrochromium alloy refining.....22

2.5.4 Interaction parameters in ferrochromium refining.....24

2.5.5 Effect of blowing conditions on the extent decarburization.....26

2.5.6 Effect of gas flow rates on decarburization.....26

2.5.7 Initial Temperature of the liquid metal.....28

2.5.8 Rate equations in AOD refining 28
2.6 Energy balance in the AOD decarburization process 30
2.7 Summary 31
CHAPTER 3 32
3. METHODOLOGY 32
3.1 Introduction 32
3.2 Description of process under study 33
3.2 Plant data collection during the decarburization process 35
3.2.1 Blow periods data measurements 35
3.2.2 Data collation and modeling 36
3.3 Reduction stage after refining in the AOD 36
Summary 37
CHAPTER 4 38
4. Modelling Methodology 38
4.1 Introduction 38
4.2 Thermodynamic analysis of plant data 38
4.2.1 Oxygen partial pressure for oxidation of C, Si and Cr 39
4.2.2 Equilibrium Partial pressure of CO from oxidation of C, Cr and Si. 40
4.3 Rate equations in the converter decarburization process 41
4.3.1 Rate equations at high carbon contents 42
4.3.2 Rate equations for low carbon levels 43
4.3.3 Equilibrium concentration of carbon 44
4.4 Mass and energy balance for the AOD process 45
4.4.1 Mass and energy balance construction procedure 46
4.4.1. Calculating the initial mass (moles) and energy of the metal bath in the converter 47

4.4.2. Calculating the mass (kmols) and energy balance for lime and dolomite 48
4.4.3 Kmols and energy calculations for FeSi in the reduction stage 50
4.4.4 Mass and energy balance calculations for AOD gases 51
4.5 Thermodynamics and Equilibrium considerations in AOD refining process 53
4.6 Interaction coefficients in metal and slag in the refining process. 54
4.5.1 Activity coefficient calculations in metal phase 55
4.5.2 Activity coefficient calculations in the Slag Phase 56
CHAPTER 5 59
5. RESULTS AND DISCUSSION 59
5.1 Introduction 59
5.2 Carbon removal trend with decarburization for plant data 59
5.3 Mass balance for AOD refining stage 64
5.3.1 Decarburization process at high carbon content during the first stage of the blow 65
5.3.2 Comparison of the final chromium composition based on models and plant data 66
5.3.3 Effect of initial temperature on the extent of decarburization 68
5.4 Effect of metal bath composition (Si, Cr and C) on the distribution ratio of oxygen 70
5.5 Effect of initial chromium content in the bath 72
5.6 Effect of O_2 partial pressure on the extent of decarburization 72
5.7: Effect of CO partial pressure on the extent of decarburization 75
5.8 Fitting of model and plant data at lower carbon levels 76
5.8.1 Comparison of modelled and plant data in terms of carbon removal 76
5.9 Effect of gas flow rate on decarburization 77
5.10 Relationship between Chromium content and Cr activity in the metal bath 79
5.11 Effect of chromium on the activity of carbon in the alloy bath 80
5.12 Relationship between Cr_2O_3 content and the activity of Cr_2O_3 in slag 82
5.12 Nitrogen solubility in the alloy bath during decarburization 85

5.13 Financial modelling of the AOD refining process 86

Summary 87

CONCLUSION 89

RECOMMENDATIONS 92

REFERENCES 95

APPENDICES 101

List of Figures:

Figure 1.1: High carbon ferrochromium alloy prices for the past 7 years (infomine.com) 4

Figure 2.1: Slag ternary diagram for typical stainless steel slags (slag atlas, 1995) 22

Figure 3.1: Process flow (adapted from the process under study) 34

Figure 5.1: Change in carbon content of the bath as a function of blowing time for 9 random heats 60

Figure 5.2: Drop in carbon content with blowing interval 61

Figure 5.3: Change in carbon content (%ΔC) with blowing time 62

Figure 5.4: Relationship between the %Cr/%C ratio and rate of decarburization during the first stage of blow 63

Figure 5.5: Relationship between Cr/C ratio and rate of decarburization during the second stage of the blow 63

Figure 5.6: Comparison of model results vs. plant data for the first stage of the blow 65

Figure 5.7: Comparison of final Cr in the alloy bath for the first stage of the blow at high carbon content 67

Figure 5.8: Comparison of final %Cr in the alloy bath predicted from rate equation model and plant data during the second stage of the blow 67

Figure 5.9: Effect of initial temperature on the extent of decarburization at high carbon content 69

Figure 5.10: Effect of initial temperature on end point carbon at low carbon contents 70

Figure 5.11: Relationship between initial temperature and distribution ratios of blown oxygen for Si, Cr and C 71

Figure 5.12: Effect of initial temperature on distribution ratios of blown oxygen for carbon.....71
Figure 5.13: Effect of initial % chromium on decarburization 72
Figure 5.14: Relationship between carbon mass % vs P_{O2} 73
Figure 5.15: Relationship between temperature and partial pressure at higher carbon levels.....74
Figure 5.16: Relationship between temperature and oxygen partial pressure at lower carbon levels 75
Figure 5.17: Calculated partial pressure of CO plotted as a function of mole fraction of carbon in the bath.....76
Figure 5.18: Comparison of the decarburization between modelled and plant data.....77
Figure 5.19: Effect of oxygen flow on decarburization in the first stage of blowing.....79
Figure 5.20: Effect of oxygen flow decarburization for the second stage of the blow.....79
Figure 5.21: Relationship of chromium content and activity of chromium in the alloy bath.....80
Figure 5.22: Effect of chromium on the activity of carbon at high carbon contents (first stage of blowing) 81
Figure 5.23: Effect of chromium content on activity of carbon at high carbon contents (second blowing stage).....81
Figure 5.24: Relationship between chromium oxide and activity in slag.....83
Figure 5.25: Relationship between temperature and chrome oxide activity.....84
Figure 5.26: Effect of slag basicity on activities of chrome oxides.....84
Figure 5.27: Relationship between %Chromium and nitrogen activity.....86

List of Tables

Table 2.1: Classification of high carbon ferrochromium and charge chrome alloys (Gasik, 2013) 7
Table 4.1: Analyses of Material inputs into the AOD 47
Table 4.2: Moles and Energy for metal @1600 ^{o}C.....48
Table 4.3: Moles and Energy calculations for FeSi.....50
Table 4.4: Moles and Energy calculations for Argon at 25 ^{o}C 52
Table 5.1: Summary of models used in the calculations of mass balance in the AOD 64

List of Appendices

Appendix 1: AOD logsheet used in process under study.....101
Appendix 2: Initial gas flows and gas ratios in model calculations.....102
Appendix 3: Initial alloy bath analysis as charged into the AOD from the EAF 102
Appendix 4: Lime analysis as added into the AOD.....102
Appendix 5: Dolomite analysis is added into the AOD.....103
Appendix 6: FeSi analysis as added into the AOD.....103
Appendix 7: Process input calculation summary.....103
Appendix 8: Process output summary for mass and energy balance model.....105
Appendix 9: Activity and activity coefficients calculations for mass and energy balance model 106
Appendix 10: first order interaction coefficient in liquid iron.....106
Appendix 11: Calculated interaction coefficients for the energy and mass balance model 107
Appendix 12: Activity coefficients at infinite solutions.....107
Appendix 13: Interaction energy between cations of major steel making slags.....107
Appendix 14: Molar weights for oxides and elements in the energy and mass balance model..108
Appendix 15: Initial analysis of hot metal charged into the AOD for the process under study .109
Appendix 16: Second blowing stage initial data from the process under study 110
Appendix 17: Financial modeling of the AOD and EAF process.....111

ABBREVIATION NOTATION AND NOMANCLATURE

AOD	Argon Oxygen Decarburizer
CLU	Creusot Loire Uddeholm
EAF	Electric Arc Furnace
CRK	Ferrochrome Converter
SAF	Submerged Arc Furnace
UTCAS	Real time dynamic process control software
MCFeCr	Medium carbon ferrochromium alloy
HCFeCr	High carbon ferrochromium alloy
LCFeCr	Low carbon ferrochromium alloy
DC	Direct Current
VOD	Vacuum Oxygen Decarburizer
HSC v.7	H – enthalpy, S – entropy, C – heat capacity

1. INTRODUCTION

The production of medium and low carbon ferrochromium alloys is not a common practice within the South African ferroalloys industry, as most companies tend to focus on the production of high carbon ferrochromium and charge chrome alloys. Companies such as Samancor Chrome have closed their IC3 plant which was used for the production of low and medium carbon ferrochromium alloys due to unfavourable market costs and high electricity consumption (MetalBulletin, 2015).However, the increased demand for low and medium carbon ferrochrome alloys in the production of special alloys and stainless steel has resulted in the development of a number of processes to reduce the content of carbon in the ferrochromium alloys.

Processes such as the Simplex, Duplex, Perrin and converter decarburization were developed in order to reduce the amount of carbon dissolved in ferrochromium alloys (Bhardwaj, 2014). The use of Argon Oxygen Decarburizers (AODs) and Creusot Loire Uddeholm (CLU) converters has traditionally been used for stainless steel production (Pretorius and Nunnington, 2002), but has since found widespread applications in the production of low and medium ferrochromium alloys (Kienel et al, 1987).

High carbon ferrochromium and charge chrome alloys are produced from the reduction of chrome lumpy ore or chrome concentrate from chrome fines concentration. Submerged arc furnaces in the production of high carbon ferrochromium and charge chrome alloys has become the main technology used since it is economical (Gasik, 2013). South Africa has over 75% of the world's chromite reserves and with a huge reserve of coal (which is used to produce metallurgical coke, the main reductant in carbothermic reduction of chromite ores), thus making South Africa one of the major producers of charge chrome (< 55 wt. %Cr) in the world (Basson et al, 2007; Cramer et al, 2004).

The present study is based on a South African company which utilizes electric arc furnaces (EAFs) and Argon Oxygen Decarburization process (AODs) to produce medium carbon ferrochromium alloy containing less than 1.0 wt. % carbon and +/- 65 wt. % chromium in the final alloy. In this process, high carbon ferrochrome fines are melted in an EAF, and the alloy melt is tapped into the AODs for converter refining, and subsequently into casting ladles for ingot casting or granulation. Typically, the initial carbon levels in the HCFeCr melts are around 4-6 wt. %, and the target is to oxidize out the dissolved carbon to less than 1.0 wt. %. Slag

formers are added in the form of burnt lime (CaO) and dolomite (MgO·CaO), as well as fluorspar to improve slag properties and to facilitate the dissolution of lime in the slag (Pretorius and Nunnington, 2002). Essentially, the target basicity of the slag is at least 1.8 ($(CaO+MgO)/SiO_2$). The current melting furnace utilizes refractory lining made of magnesia based bricks depending on desired slag regime and cost. From the EAFs, the molten material is tapped into transfer ladles before charging into manually operated AODs where the refining process takes place.

During the decarburization stage, oxygen is blown into the AODs, along with an inert gas (N_2 or Ar), which helps lower the partial pressure of the produced CO during oxidation of carbon. After the oxidation stage, ferrosilicon is added in the reduction stage of the blowing process to recover chromium that has been oxidized to slag (Pretorius and Nunnington, 2002). In most cases, the pick-up of silicon in the metal does not exceed 0.5 wt. %. When the desired liquid low or medium ferrochromium metal composition is achieved, the refined ferrochromium alloy is then tapped into a teeming ladle, and cast into ingots or is granulated.

The AODs under study in this investigation are manually operated. Initially the AODs were automatically operated, but the automatic operating model made the refining process take too long and faced challenges in temperature control due huge discrepancies between the actual measured temperature and model prediction. In addition to these discrepancies, operating costs (particularly O_2, N_2 and refractory lining) of the process became too high thereby reducing the profit margin. Since the switch from automatic to manually operated AODs, no technical studies and research has been done to optimize the operation through the standardization of the critical process parameters.

As a result, achieving process consistency in the operating parameters per heat, such as slag quality control, decarburization time, gas flow rates and ratios has never been achieved. Based on the aforementioned, the main purpose of this research project is to conduct a parametric and thermodynamic modeling of the AOD process based on the key process parameters, link the scientific models to actual process data, and to optimize the AOD refining process based on the results obtained from the thermodynamic models and parametric studies.

SIGNIFICANCE OF THE STUDY

Ferroalloys are defined as alloys of iron and contain one more or elements such as chromium, manganese or silicon in significant quantities. These alloys are critical to improving the properties of steels. For the purposes of this study the ferroalloy of concern involves the refining of high carbon ferrochromium alloys. The main element in this ferro alloy is chromium and is mainly used in the stainless steel production Turkdogan and Fruehan, 1999). Chromium is responsible for increasing the corrosion resistance of stainless steel by forming a thin chrome oxide layer on the surface which is stable and inert to chemical attack and reactions (Holappa, 2002). Chromium as an alloying element is generally added in the form of high carbon ferrochromium alloy (HCFeCr) but the carbon is an impurity especially in the production of low carbon stainless steels and super alloys.

With increasing demand for improved properties in steel, impurities in steels have become a major focus (Pande et al, 2010). Typically, the preference of lower carbon content in steel has been a major driver in the production and consumption of low and medium carbon ferrochromium alloys. The lower carbon content enhances the steel's mechanical properties such as increased drawability and formability (AK Steel, 2016) by reducing the precipitation of chromium carbides. Formation of these chromium carbides leads to intergranular corrosion resulting in weld decays and failures at high temperatures due to steel sensitization which is associated with high carbon contents in stainless steels (Bhonde et al, 2007; Totten et al, 2003).

In addition, market prices of low and medium carbon FeCr alloys are comparatively higher than for high carbon ferrochromium and charge chrome alloys. For example, the current market prices for high carbon ferrochrome (7-9 wt. %C) range from USD$1.76-2.20/kg, whereas the refined medium carbon ferrochromium alloys (0.8-1.0 wt. %C) at the time of the study was on average USD$3.08/kg (infomine/commoditymine, 2016). In essence, higher market prices for medium and low carbon ferrochromium alloys justify additional investments in the refining processes. Prices for commodities quoted in this section are prices at the time of the study and are subject to fluctuations depending on market conditions (figure 1.1).

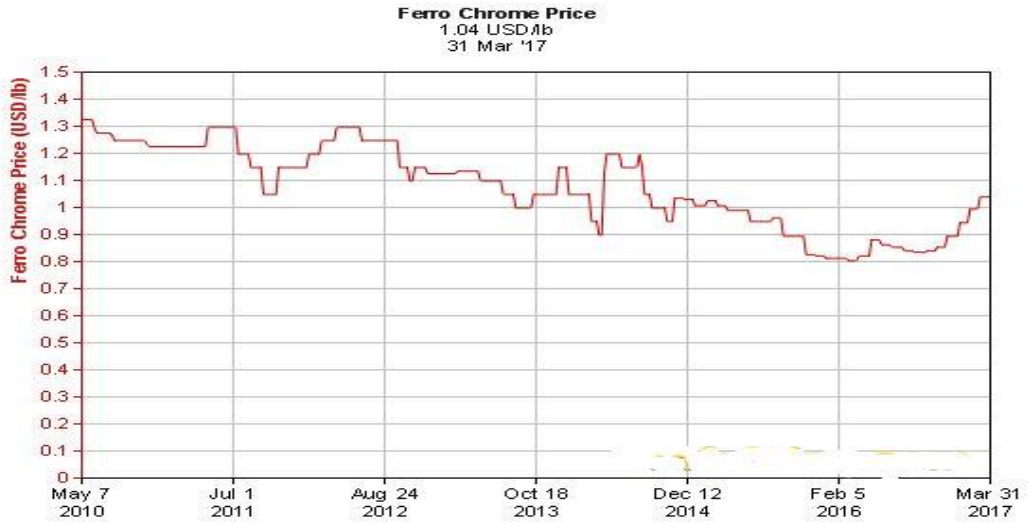


Figure 1.1: High carbon ferrochromium alloy prices for the past 7 years (infomine.com)

The cost of producing low/medium carbon ferrochromium alloys is driven by additional infrastructure required for decarburization. In particular, the AOD converter costs are mainly influenced by refractory materials consumption and the cost of gases. In other operations, alternative gas options have been applied such as introduction of dry steam, in order to reduce converter costs when using argon as the inert gas (Beskow et al, 2010). Nitrogen has also been utilized as a substitute to try and bring costs down (Turkdogan and Fruehan, 1999; Wei and Zhu, 2002).

The process under study has experienced high AOD operational costs as no study was done on the optimization of different process parameters thereby leading to poor costs control and alloy recovery optimization of the process. The findings of this study will improve the parametric control of the decarburization process for production of low/medium carbon ferrochromium alloys using AODs. This will aid in the reduction of operational costs which can be the basis of the creation of cost models based on process consumables such as refractory linings, oxygen, argon, nitrogen, among other cost drivers, which will be tried for different rates of decarburization.

RESEARCH OBJECTIVES

The main objective of this study was to investigate the thermodynamic and parametric modeling in the refining of high carbon ferrochrome alloys in manually operated AODs in the production of medium carbon ferrochrome alloys. The effect of key process parameters on the overall process performance and final product quality was analyzed. This in turn will lead in creation of models to mimic the refining process to produce predictive changes in process parameters to attain a specific required product specification. In detail, this project entails to:

- To determine optimum parameters for the refining process of high carbon ferrochromium alloys to produce medium carbon ferrochromium alloys using manually operated AODs
- To develop thermodynamic and mass and energy balance models (applicable) in the converter refining process of high carbon ferrochromium alloys using manually operated AODs,
- To apply the thermodynamic and mass and energy balance models to analyse the effects of varying different process parameters on the refining process based on plant data
- To develop a cost model for the production of medium based on key process variables such as chromium losses to slag, refractory materials consumption, consumables usage, and other opportunity costs such as penalties and productivity variance.

2. LITERATURE REVIEW

2.1. Introduction

The production of high carbon ferrochromium and charge chrome alloys through the reduction of chrome ore by metallurgical coke or coal, with fluxes has traditionally been done by use of submerged arc furnaces (SAF). However carbon is an impurity in the production and use of super alloys and some low carbon stainless steels, thereby driving the need to produce lower carbon content ferrochromium alloys. In the past Metallothermic reduction techniques (aluminothermic and silicothermic) have been able to produce ultra-low carbon with carbon contents ≤ 0.05 wt. % in the final alloys (Gasik, 2013).

Other techniques of producing low carbon ferrochromium alloys include refining of FeCr by chrome ore to reduce the carbon content through the reduction of Cr_2O_3 by carbon. In addition to this technique, development of converter refining has contributed to the production of lower carbon ferrochromium alloys from high carbon ferrochromium and charge chrome alloys. In essence, use of converters include the use of argon oxygen decarburizers (AODs), ferrochrome converters (CRK) and Creusot-Loire Uddeholm (CLU) coupled with the injection of an oxidant and an inert gas into vessels through the tuyeres and/or lance to remove the carbon in the molten alloys (Heikkinen, 2010).

Understanding of the different oxidation reactions and kinetics of these reactions in the AODs is based on the knowledge from stainless steel production. It is now possible to an extent to predict the effect of changes in operational parameters such as gas flow rates during ferroalloys converter refining (Wei & Zhu, 2002).

2.2 High Carbon Ferrochrome production

Ferrochromium alloys are generally produced in submerged arc furnaces (SAFs) from the carbothermic reduction of chrome ores. These alloys are a source of chromium, which is a major alloying element in the production of high value steel products. Table 2.1 summarizes the classification of high carbon ferrochromium and charge chrome alloys according to mainly the chromium content in the alloys.

Table 2.1: Classification of high carbon ferrochromium and charge chrome alloys (Gasik, 2013)

Alloy Type	%Cr	%Si	%C	%P	%S
High Carbon Ferrochromium	60 - 70	<2	<8	<0.015	<0.02
		2 - 3	<6	<0.03	<0.04
				<0.05	<0.06
Charge Chrome	50 - 55	2 - 3	<8	<0.015	<0.02
		3 - 4		<0.03	<0.04
		4 - 5		<0.05	<0.06

As shown in Table 2.1, high carbon ferrochrome alloys typically contain carbon between 6-8 wt. % C, and chromium content in the range 60-70 wt. % Cr. The production of such alloys requires chromite ores that have higher Cr/Fe ratio typically above 2. Charge chrome is produced from chromite ores with lower Cr/Fe ratio (usually between 1.5-1.6) and Cr levels of 50-55 wt. %, and sometimes even lower than 50 wt. % (Gasik, 2013). Chromite ore typically exists in the form of a spinel ($(Fe,Mg)O.(Cr,Fe,Al)_2O_3$) (Gasik, 2013).

The carbothermic smelting route taken has an impact on the composition of particular elements such as Si, S and P. The type and quality of reductant used will also impact on the final product quality. Usually reductants used are carbon based (coke, coal, charcoal, anthracite, etc.), and these are the main sources of S and P. The quality of the ore will have an impact on the smelting operations. In particular, the quality of raw materials can have significant impact on the metallurgical efficiencies in the furnace (Gasik, 2013).

The reaction for the reduction of chromite ore is shown in equation 2.1 (Ugwuegbu, 2012):

$$Cr_2FeO_4 + 4C = 2Cr + Fe + 4CO \quad [2.1]$$

Generally, submerged arc furnaces are used for smelting of Cr_2O_3 to Cr. The reduction reactions are promoted by use of reductants such as solid carbon in the form of either metallurgical coke or coal, or a combination of both. Solid-gas reduction also occurs with CO and ore interaction as illustrated by equations 2.2 and 2.3 (Chakraborty et al, 2005).

$$Cr_2O_3 + 3CO = 2Cr + 3CO_2 \quad [2.2]$$

$$C + CO_2 = 2CO \quad [2.3]$$

The chromium produced from chrome ore during carbothermic reduction will react with carbon forming chromium carbides such as Cr_3C_2, Cr_7C_3 and $Cr_{23}C_6$ (Gasik, 2013).

The DC arc furnace has a single preformed electrode with a hollow centre that is used to feed charge into the furnace. This electrode acts as the cathode and there is an anode at the bottom of the furnace. The DC furnaces use direct current, unlike the SAF, which utilizes alternating current. The DC furnaces are adaptable to the smelting of ore fines or concentrates (Hockaday et al, 2010).

In the submerged arc furnace, chrome ore is charged into the furnace, together with fluxes such as limestone or quartz to adjust the slag basicity. Most of the reduction of Cr_2O_3 occurs in the coke bed which is located below the electrodes. The initial slag that is formed in the furnace contains significant amount of chromium which will be in the form of alloy entrained in the slag or slightly altered chromite.

The extent to which the spinel dissolves in the slag is also dependent on factors such as the amount of slag produced, the partial pressure of oxygen, the length of the residence time the material spends in the high temperature zone of the furnaces and slag composition. Of importance to note is also the chromium activities in the slag as this will impact on the chromium recovery of chromium in the slag melt, as this impacts on the financial viability of the process and difficulties associated with discarding of chromium-containing slags as a waste product (Gasik, 2013; Holappa and Xiao, 1992).

In the recent years, technology has also been developed to smelt chrome fines and concentrates by the use of plasma furnaces. This development has been driven by the flexibility of plasma furnaces to treat fines and easier and more rapid response to control compared to submerged arc furnaces (Mac Rae, 1992; Slatter et al, 1986). The high carbon content in the high carbon ferrochrome or charge chrome is a result of the carbon coming from the reductants in the form of coke or coal, which then exists as metal carbides of iron and chromium in solid ferrochrome. However, the high carbon in the alloy has negative impacts on the alloy mechanical properties.

In general some stainless steels and super alloys require ultra-low carbon contents. In some stainless steels, higher carbon contents cause sensitization of the steels at elevated temperatures as a result of the chromium carbides precipitating along grain boundaries. As a result, the formation of carbides result in the areas adjacent to the grain boundaries becoming 'starved' of Cr and less corrosion resistant, leading to corrosion of the metal. As a result, there is need to reduce the carbon content in high carbon ferrochromium and charge chrome alloys that are used in the production of low carbon stainless steels (Bhonde, 2007; Gasik, 2013).

2.3 Production of Low and Medium Carbon Ferrochrome alloys

Low and medium carbon ferrochromium alloys have found widespread uses in the manufacture of super alloys and super grades of stainless steels due to their lower carbon content. Lower carbon content in these alloys improves the chemical and mechanical properties of stainless steels and other super alloys, and this is principally achieved by using low carbon-containing alloy additives such as low and medium carbon ferrochromium alloys (Heikkinen et al, 2011).

Typically, production of medium carbon ferrochromium alloy can be done through oxygen blowing in a converter refining of HCFeCr or by the silico-thermic reduction of chromite ore and concentrates. Several techniques are used to lower the carbon content in ferrochrome alloy, and can be characterized as conventional processes, such as metallothermic processes, and non-conventional methods that include processes such as decarburization of solid FeCr by vacuum heat treatment process and use of an oxidant such as iron oxide or other oxidizing mixtures such as steam and CO_2 gas (Bhardwaj, 2014).

2.3.1 Unit processes in the production of low and medium carbon ferrochromium alloys

The production of medium and low carbon ferrochrome alloys has been mainly driven by the undesirable properties of carbon in ultra-low carbon stainless steels. There has been a drive in production of ultra-low carbon through the use of processes such as aluminothermic and silicothermic reduction. Converter technology has also revolved through use of oxygen, steam and in some cases use of CO_2 gas. Vacuum oxygen decarburization processes (VODs) have also been used to produce ultra-low carbon ferrochrome (Wang et al, 2015; Rick et al, 2011)

The Perrin process is one of the processes used in the production of LCFeCr alloys, and involves the use of silico-chromium/ferrosilicon as a reductant. In the initial stages, chrome ore

concentrate is blended with lime and charged into a kiln, before charging into the furnace for melting (Shoko et al, 2004). The slag produced from the first stage of the process still contains a quantifiable amount and contains in the range 24-26 wt. % Cr_2O_3, and is further reacted with ferrosilicon chrome to recover the chrome units (Bhardwaj, 2014)

The Duplex process is also another method which involves a silico-thermic reduction of a lime-chromite slag to produce low carbon ferrochromium alloy (Ghose et al, 1983). In this process, the ferrosilicon/silico-chromium is crushed to a fine size of 5-10mm and is then mixed with lime and fed into a kiln before being charged into the electric furnace for melting (Ghose et al, 1983). An ore-lime melt produced in an electric arc furnace is tapped into a ladle and contains approximately 40 wt. %CaO and between 25 –28 wt. % Cr_2O_3 (Ghose et al, 1983).

Powdered (Ferrosilicon chromium alloy) FeSiCr is then added into the ladle to produce an alloy with between 12-14 wt. % silicon content. The amount of FeSiCr added depends on the analysis of the FeSiCr, the lime-ore melt and the desired product quality from this process. The metal and slag from the ladle are then poured and mixed thoroughly in a transfer ladle to facilitate the reduction of Cr_2O_3 in the slag. The transfer ladle is deslagged and the remaining metal is then thrown back into the arc furnace with a new ore-lime melt batch to produce a final metal with $\leq$ 1 wt. % Si (Bhardwaj, 2014).

The third process used in the production of LCFeCr alloys is the Simplex process, in which the high carbon ferrochrome produced from a submerged arc furnace is crushed and milled in a ball mill to produce a powdered material. The milled powder is then mixed with Cr_2O_3 and Fe_2O_3 then briquetted before being decarburized by annealing at about 1350^oC in a vacuum (Bhardwaj, 2014).

2.4. Refining process of High carbon Ferrochromium alloys

As discussed in section 2.3, carbon has detrimental effects in some stainless steels and super alloys as it reduces chemical and mechanical properties of these alloys. The need to lower carbon content has driven technology and innovations and these have taken into account the costs associated with lowering of C. Methods such as triplex process, metallothermic reduction, converter and vacuum techniques were employed so that ultra-low carbon ferrochrome could be directly produced (Bhonde et al, 2007).

With the advent of VODs and AODs, the chemical energy released from the oxidation of Si and C in the high carbon ferrochromium alloys could be properly harnessed for fines re-melting instead of reducing Cr_2O_3 in chrome ore, resulting in reduced process costs for the refining processes (Rick et al, 2015). In detail, some of the processes used in the production of low carbon FeCr alloys are discussed in Sections 2.4.1 – 2.4.6.

2.4.1 Refining of ferrochrome by chromium ore

The refining of HCFeCr alloys using Cr ore is done in a furnace based on the main assumption that the chromium in the alloy exists as chromium carbides (Cr_7C_3) (Elyutin et al., 1957). The chromite is added into the (refining) furnace, and can be represented by the equation 4.

$$\frac{2}{3}Cr_7C_3 + \frac{1}{2}FeCr_2O_4 = \frac{17}{3}Cr + \frac{1}{2}Fe + 2CO \qquad [2.4]$$

The viscosity of high chromium refining slag and high melting point (approx. 2175K) makes this whole process difficult. This is due to the difficulty in separation between metal in slag due to restriction to flow because of highly dense slag. Slag fluidity is also a function of temperature and a high slag melting point will result in a viscous slag at operating temperatures in the furnace (Bhonde et al, 2007). For decarburization to occur in this process, high temperatures are needed (Bhardwaj, 2014).

2.4.2 Metallothermic Reduction

Metallothermic processes are usually exothermic in nature. Metallic silicon (Si) and aluminum (Al) are used in the silicothermic and aluminothermic processes, respectively. During the metallothermic reduction, he Al and Si are oxidized and this results in a sharp generation of heat which is then utilized in the smelting process (Ghose et al, 1983). In essence, the aluminothermic reduction is used to produce ultra-low carbon ferrochromium alloys, while the silicothermic reduction is used to produce low carbon ferrochromium alloys (Seetharaman et al, 2014).

2.4.2.1 Silico-thermic process

In the silicothermic process, a mixture of chrome ore and lime is smelted in an electric arc furnace (EAF) to produce a lime-ore melt. The resulting lime-ore melt is then tapped into a ladle where it is mixed with ferrosilicon chrome alloy and reaction is quite exothermic, as silicon being the reductant, reduces the Cr_2O_3 in the melt to Cr. This resulting slag produced as a result

of this reaction between ferrosilicon alloy and the lime-ore melt, is a calcium silicate slag. The calcium silicate slag is then taken into a second ladle and mixed with molten high carbon ferrochrome, since the slag still contains chromium oxide that can be recovered. The product of this reaction is an intermediate product of ferrochrome silicon (Seetharaman et al, 2014).

Low carbon ferrochrome can be produced using silico-chrome/ferrosilicon chrome as a reducing agent. An increase in silicon content will decrease carbon solubility in the metal (Bhardwaj, 2014). The silico-thermic reduction process is capable of producing alloys with carbon content below 0.03 wt. %C, making it more preferable where very low carbon levels are desired and such low carbon contents cannot be obtained using oxygen in the AOD process.

The Perrin process is a typical example of the silicothermic reduction process. The ferrosilicon chromium alloy used in this process (35 – 43 wt. % Si) is produced in a smelting furnace such as SAFs, whilst chrome ore and lime are mixed in a different electric furnace to produce a lime-ore melt contains between 24-26 wt. % Cr_2O_3. These two products (FeSiCr alloy and lime-ore melt), produced from different furnaces, are then intermittently mixed in a mixing ladle (mixing commonly called 'cocktailing'). The alloy produced in this mixing ladle has an average analysis of 65-72 wt. % Cr and C of 0.03-0.05 wt. %. In this process, all reactions occur in the liquid phase and reactions highly exothermic. The main disadvantage of this process is the need to synchronize all the processes to ensure no freezing of liquid material at any stage in the process (Ghose et al, 1983).

The Duplex process is relatively simpler than with the Perrin process, as it uses ferrosilicon chromium alloy in the solid form. In this process, ferrosilicon chromium alloy contains Si which is the main reductant reducing Cr_2O_3 to Cr in the lime-ore melt. The average analysis of FeSiCr used is 38-40 wt. % Cr, 43-45 wt. %Si and 0.03-0.05 wt. % C, crushed to between 5-10mm in size.

The lime-ore melt from the EAF having an analysis of approx. 25-28 wt. %Cr_2O_3 and 40 wt. %CaO, is mixed in a ladle with the ferrosilicon chromium alloy of 12-14 wt. %Si (which is produced from a SAF). This mixture is then intermittently mixed in a transfer ladle in order to recover as much residual Cr_2O_3 from the slag as possible and achieve a slag of <1 wt. %Cr_2O_3. This slag is then discarded and the resultant intermediate alloy charged back into the furnace with the lime-ore melt, reducing silicon in the metal to <1 wt. %. The final slag usually contains

approx. wt. 3%Cr_2O_3, which is generally higher than in the Perrin Process (Bhardwaj, 2014; Ghose et al, 1983).

2.4.2.2 Alumino-thermic technique

The aluminothermic reduction process mainly applies for the in-situ production of ultra-low ferrochromium alloy with at a smaller scale. The slag produced from this process is refractory (Al_2O_3 + Cr_2O_3) with a high melting point so lime (CaO) is added to the process in order to lower the melting point of the slag, thus also reducing the overall reaction temperature for the process. This slag is then kept fluid by addition of aluminum (Al) and $NaNO_3$ into the charge. These additions will help in aiding metal recovery from slag. The reactions below illustrate the process occurring (Gasik, 2013).

$$\frac{2}{3}Cr_2O_3 + \frac{4}{3}Al = \frac{4}{3}Cr + \frac{2}{3}Al_2O_3 \quad \Delta G^o = -309 + 0.004T \qquad [2.5]$$

$$K = (a_{Al_2O_3}^{2/3} \times a_{Cr}^{4/3})/(a_{Al}^{4/3} \times a_{Cr_2O_3}^{2/3})$$

Where:

α_i represents activities of Al_2O_3, Al, Cr and Cr_2O_3

ΔG^o is the standard Gibbs free energy

Aluminium as shown in equation 2.5 is used as the reductant of which the oxidation of Al is exothermic and generates temperatures in the range 1800-2500^{o}C. In addition aluminothermic reduction is promoted by lowering the Al_2O_3 activity in the generated slag. This can be achieved through addition of fluxes such as lime. By preheating the feed to around 500^{o}C, the aluminothermic reduction process is accelerated (Bhardwaj, 2014).

2.4.3 Converter Refining

Converter technologies have widely been used in secondary metallurgy to refine melts that have been produced in a primary process, for example SAF or EAFs, to reduce the carbon content in the alloy (Heikkinen et al, 2011). There are different types of converters currently being applied, namely, the Creusot Loire Uddeholm (CLU) and Argon-Oxygen Decarburization (AOD).

The different converters basically use same principle (of blowing oxygen) for decarburization. Basically, carbon is driven out of the bath through oxidation when oxygen is blown into the

alloy bath through the tuyeres and/or top lance with an inert gas like Ar or N_2. Steam has been used in other instances as well as advances in using CO_2 as an oxidant (Rick, 2010).

2.4.3.1 Utilization of gases in converter refining

The use of the AODs has dominated the stainless steel refining to achieve low carbon contents since the introduction of the technology in the 1960s (Rick, 2010). In the AOD, oxygen is blown with Ar or N_2 as the inert gas. The oxygen is the oxidant used for decarburization. The oxidation reactions are exothermic, thereby raising bath temperature and as a result, no external heat source is used (Wei and Zhu, 2002). The inert gases help lower the partial pressure of CO gas and help drive carbon removal.

The gases are introduced into the metal bath through the tuyeres at the bottom or a top lance, depending on converter design. The gases also mix the bath making it turbulent, therefore increasing contact area between slag and metal and promoting slag-metal interface reactions (Wei and Zhu, 2002; Bhonde et al, 2007). The molten metal charged into the AOD comes from either an EAF (after scrap, high carbon ferrochromium or charge chrome alloys melting), or directly from the SAF as molten metal charged directly to the AOD (Wei and Zhu, 2002).

Of importance in any AOD operation, is the calculation and determination of production costs. These production costs include the cost of raw materials being charged into the converter, the tap-to-tap time which includes duration of each blowing operation and the life cycle and cost of refractory material used to protect converter shell (Song et al, 1992).

Due to the cost of Ar and problems with nitrogen pick-up into the metal, processes such as the CLU process were developed to lower costs of decarburization, through use of a cheaper alternative to Ar. This process uses the fundamental background expressed in the equation [2.6]. This technology utilizes superheated steam which is mixed with oxygen, compressed air and nitrogen/argon as bottom blown gases and the oxygen as a top blown gas (Beskow, 2010).

$$H_2O_{(g)} + \frac{241.9kJ}{mol} = H_{2(g)} + 1/2O_{2(g)} \qquad [2.6]$$

Rick (2010) stated that the use of a kg of steam equated to a substitution of 1.25nm^3 of Ar or N_2, 0.625nm^3 of O_2 and approximately 10kg of scrap. The use of steam also helps in cooling the

bath thereby eliminating need for cooling scrap because the reduction of steam consumes heat due to the endothermic nature of the reaction. According to Rick (2010), nitrogen pick-up is also eliminated through the use of steam, and the reaction of dry steam in the converter decarburization is depicted by equation 2.7:

$$Cr_{23}C_6 + 6H_2O = 23Cr + 6H_2 + 6CO \quad [2.7]$$

As shown in equation 2.7, H_2 acts as the inert gas and O_2 is the oxidant. The use of steam will also have an adverse effect of increasing hydrogen content in the metal, which is undesirable (Bhonde, 2007).

In South Africa, Columbus Steel in Middelburg implemented this method in 2008 (Beskow, 2010). With the use of steam, Columbus Steel managed to reduce their gas consumption costs by reducing of the amount of crude argon consumed in the process by 20-25%, thereby making it possible for them to schedule production independent of argon availability (Beskow, 2010). Due to the endothermic nature of the reaction with steam, it has the added advantage when there is heat surplus in a converter by acting as an economic coolant compared to scrap addition during the refining process (Bhonde, 2007).

Use of carbon dioxide in the decarburization process has been investigated and applied to decarburization as shown in the equation 2.8.

$$Cr_{23}C_6 + 6CO_2 = 23Cr + 12CO \quad [2.8]$$

The reaction above is endothermic and can only be thermodynamically feasible at high temperatures and low CO partial pressure. (Bhonde et al, 2007). Wang et al (2015) concluded that additions such as coolants were not necessary in a process where CO_2 was used as the oxidant, as the endothermic decarburization reaction by CO_2 consumed the excess energy. Furthermore, bath temperature and temperature increases can be controlled by partially introducing carbon monoxide to compensate for some oxygen in the AOD.

In addition, the use of CO as an oxidant improved chromium yield as a result of the weaker oxidation ability of carbon monoxide thus reduced chromium oxidation. Use of CO also leads to

improved refractory life span due to less thermal shock as is observed in the use of oxygen as the excess energy from the oxidation reactions damages refractory lining (Wang et al, 2015).

2.5 Reactions & thermodynamic considerations in the converter refining process

In general, converter refining takes lesser time than conventionally taken in a process like the silico-thermic method, thereby making it cheaper than most pyrometallurgical operations that may require many furnaces. The use of oxygen as the oxidant, and the exothermic nature of the oxidation reactions, renders the process less costly, as electric energy is only used for auxiliary movement of the vessels. Generally, the main reactions occurring in converter refining processes are the oxidation reactions of carbon, chromium and silicon (Turkdogan & Fruehan, 1998).

As already discussed, the CLU process uses dry steam, oxygen, argon compressed air, and nitrogen in the decarburization process. The steam decomposes into hydrogen and oxygen at elevated temperatures and since the endothermic decomposition reaction makes the temperature control in the CLU efficient thereby eliminating need for adding scrap as a coolant. As a result, this makes the CLU ideal for producing medium carbon ferrochrome and ferromanganese, especially in the later process where the evaporation of manganese from the bath due to high temperatures is a serious health and environmental concern (Rick, 2010: Bellow et al, 2015).
The CRK converter is commonly used as an intermediate converter, mainly for silicon and carbon removal and for scrap melting, while avoiding the oxidation of chromium. The CRK vessel design is similar to that of an AOD reactor, but the main difference is mostly on the purpose of use (Heikkinen, 2012). In the CRK process, oxygen is blown through the tuyeres or via the top lance into the bath to reduce Si from initial 4-5 wt. % to below 0.5 wt. %. The carbon is also reduced from around 6-7 wt. % to 3 wt. %.

The main reason for not decarburizing to carbon contents lower than 3 wt. % is to minimize the oxidation of chromium oxidation, which essentially tends to increase as the carbon content in the bath decreases (Heikkinen, 2012). From the work done by Heikkinen et al (2011), when the Si content in the bath decrease to between 0.3-0.6 wt. %, the carbon oxidation becomes the more favourable reaction with oxygen until to below approx. 2.5 wt. %, thereafter the chromium oxidation becomes significant in the CRK converter.

Traditionally, the AOD converter has been widely adopted in the stainless steel and medium/low carbon ferrochrome production (Wei and Zhu, 2002). In the production of medium and low carbon ferrochromium alloys, the AOD converting process utilizes molten alloy from the EAF or SAF in the form of high carbon ferrochrome and/or charge chrome. Depending on AOD vessel design, the oxygen is blown into the converter, either from the bottom or from top lances. The key reactions in the AOD vessel involve the oxidation of C and Si, and consequently Cr, which is then recovered in the reduction stage by addition of FeSi (Wei & Zhu, 2010). The typical oxidation reactions that occur in the converter are shown in equations 2.9-2.12.

$$[C] + \frac{1}{2}O_2(g) \rightarrow \{CO\}_{(g)} \quad [2.9]$$

$$2[Cr] + \frac{3}{2}O_2(g) \rightarrow (Cr_2O_3) \quad [2.10]$$

$$[Si] + O_2(g) \rightarrow (SiO_2) \quad [2.11]$$

$$[Fe] + \frac{1}{2}O_2 \rightarrow (FeO) \quad [2.12]$$

Other independent reactions also occur during the decarburization stage, and these are shown in equations 2.13-2.15 (Wei and Zhu, 2002):

$$[C] + (FeO) \rightarrow \{CO\} + [Fe] \quad [2.13]$$

$$\Delta G_C = \Delta G_C^{\circ} + RT \ln(P_{CO} /(a_{[C]} \times a_{(FeO)})$$

$$2[Cr] + 3(FeO) \rightarrow (Cr_2O_3) + 3[Fe] \quad [2.14]$$

$$\Delta Gc = \Delta G^{\circ}c + \Delta G^{\circ}_{Cr} + RTln\,(a_{Cr_2O_3} /(a^2_{[Cr]} \times a^3_{(FeO)}))$$

$$[Si] + 2(FeO) \rightarrow (SiO_2) + 2[Fe] \quad [2.15]$$

$$\Delta G_{Si} = \Delta G_{Si}^{\circ} + RT\, ln \frac{a_{(SiO2)}}{a_{[Si]}a^2_{(FeO)}}$$

The equations above show the Gibbs free energy changes, ΔG, which is a measure of the thermodynamic driving force for the reactions to occur. Thermodynamic principles state that if $\Delta G^o < 0$ at any particular temperature, then the reaction is spontaneous and non-spontaneous if the $\Delta G^o > 0$. Therefore, at process temperatures the oxidation reactions referred to in equations 2.9-2.15 are thermodynamically feasible (Wei and Zhu, 2002).

2.5.1 AOD decarburization process

In general, the AOD converting process uses oxygen for decarburizing (Wei and Zhu, 2002). As shown in equation [2.9], oxygen reacts with carbon to form carbon monoxide. In the initial stages of the blow, the Oxygen: Nitrogen/argon ratio is usually high, and the ratio is dependent on the analysis of the liquid metal coming from the EAF. In a typical AOD, the oxygen and nitrogen/argon are blown into the bath through the tuyeres at the bottom of the vessel or a top lance, thereby stirring the bath as well (Wei and Zhu, 2002).

According to Fruehan (1976) and Wei and Zhu (2002), the oxygen blown through the tuyeres also oxidises Cr to form chromium oxide (Cr_2O_3) , and the Cr_2O_3 in turn oxidises the carbon as it rises through the metal bath due to the mixing effect of nitrogen or argon. Fruehan (1976) further assumed that the carbon oxidation is mainly determined by the rate of oxygen being blown for higher carbon levels, while for lower carbon levels the oxidation is mainly determined by the rate of carbon mass transfer from the bulk of the melt to the bubble surface.

Furthermore, Fruehan stated that the carbon oxidation by Cr_2O_3 was mainly controlled and dependent on the mass transfer of carbon to the surface of the inert gas bubbles, resulting in Cr_2O_3 being reduced to Cr. However, Wei and Zhu (2002) also clarified that the mass transfer of carbon to the reaction sites was only rate determining at lower carbon contents, whereas at higher carbon composition the rate of oxygen blown into the metal bath controls the extent of decarburization.

2.5.1.1 Thermodynamics of the decarburization reaction involving dissolved oxygen

The oxygen blown into the converter through the tuyeres and/or the top lance reacts with carbon as illustrated in equation [2.16].

$$[C] + [O] = \{CO\}_{gas} \qquad K = \frac{P_{CO}}{a_C \times a_O} = e^{-\frac{\Delta G^o}{RT}} \qquad [2.16]$$

Where:

K is the equilibrium constant

P_{CO} is the partial pressure of carbon monoxide

R is the molar gas constant

α_i is the activity of carbon and oxygen.

Where K is the equilibrium constant, P_{CO} partial pressure of CO, R molar gas constant, T is temperature (in K), a_C activity of carbon, and ΔG^o is the standard Gibbs free energy for the reaction. In order to drive the reaction forward, lowering the CO partial pressure or increasing oxygen activity will promote oxidation of carbon. However, an increase in partial pressure of oxygen will also result in the oxidation of loss of Cr to slag as shown in equation 2.17 (Heikkinen et al, 2011).

$$2[Cr] + 3[O] = (Cr_2O_3) \qquad K = \frac{a_{Cr2O3}}{a_{Cr}^2 \times a_O^3} = e^{\frac{-\Delta G^o}{RT}} \qquad [2.18]$$

The best option to reduce chromium oxidation is by lowering the partial pressure of CO in the bubbles, and this can be done through introduction of a diluent inert gas (Heikkinen et al, 2011). Nitrogen and argon gases are the main gases used as inert gases in the decarburization process, but nitrogen is preferred since is relatively cheaper than argon Heikkinen et al, 2011; Wei and Zhu, 2002). However, the use of nitrogen presents challenges such as the dissolution into alloy will have a negative effect. Nitrogen is known to cause strain ageing, reduce ductility and embrittlement of the heat affected zone (HAZ) for welded steels (Satyendra, 2013).

In addition to lowering the partial pressure of CO is the AOD, the use of inert gases such as N_2 and/or Ar also facilitates the attainment of higher equilibrium Cr percentages in the bath, thereby attaining lower carbon contents with minimum Cr loss to slag (Heikkinen et al, 2011; Wei and Zhu, 2002). Inert gas blowing in the AOD has other advantages such as stirring of the bath to ensure good contact area between the slag and metal interfaces (Heikkinen et al, 2011). This is achieved by reducing the oxygen to nitrogen and/or argon ratio leading to more nitrogen or argon and hence, less oxygen in the bath, resulting in reduced Cr oxidation (Heikkinen et al, 2011)

2.5.1.2 Reduction stage

When the desired carbon levels have been achieved in the decarburization stage, the next stage is to recover most, if not all, of the chromium that would have been oxidised to slag. Essentially, the reduction is stage mainly involves the reduction of Cr_2O_3 to elemental Cr by using

ferrosilicon as a reductant (Heikkinen, 2013). In this case, the ferrosilicon reduces the metal oxides as illustrated in in equation 2.19.

$$3[Si] + 2(Cr_2O_3) = 4[Cr] + 3(SiO_2) \quad [2.19]$$

During the reduction stage in the AOD, the mixing of the metal bath is achieved by stirring with an inert gas such as argon. In the case where nitrogen has been used as a carrier gas during the oxidation stage, the introduction of argon gas also helps in the removal of any dissolved nitrogen in the bath as argon has a higher partial pressure and a heavier molecule than nitrogen (Wei and Zhu, 2002). Addition of FeSi to the AOD is done at the reduction stage to reduce Cr_2O_3 from slag to Cr, thereby reducing losses to slag (Pretorius and Nunnington, 2002).

2.5.2 Thermodynamic considerations for metal & slag in ferrochrome refining

The metal and slag control in the AOD process is essential in order to get the desired slag and metal quality. As such, it is important to understand the thermodynamic behaviour of metal and slag in the AOD converter. The slag chemistry and slag volume influence the bath temperatures by insulating the bath against excessive heat losses, protecting the refractory lining, and also in promoting the desulphurization of the metal bath (Pretorius and Nunnington, 2002). The desulphurization of the bath by slag-metal reactions takes place according to equation 18 (Pretorius and Nunnington, 2002):

$$[S]_{bath} + (CaO)_{slag} = (CaS)_{slag} + [O]_{bath} \quad [2.20]$$

AOD converting process utilizes basic slags: target basicity 1.8 Essentially, the typical slag composition targeted for basicity calculations at the process under study is in the range CaO ≥ 40 wt. %, MgO 10-12 wt. % and SiO_2 ≤ 30 wt. % Pretorius and Nunnington, 2002). Basically, the use of basic slags and compounded by the reduced oxygen potential in the metal bath, create the ideal conditions for the desulphurization process (Pretorius and Nunnington, 2002).

The slag basicity can be calculated as shown in equations 2.21-2.22 (Pretorius and Nunnington, 2002).

$$B = \frac{CaO+MgO}{SiO_2} \geq 1.8 \quad [2.21]$$

$$B = \frac{CaO}{SiO_2} \geq 1.5 - 1.6 \quad [2.22]$$

In general, high slag volumes also have the negative effects on the efficiency of the AOD process, particularly in reducing the carbon removal, negatively affects the desulphurization, and also the dissolution reactions in the reduction stage. This in turn can be compounded by slag carry over from the EAF or SAF, increasing slag volume in the converter (Pretorius and Nunnington, 2002). Therefore, the volume of slag in the refining process has to be minimized as much as possible in order to enhance the escape of CO gas, and also to reduce the wear of refractory materials (Pretorius and Nunnington, 2002; Xiao and Holappa, 1992).

Burnt lime and dolomite are used as sources of CaO and MgO (basic oxides) needed for increasing basicity. The use of fluorspar as an additive is also practiced as it improves the lime dissolution kinetics, particularly in the reduction stage. The addition of FeSi results in the formation of $CaSiO_4$, an inter-mediate phase, due to reaction of SiO_2 with the lime during the reduction stage (Pretorius and Nunnington, 2002).

The $CaSiO_4$ produced further reacts with SiO_2 to form $CaSiO_3$, which then melts gradually to form the final slag. The use of CaF_2 improves slag fluidity, hence promote better mass transfer rates, and consequently improve desulphurization process, as well as metal-slag separation, thereby reducing metal loss to slag in the converter upon tapping (Pretorius & Nunnington, 2002; Chuang et al, 2002).

Figure 2.2 is a typical slag ternary diagram depicting the composition of stainless steel slags (Pretorius and Nunnington, 2002). Ideally, a typical slag should have the analysis already described in equations 2.21 and 2.22. The ternary diagram shown in Figure 2.2 gives an indication of the liquidus temperatures for that particular analysis of slag desired.

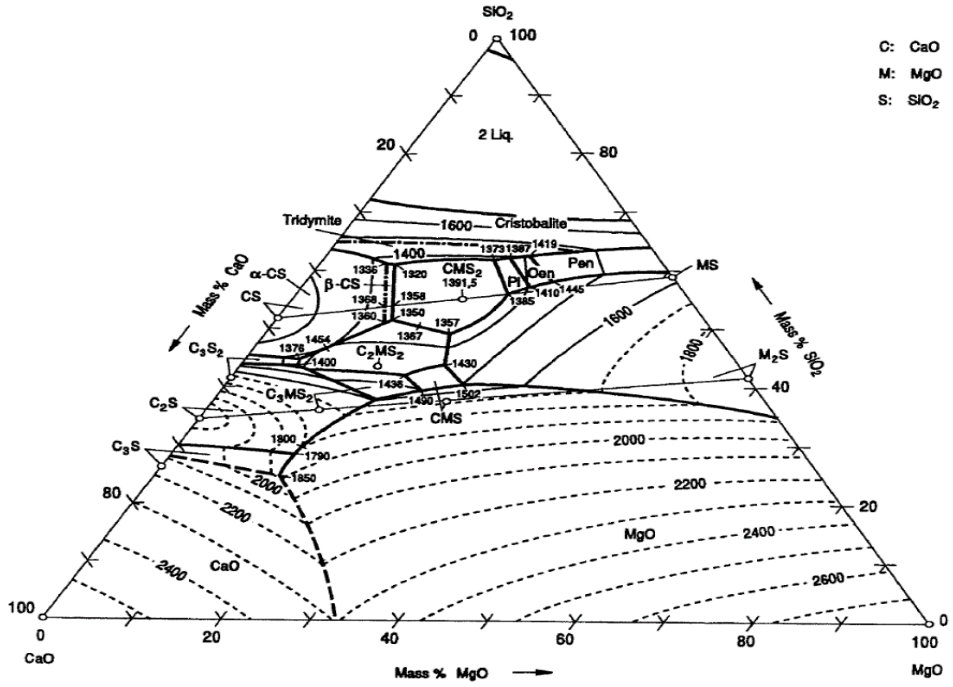


Figure 2.1: Slag ternary diagram for typical stainless steel slags (slag atlas, 1995)

Poor and inconsistent slag control and monitoring in the AOD converter often results in high losses of chromium to slag and this is particularly coupled with the negative impacts of high slag viscosity which can lead to the high loss of metallics (Pretorius and Nunnington, 2002; Ban-Ya, 1993).

The use of fluxes in the smelting operations is done to modify the slag composition to ensure that a slag with the required properties is produced. Typical fluxes used in high carbon ferrochrome/charge chrome production are quartz, dolomite or lime. The quality of the slag produced will have an impact as well on the process metallurgy melting temperatures as well as the tapping conditions of the furnace (Gasik, 2013).

2.5.3 Activities of Cr and C in ferrochromium alloy refining

The co-existence of the solute atoms such as Cr, C and O in the bath has been extensively studied in order to understand the bath refining process for Fe-C-Cr system (Ohtani, 1956; Fruehan and Turkdogan, 1999; Richardson and Dennis, 1953). Richardson and Dennis (1953) investigated the effect of Cr on the activity coefficient of carbon in a Fe-Cr-C bath by using experiments which determined the conditions of equilibrium in the CO/CO_2 mixture reaction

with C in the Fe-C-Cr melts. The authors used a binary Fe-C system to determine the activity of C in liquid Fe + C solutions and experimental results allowed for better accuracy in the determination of carbon and iron activities.

The C effect at a particular temperature on the activity coefficient of Cr can be depicted by the interaction coefficient, γ_{Cr}^{C} (Ohtani, 1956). From these findings, Ohtani (1956) proposed the relationship between the interaction coefficient and the activity coefficient of Cr as:

$$\gamma_{Cr}^{C} = \gamma_{Cr}/\gamma'_{Cr} \quad [2.23]$$

Where

γ_{Cr} Is the activity coefficient of Cr in Fe-C-Cr alloys

γ'_{Cr} is the activity coefficient of Cr in Fe-Cr

From the experimental work done by Ohtani (1956), it was shown that Fe-Cr alloys obey Raoult's law, and that the alloys tend to show a negative deviation from Raoult's law when C is added as a third element to Fe-Cr binary alloys. Essentially, Raoult's law states the partial pressure of each component in an ideal liquid mixture can be obtained from the product of that specific component with its composition (mole fraction) in that particular mixture in question (Gaskell, 2013).

In addition to the influence of C on Cr, the effect of Cr on C was also investigated, and the relationship is represented as shown in equation 2.24 (Ohtani, 1956):

$$\gamma_{C}^{Cr} = \gamma_{C}/\gamma'_{C} \quad [2.24]$$

Based on the studies by Richardson and Dennis (1953) to determine the equilibrium for CO/CO_2 mixtures with C in Fe-C-Cr alloys, it is possible to evaluate effect of Cr on the activity coefficient of carbon in the bath. The results obtained from this by the authors work made it possible for calculation of thermodynamic properties for Fe-C with better accuracy. Ohtani (1956) proposed that chromium has affinity for carbon and was shown by the change in solubility of graphite on addition of chromium in Fe-Cr-C alloys. This was attributed to the drop in carbon activity in iron solutions upon addition of chromium.

According to Ohtani (1956), the interaction energy between Cr and C is higher than that of Fe-C atoms, and hence the distribution of C in relation to Cr atoms is not random. Ohtani (1956) further proposed that carbon atoms in molten Fe-Cr-C alloys tend to preferably agglomerate around chromium atoms than iron atoms thus exist with a higher proportion of Cr atoms around them. Therefore, the affinity between the Cr and C atoms makes it difficult for the decarburization to occur in the converter, especially at lower C contents (Ohtani, 1956). In other words, the Cr content in the metal bath will affect the extent to which C can be oxidized, without the co-oxidation Cr (Ohtani, 1956).

2.5.4 Interaction parameters in ferrochromium refining

Interaction parameters are defined as a measure of interactions that occur between atoms or molecules in a solution. This can be the interaction between these molecules/atoms with one another or with the medium or solvent in which they are dissolved (Tados, 2013; Ohtani, 1956). From the work done by Fuwa and Chipman (1959) on the activity of carbon in Fe-C-X systems reveal, the researchers concluded that interaction parameters are linked to sites of the elements (X) on the periodic table and tend to vary with the atomic number of the element X.

Wada et al (1951) stated that the interaction parameters were related to the excess free energy of mixing, that is, the interaction parameters depended on interaction energies between solute and solvent atoms (or solute and solute atoms). Wagner (1952) developed the first order free energy interaction coefficients for dilute multi-component solutions, which is the coefficient in the Taylor series expansion for the logarithm of the activity coefficients and represented as shown in equations 2.25 and 2.26:.

$$\varepsilon_i^{(j)} \equiv [\frac{\partial ln\gamma_i}{\partial X_j}]_{X_1 \to 1} \qquad [2.25]$$

$$ln\gamma_i = ln\gamma_i^o + \sum_{j=2}^{m} \varepsilon_i^{(j)} X_j + higher\ order\ terms \qquad [2.26]$$

Bale and Pelton (1989) developed modifications to the unified interaction parameter formalism. The formalism proposed by Pelton and Bale (1989) reduces to the formalism developed by Wagner (1952) at infinite dilution (by neglecting all other higher orders except for the first order terms) to an expression that is linear with respect to molar fractions of solutes in dilute alloy as shown in equation 2.26.

The advantage with the unified interaction parameter formalism over the standard formalism is that it remains thermodynamically consistent at finite concentrations whereas the latter does not. It should be noted however that at infinite dilutions, the unified interaction parameter formalism reduces to standard formalism and keeps the numerical values of parameters as well as the notation (Bale and Pelton, 1966). This calculation for interaction parameters and activity coefficients was used in the process under study to calculate activities and activity coefficients for Cr, C, Si for the study and mass and energy balance model development.

Taking a system with (N+1) components, where there is N solutes and a solvent, and limiting it to first order interaction parameters, the unified interaction parameter formalism can be expressed as shown in equation 2.26 (Bale and Pelton, 1966).

$$ln\gamma_i = ln\gamma_i^o + ln\gamma_{Solvent} + \varepsilon_{i1}X_1 + \varepsilon_{i2}X_2 + \varepsilon_{i3}X_3 + \cdots + \varepsilon_{iN}X_N \quad [2.26]$$

In addition/furthermore/, the equation for the activity coefficient of the solvent is expressed as;

$$ln\gamma_{solvent} = -\frac{1}{2}\sum_{j=1}^{N}\sum_{k=1}^{N}\varepsilon_{jk}X_jX_k \quad [2.27]$$

Where;

X_i is the mole fraction of a component i.

ε_{ij} interaction coefficients

γ_i activity coefficient of component i.

$\gamma_{solvent}$ activity coefficient of solvent

For first order interaction parameters in ternary systems with a solvent and two solutes, namely solute 1 and solute 2, the following quadratic formalisms were derived (Pelton and Bale, 1989).

$$ln\gamma_{solvent} = -\left(\frac{\varepsilon_{11}}{2}\right)X_1^2 - \left(\frac{\varepsilon_{22}}{2}\right)X_2^2 - \varepsilon_{12}X_1X_2 \quad [2.28]$$

$$ln\gamma_1 = ln\gamma_1^o + \left[-\left(\frac{\varepsilon_{11}}{2}\right)X_1^2 - \left(\frac{\varepsilon_{22}}{2}\right)X_2^2 - \varepsilon_{12}X_1X_2\right] + \varepsilon_{11}X_1 + \varepsilon_{21}X_2 \quad [2.29]$$

$$ln\gamma_2 = ln\gamma_2^o + \left[-\left(\frac{\varepsilon_{11}}{2}\right)X_1^2 - \left(\frac{\varepsilon_{22}}{2}\right)X_2^2 - \varepsilon_{12}X_1X_2\right] + \varepsilon_{22}X_2 + \varepsilon_{12}X_1 \quad [2.30]$$

The above equations are valid for all compositions and are analogous to the quadratic formalism proposed by Darken (1967), which is thermodynamically consistent at finite concentrations. With the determination of these models for activities and activity coefficients, the same models were used to determine the interaction between interaction of Cr, Si and C with Fe as the solvent (and the oxides of these elements) in the refining of high carbon ferrochromium alloy in the bath in order to predict behaviour of these elements and oxides in the converter refining.

2.5.5 Effect of blowing conditions on the extent decarburization

In the refining stage, the carbon content in the bath gets depleted as decarburization proceeds until critical carbon level is attainted. Turkdogan and Fruehan (1999) defined the critical carbon as that carbon content below which chromium oxidation commences. These authors further stated that critical carbon level increased with the chromium content (or activity of chromium) in the alloy bath. However critical carbon in the refining process is determined by a number of factors such as thermodynamic and kinetics considerations, temperature and chemical composition of the alloy bath, blowing rates of argon and oxygen (or any other inert gas used), the configuration and geometry of the vessel, activity coefficients of the individual elements in the alloy bath and the mixing and stirring effect of the blown gases (Wei and Zhu, 2002).

According to Wei and Zhu (2002), the blowing time is a function of gas flow rates and a balance between ratios of oxygen to nitrogen or argon (Wei and Zhu, 2002). When carbon reaches a critical content, Cr loss to slag increases with further blowing time and the Cr loss to slag can be represented as shown below in equation 2.31;

$$\Delta[\%Cr] = \frac{4M_{Cr}}{3W10^{-2}} N_{O_2} t - \frac{10^{-2}W}{2M_c} \Delta[\%C] \qquad [2.31]$$

Where M_{Cr}, M_c are molecular weights for Cr and C respectively, W weight of steel, N_{O_2} molar flow rate of O_2 and Δ[%C] change in carbon content (Turkdogan and Fruehan, 1999).

2.5.6 Effect of gas flow rates on decarburization

Volumetric gas flow rates have an influence on oxidation reactions that occur within a converter. The O_2:Ar gas ratios play a major role in the efficiency of the decarburization process (Wei et al, 2010). A reduction in O_2: Ar ratio with the blowing intervals improves the effectiveness of the

refining process. Fruehan (1976) stated that the oxygen volumetric flow rate was critical for decarburization at higher carbon levels in the alloy bath. Wei and Zhu (2002) went on further to state that the gas flow rate has a significant effect on decarburization and the oxidation of elements in the alloy bath. At critical carbon, the reduction of oxygen gas flow rate and increase in argon flow rate dilutes the carbon monoxide produced from carbon oxidation, thereby promoting further carbon oxidation at lower carbon contents in the bath (Wei and Zhu, 2002).

As decarburization proceeds, the %C remaining in the bath becomes rate determining, as an increase in nitrogen and decrease in oxygen flow rates will promote decrease in partial pressure of CO and thereby promoting further decarburization (Wei et al, 2010). The inconsistent control of gas flow rate translates to higher operational costs due to un-optimized gas consumption and blow times. The inconsistent blowing cycles will increase costs on gases, reduced refractory lifespan, Cr loss in slag, and overally, decreased productivity. It is quite prudent to have a standardized blowing rate with consistent gas flows to improve on process efficiencies.

The decarburization rate increases as the blowing process proceeds, and this results in the increase of the bath temperature from the exothermic oxidation reactions. During this stage, the decarburization rate is directly influenced by the volumetric flow rate of the oxygen gas. As the carbon level decreases, it reaches a critical point value (critical carbon level) where the decarburization rate then becomes more dependent on mass transfer of the carbon in the bath (Wei et al, 2010).

According to Turkdogan and Fruehan (1998), the critical carbon content during refining, is that carbon content below which Cr in the bath starts getting oxidized. The critical carbon will increase with decrease in bath temperature and increase in Cr content or Cr activity (Turkdogan and Fruehan, 1999). When oxygen is blown into the converter, Cr gets oxidized first to Cr_2O_3, which is further reduced by the solid carbon as it rises into the slag-metal emulsions (Turkdogan and Fruehan, 1999):

$$Cr_2O_3 + 3C = 2[Cr] + 3\{CO\} \quad [2.32]$$

$$\frac{d\%C}{dt} = -\frac{\rho}{W}\sum_i m_i A_i[\%C - \%C_i^e] \quad [2.33]$$

Where ρ is the steel density, W is weight of the metal, m_i is mass transfer coefficients, A_i the surface areas, $\%C^e_i$ equilibrium carbon content, and subscript , i, individual reaction sites e.g. top slag or rising bubble.

2.5.7 Initial Temperature of the liquid metal

In most cases, crude steel/FeCr from EAF/SAF is conveyed to the AOD in a transfer ladle as liquid alloy. The initial temperature of the metal charged into the converter is important. In other words, a lower carbon content and lower Cr loss in slag is achievable at the end of the refining stage with a higher starting temperature of the liquid metal. This will impact positively on the amount of FeSi needed for recovery of Cr from slag (Wei and Zhu, 2002; Fruehan, 1976; Turkdogan and Fruehan, 1999). Due to the manual process implemented in this process data, the impact of initial temperature on decarburization has not been observed.

Wei and Zhu (2011) studied the impact of initial temperature on decarburization. All other process parameters were kept constant and the initial temperature of the bath was varied by +/- 10K. It was observed that an increase by 10K resulted in a decrease in the final end point carbon, and a decrease of initial temperature by -10K resulted in an increase in end point carbon content. It was however noted in that study that consistent implementation of this study on process level was difficult as every heat characteristic differs from the next heat in process operation.

2.5.8 Rate equations in AOD refining

The rate of decarburization can be described by rate equations which can be used as predictive models in the refining process. At higher carbon levels in the alloy bath, the oxygen flow rate determines carbon oxidation and carbon liquid mass transfer to reaction interface is rate limiting at lower carbon contents (Wei and Zhu, 2002; Fruehan, 1976). By considering these conditions of carbon oxidation for higher and lower carbon levels, it is possible to model rate equations for oxidation of elements in the alloy bath (Wei and Zhu, 2002). Wei and Zhu (2002) and Fruehan (1976) defined lower carbon contents as that carbon content below the critical carbon content where carbon mass transfer becomes rate limiting and not the oxygen flow rate into the alloy bath.

2.5.8.1 Rate Equations at higher carbon levels

The rate of decarburization for the refining process at higher carbon levels in the metal bath is mainly dependent on the rate of oxygen blown into the process (Wei and Zhu, 2002; Fruehan, 1976). The average losses of the main elements in the bath like silicon, carbon and chromium are described in the equations 2.34 – 2.36 below (Wei and Zhu, 2002; Fruehan, 1976; Diaz et al, 1997).

$$\frac{d[\%C]}{dt} = -\frac{2\eta Q_O}{22400} \times x_C \times \frac{100 * M_C}{W_m} \quad [2.34]$$

$$\frac{d[\%Cr]}{dt} = -\frac{2\eta Q_O}{22400} \times x_{Cr} \times \frac{100 * M_{Cr}}{1.5 * W_m} \quad [2.35]$$

$$\frac{d[\%Si]}{dt} = -\frac{2\eta Q_O}{22400} * x_{Si} * \frac{100 * M_{Si}}{2 * W_m} \quad [2.36]$$

where

Q_O is flow rate of oxygen.

M_i is the molar mass of the substance, i.

X is the molar fraction of each element, i:

W_m is the mass of the alloy bath charged into the converter:

η is the utilisation ratio of oxygen.

2.5.8.2 Rate Equations for the low carbon contents

The authors Wei and Zhu (2002) and Fruehan (1976) defined lower carbon contents in the alloy bath to be lower than the critical carbon of the alloy bath under which carbon mass transfer to the reaction interface becomes rate limiting and not oxygen flow rate into the alloy bath. At low carbon concentrations the main oxidation reactions are that of chromium and carbon, and these reactions increase the alloy bath temperature as these reactions are exothermic in nature. The equation that appropriately describes this scenario is equation 2.37 (Wei & Zhu, 2002).

$$-W_m \frac{d[\%C]}{dt} = A_{rea} \rho_m k_c ([\%C] - [\%C]_e) \quad [2.37]$$

Where:

W_m - mass of liquid alloy (g)

[%C] - mass % of concentrate of carbon in molten alloy (wt. %)

A_{rea} – total reaction interface (cm^2)

ρ_m – density of alloy (g/m^3)

k_c – mass transfer of carbon in molten alloy (cm/s)

$[\%C]_e$ – equilibrium concentration of carbon in molten alloy at reaction interface (wt. %)

2.6 Energy balance in the AOD decarburization process

It is important to look at the energy balance and requirements for decarburization. The energy in the converter comes from oxidation reactions of carbon, chromium and silicon as illustrated in equations in equations 2.9 – 2.15 (Heikkinen et al, 2011). These oxidation reactions release heat as the elements in the metal bath get oxidised (Wei and Zhu, 2002). The molten alloy charged into the converter along with all the gases (argon/nitrogen, oxygen and the exhaust gases) all carry heat in the converter. Slag formers added in the form of lime and dolomite also take in heat in the formation of slag (Wei and Zhu, 2002) Wei and Zhu (2002) went on to state that as heat rises in the converter due to the oxidation reactions of the elements (of which the reactions are exothermic), heat losses through exhaust gases, radiation when converter is tilted to take samples and check bath temperature, and by conduction and adsorption through the refractory lining are experienced. Pretorius and Nunnington (2002) also stated that large amounts of slag formers could lead to high volumes of slag and insulate the bath hence affecting high refractory wear and inhibit carbon removal efficiency.

A general expression of energy balance (Wei & Zhu, 2002) during decarburization is as shown in Equation 2.38:

$$\Delta H_C + \Delta H_{Si} + \Delta H_M + E = C_p' \Delta T + q_o t \qquad [2.38]$$

$\boldsymbol{\Delta H_C}$ is the heat of oxidation of Carbon

$\mathbf{\Delta H_{Si}}$ is the heat of oxidation of Silicon

$\mathbf{\Delta H_M}$ is the heat of oxidation of Chromium and Iron

E is the electrical energy

$\mathbf{C_p'}$ is apparent heat capacity of the metal/refractory system

Δ**T** is the temperature change during the decarburization period

$\mathbf{q_o}$ represents steady state external heat loss rate

t is the total elapsed time from start of oxygen blowing until the start of the reduction stage.

Some of the bath temperature is partly lost due to conduction and adsorption by the refractory lining and shell during the refining process. When the converter is tilted to facilitate sampling and temperature checks, radiation losses are also experienced. Additions of coolants for temperature control also lower bath temperature (Wei & Zhu, 2002).

2.7 Summary

High carbon ferrochromium and charge chrome alloy production is mainly through the carbothermic process (with use of SAF) where carbon is used as the main reductant and fluxes such as limestone and quartz are used to achieve required slag chemistry and properties (Gasik, 2013). Technology advancement has resulted in the development of plasma furnaces in the manufacture of high carbon ferrochromium and charge chrome alloys through the smelting of chromite fines. However the use of high carbon ferrochromium and charge chrome in the production of stainless steel has led to the development of technology for carbon removal as carbon is an impurity in super alloys and low carbon stainless steels production.

Different technologies such as the metallothermic processes and ferrochromium alloy refining with chrome ore have been developed to lower carbon content. However the development of converter refining has found greater use as it is cheaper. Of particular interest in the converter technology is the use of converter technology mainly in the production of stainless steel. However, this technology has been harnessed in the production of medium carbon ferrochromium alloy to reduce carbon content in the alloy. The process under study has harnessed the use of AOD technology in the production of medium carbon ferrochromium and forms the basis of this investigation.

CHAPTER 3

3. METHODOLOGY

3.1 Introduction

The parametric study in the decarburization process of high carbon ferrochromium alloys in the AOD converter enhances the understanding and process control of the thermodynamics involved in the process. The carbon in the liquid alloy is oxidised to CO gas which is then driven out of the bath, thereby lowering the carbon in the metal (Wei &Zhu, 2002). Chromium is also oxidised particularly around the tuyere area, and then as the Cr_2O_3 rises with the argon/nitrogen bubbles it oxidizes the carbon thus getting reduced to chromium (Fruehan, 1976). Fruehan (1976) also assumed that at lower carbon levels, the liquid mass transfer of carbon to the bubble surface determines the carbon oxidation by Cr_2O_3 but at higher carbon levels, it is primarily determined by the amount and rate of oxygen flow blown into the vessel.

In this study, the process under study was investigated to evaluate process performance for manually operated AODs in the manufacture of medium carbon ferrochromium alloy. The AOD processing route has been traditionally used for stainless steel production, and most research done has been to understand thermodynamics and kinetics for stainless steel production (Wei and Zhu, 2002; Freuhan, 1956). The automated operation was abandoned after the simulation prediction for temperature and carbon levels deviated significantly from the results obtained from sampling and manual temperature measurements, rendering process control difficult. The UTCAS system (real-time dynamic process control software) was used to run the AOD on automatic, but was since stopped though data like pressure and volumetric flow can still be obtained on the display.

Actual gas flows and gas pressures were displayed on the screen from the UTCAS display, and these values were then used to calculate normal gas flow rates for the plant data collected. The use of nitrogen as the inert gas of choice was chosen for the process under study, as the cost of argon gas was higher than that of nitrogen. Since the onset of the manual operation, no scientific study has been undertaken to improve process performance. Plant data was collected for 30 AOD heats in order to understand the decarburization rates and effect of different parameters on the process over a 30 day interval. The limited time frame for data collection was a result of time

constraints for compiling of the final thesis, thus extended data collection interval was not possible for the plant under study. This process data was collected by the control room operator that is filled onto an AOD log-sheet (template shown in the Appendix 1).

3.2 Description of process under study

The process under study involves the utilization of EAFs to re-melt high carbon ferrochromium alloy fines (> 10mm in size) with analysis of the metallic fines ranging from 63 – 68 wt. % Cr, 0.7 – 1.5 wt. % Si and carbon > 7 wt. %. The process flow is shown in figure 4. The high carbon ferrochromium alloy fines are charged into the electric furnaces mixed with a blend of slag formers (burnt lime and dolomite), which form the basis for slag formation. The melting process in the furnace on average has duration of 3hrs. When the melting is complete, the electric furnaces are tilted to tap the slag into the slag pots.

Upon attaining a temperature of approximately 1700^{o}C after the last deslagging, the molten alloy is then tapped into a transfer ladle and the net weight of the alloy measured. Care is taken to ensure that slag carry over to the AOD is avoided. This is to ensure that the slag volume in the converter is controlled. A high slag volume in the converter has been observed to reduce rate of decarburization and high temperatures in the bath (> 1760^{o}C) resulting in reduced oxygen:nitrogen gas ratios to try and lower the bath temperature (Wei and Zhu, 2002; Pretorius and Nunnington, 2002). The high slag volume insulates the bath, resulting in very high bath temperatures being experienced (Pretorius and Nunnington, 2002).

The tapped molten alloy is charged into the AOD when the transfer ladle is transported using an overhead crane. The AOD is titled to allow for transfer of molten alloy to the vessel. At this moment, a quick immersion thermocouple (QIT) is used to measure the initial temperature of the bath. The converter is then tilted back to the vertical position where the first stage of blowing takes place. The first stage of the blowing process involves decarburizing a carbon content >2 wt. %. This stage also involves blowing a gas flow ratio of 3:1 oxygen and nitrogen, as at this stage carbon is sufficiently high and the rate of oxygen blown into the AOD by the two bottom tuyeres is rate determining (Fruehan, 1976).

When the measured carbon level is less than 2 wt. %, this signifies the start of the second stage of blowing. In this stage, the carbon is considered low enough to adjust the oxygen:nitrogen ratio

to 1:1 respectively. The carbon content is sufficiently low for carbon content liquid mass transfer to the nitrogen bubbles as the Cr_2O_3 rises in the bath, to be rate determining. This means the rate of oxygen flow into the converter is no longer determining the decarburization process (Wei and Zhu, 2002; Fruehan, 2002).

Upon attaining a carbon content of > 1 wt. % carbon, the decarburization process moves into the reduction phase, where ferrosilicon alloy (FeSi) is added in order to recover the chromium that has been oxidized to slag. In this stage of the process, silicon in the FeSi reduces Cr_2O_3 to Cr and this chromium reports to the metal bath. To reduce loss of metallic elements to slag, fluorspar is added to improve slag fluidity and also reduce alloy entrainment in slag (Pretorius and Nunnington, 2002). Argon is then blown into the metal bath and oxygen and nitrogen discontinued. The argon is meant to stir the bath during reduction stage (Wei and Zhu, 2002). The metal is then tapped into molded pans and sent for crushing once it has sufficiently cooled to be crushed.

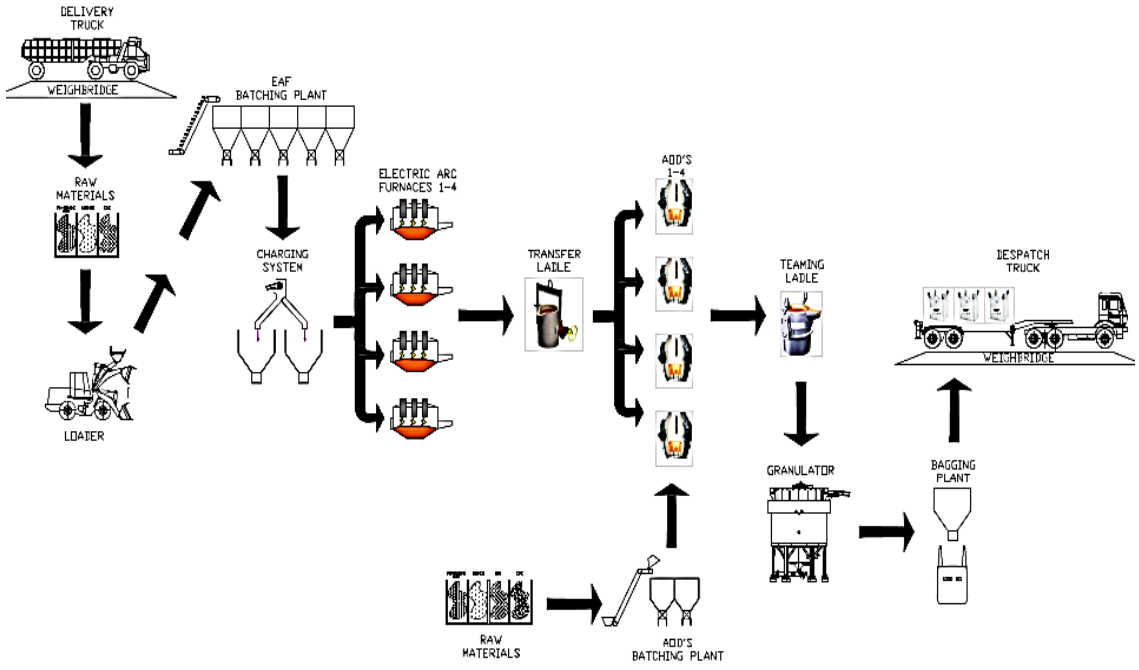


Figure 3.1: Process flow (adapted from the process under study)

For the duration of the time interval under study, same operating conditions (such as the quality of the high carbon fines melted) remained the same, thus eliminating influence of change in process conditions, which can change process performance.

3.2 Plant data collection during the decarburization process

The aim of collecting this data was to study the process parameters and their influence on the decarburization process. The molten metal tapped from the EAF was conveyed to the AOD using a transfer ladle hooked to an overhead crane, and the mass of the molten alloy was determined and recorded onto the log sheet. This formed the basis of calculating the initial molten metal weight charged into the AOD.

Samples of the molten alloy were taken from the EAF during tapping stage, and then sent to the laboratory for chemical/ compositional analysis. The analyses of major elements C, Si, Cr and Fe were conducted using a Spectromaxx Metal Analyzer, and the results were then taken to the EAF and AOD control rooms, and recorded on the log sheets. The initial temperature of the melt charged into the converter was also measured using dip/QIT thermocouples. Slag samples were also taken for analysis on the X-ray Fluorescence Analyzer.

Once the molten metal has been transferred to the AOD, the decarburization process commences, and during the first and second blowing stages, the metal melt samples were also taken in order to check the extent of decarburization and to optimize the process gas flow rates, gas pressure, and bath temperatures for optimal process control. These process parameters were recorded, and gas flow rates and system pressure measurements based on the UTCAS system (computer control system designed for converter refining).

The exact masses of slag formers and FeSi added were obtained from the scales at the AOD batching plant. The final weight, analysis and temperatures were also measured after the final specifications were achieved on Carbon and Silicon.

3.2.1 Blow periods data measurements

First stage of the blowing process involved blowing oxygen and nitrogen at higher carbon levels in the alloy bath, and was done for at least 20 mins after addition of slag formers and initial temperature measurement.

The initial temperature measured at the AOD was a function of the temperature at which the same tap was made at the EAF, and the time it took to transfer the same tap from the EAF to the AOD. This would influence temperature pick up in the AOD from the start of the blowing

process as observed, hence the lower the initial temperature, the longer it took for temperature to pick up to between 1720 – 1750^{o}C. If temperature was less than 1720^{o}C, blow 1 continued until desired temperature was reached. However, the change from first to the second blowing stage is done once carbon goes down to ≤ 2.0 wt. %. The second blowing stage involved taking down carbon from less than 2 wt. % obtained from blow 1 to around 0.8 – 1.0 wt. %. This was usually between 15 – 20 mins depending on the carbon level.

The most significant change in the second stage of blowing was the reduction in Oxygen: Nitrogen ratios. The same measurements as in blow 1 were repeated until the end of blow 2. If carbon was analyzed to be between 1.0 – 1.2 wt. % then the blow interval was further increased by another 7-10 mins. If however if it still remained above 1.2 wt. % after the second blow, then the blow time was increased by 15-20 mins. After the extension of blow 2 to accommodate for higher carbon levels, the carbon was observed to go under 1.0 wt. % and the refining stage ensued.

3.2.2 Data collation and modeling

A mass and energy balance model was constructed based on the collected plant data. The data obtained from the process log sheets for the 30 heats was interpreted in terms of mass and energy balance parameters such as interaction parameters, energy contribution of each element/oxide and Gibbs free energies, amongst other parameters.

Once the energy and mass balance model was constructed, the different parameters discussed in the literature review were manipulated, and their parametric effects on the behavior of the process were observed. The energy and mass balance model was constructed using Microsoft excel format. The rate of decarburization for the two blow scenarios (1st and 2nd stages of blowing periods) was also investigated to ascertain if models highlighted in literature could be applied to the current refining process under study.

3.3 Reduction stage after refining in the AOD

Once the desired carbon content was achieved in the refining stage (for the process under study < 1.0 wt. % C), the reduction stage of the decarburization process commenced to recover chromium lost to slag as chromium oxide (Pretorius and Nunnington, 2002). In this stage of the process, oxygen and nitrogen blowing was replaced by argon blowing and FeSi addition. The

argon stirs the bath and drives out the nitrogen, thereby lowering nitrogen content in the bath (Kienel, 2014). The reduction of Cr_2O_3 to chromium follows equation 3.1:

$$2Cr_2O_3 + 3Si = 4Cr + 3SiO_2 \quad [3.1]$$

Chromium is then recovered into the metal bath as it separates from slag. It is important however that the slag be fluid and less viscous to reduce metal entrainment in slag. For this to be achieved in the process under study, fluorspar was added (as discussed in section 2.5.2 of the literature review) to make slag more fluid (Pretorius and Nunnington, 2002).

Summary

The aim for plant data collection in this section for the process under study was to measure and investigate the effect of different process parameters, such as effect of initial temperature on decarburization process or gas flows and ratios amongst others, on the overall decarburization process. The chemical analysis of the molten metal charged into the AOD was determined first before charging the converter. The weight of the molten metal was also measured and initial temperature of bath analysed with a quick immersion thermocouple once the molten alloy was charged into the vessel. Dip thermometers and samplers were used as tools for data collection in the process for temperature and chemical composition determination respectively. All collected data was logged onto a data template (log sheet as shown in appendix 1) up until the final metal was tapped and cast into ingots. Once all the data emanating from different process parameters was collected, analysis and modeling of data was done.

CHAPTER 4

4. Modelling Methodology

4.1 Introduction

Modeling and simulation in AODs has been studied in an attempt to predict thermodynamic and process parameters effect on the decarburization process. This modeling and simulation can be used to predict outcome of the decarburization process in the AOD, making manipulation of process parameters to achieve a desired product outcome, possible (Wei and Zhu, 2002). By investigating the free energies, activities of elements/oxides, interaction parameters (amongst other parameters investigated) and as discussed in literature, modeling of the interaction of the different elements and oxides, it is possible to do thermodynamic modeling and parametric study of the effect and contribution of different process parameters to the overall decarburization process (Fruehan, 1976; Wei and Zhu, 2002).

A mass and energy balance model was constructed using thermodynamic principles and research work done by authors who investigated such parameters as interaction coefficients and Gibbs free energy, amongst others. This model was used as a predictive tool to determine conditions required to achieve a desired product outcome. Rate equations were also modeled based on literature to predict final product specifications as well. These rate equations were divided into two categories, namely rate equations at higher carbon contents (> 2.0 wt. % C) and rate equations for lower carbon contents (≤ 2.0 wt. %).

4.2 Thermodynamic analysis of plant data

Having discussed thermodynamic principles, such as the activity coefficients of Cr, Si, C, SiO_2, Cr_2O_3 and FeO highlighted in the literature, the plant data was analyzed to investigate the effect of the thermodynamic models and rate equations on the decarburization process. In addition, the slag and metal analyses were analyzed to model behaviour of the blowing process based on the model equations formulated by Heikkinen et al. (2011) that analysed behaviour of silicon, carbon and chromium in the converter.

The standard free energies (ΔG) for the reactions of Cr, C and Si were obtained by the values obtained from the modelling software, HSC Chemistry for Windows, which provides a detailed

database of thermodynamic data (Xiao et al, 2002). The Gibbs free energies values indicating the change of state from Raoultian to Henrian states, ($\Delta G_{R\rightarrow H}$), defined as energy for the change between Raoultian and Henrian standard states, and were obtained from the formula shown in equation 36, derived from work done by Sigworth and Elliot (1974).

$$\Delta G_{R\rightarrow H} = -nRTLn\gamma_i^O \quad [4.1]$$

The activity coefficients (γ_i) were obtained through calculations using the unified interaction parameter formalism (Pelton & Bale, 2007), whereas the mass% fractions (X_i) were obtained from the chemical analyses of the slag and metal samples at different times of the blow process in the converter. The activities (a_i) were then obtained by multiplying the different activity coefficients for the slags with the appropriate mole fractions of the oxides in the slag as shown in equation 4.2 (Ban-Ya & Xiao, 1993).

$$a_i = \gamma_i \times X_i \quad [4.2]$$

4.2.1 Oxygen partial pressure for oxidation of C, Si and Cr

The oxidation reactions of Cr, Si and C were taken into account so that the oxygen partial pressures could be determined. Equilibrium conditions were assumed for the oxidation reactions (Heikkinen et al. 2011). The oxidation of silicon oxidation in the metal bath with iron as the matrix was expressed as shown in equation 4.3 (Heikkinen et al, 2011)

$$Si_{Fe} + O_2(g) = (SiO_2) \quad [4.3]$$

$$K_{4.3} = \frac{a_{SiO_2}}{a_{Si}\times P_{O_2}} = \frac{a_{SiO_2}}{\gamma_{Si}\times X_{Si}\times P_{O_2}} = e^{-[\frac{\Delta G^O_{4.3}+\Delta G_{R\rightarrow H}}{RT}]}$$

The equilibrium constant equation 4.3 was expressed in terms of activity of SiO_2, Si and the partial pressure of oxygen. Rearranging equation 4.3, and expressing it in terms of oxygen partial pressure, made it possible to calculate the oxygen partial pressures for the oxidation of Si in the converter as shown in equation 4.4 (Heikkinen et al., 2011).

$$P_{O_2} = \frac{a_{SiO_2}}{\gamma_{Si}\times X_{Si}} \times e^{[\frac{\Delta G^O_1+\Delta G_{R\rightarrow H}}{RT}]} \quad [4.4]$$

Where $a_{Si} = \gamma_{Si} \times X_{Si}$

This same calculation/ procedure was also followed for the other elements Cr and C, and the equations also derived as shown in equations 4.5-4.8 (Heikkinen et al., 2011).

For Chromium oxidation;

$$\frac{4}{3}\mathrm{Cr_{Fe}} + \mathrm{O_2(g)} = \frac{2}{3}(\mathrm{Cr_2O_3}) \qquad [4.5]$$

$$\mathrm{K_{4.5}} = \frac{{a_{Cr_2O_3}}^{\frac{2}{3}}}{a_{Cr}^{4/3} \times P_{O_2}} = \frac{{a_{Cr_2O_3}}^{\frac{2}{3}}}{\gamma_{Cr}^{4/3} \times X_{Cr}^{4/3} \times P_{O_2}} = e^{-[\frac{\Delta G^{O}_{4.5} + \Delta G_{R \to H}}{RT}]}$$

$$P_{O_2} = \frac{{a_{Cr_2O_3}}^{\frac{2}{3}}}{\gamma_{Cr}^{4/3} \times X_{Cr}^{4/3}} \times e^{[\frac{\Delta G^{O}_{4.5} + \Delta G_{R \to H}}{RT}]} \qquad [4.6]$$

For carbon oxidation:

$$2\mathrm{C_{Fe}} + \mathrm{O_2(g)} = 2\mathrm{CO(g)} \qquad [4.7]$$

$$\mathrm{K_{4.7}} = \frac{P_{CO}^2}{a_C^2 \times P_{O_2}} = \frac{P_{CO}^2}{\gamma_C^2 \times X_C^2 \times P_{O_2}} = e^{-[\frac{\Delta G^{O}_{1} + \Delta G_{R \to H}}{RT}]}$$

$$P_{O_2} = \frac{P_{CO}^2}{\gamma_C^2 \times X_C^2} \times e^{[\frac{\Delta G^{O}_{1} + \Delta G_{R \to H}}{RT}]} \qquad [4.8]$$

The data collected was then taken and the oxygen partial pressures calculated for each heat.

4.2.2 Equilibrium Partial pressure of CO from oxidation of C, Cr and Si.

The equilibrium partial pressures for carbon monoxide for the set of plant data were also determined. In this case, the reduction reactions for SiO_2 and Cr_2O_3 to elemental Si and Cr respectively were taken (Heikkinen et al., 2011). The reduction reactions were taken at equilibrium, and the equilibrium constants were then rearranged in terms of the carbon monoxide partial pressures. In addition, the oxidation of C to form CO was also taken into account, and the thermodynamic relationships are shown in equations 4.9- 4.11.

For silica reduction:

$$2\mathrm{C} + \mathrm{SiO_2} = \mathrm{Si} + 2\mathrm{CO} \qquad [4.9]$$

$$\mathrm{K} = \frac{a_{Si} \times P_{CO}^2}{a_C^2 \times a_{SiO_2}} = e^{-[\frac{\Delta G^{O}_{1} + \Delta G_{R \to H}}{RT}]}$$

Rearranging equation 4.9 gives:

$$P_{CO} = \sqrt{\frac{a_C^2 \times a_{SiO_2}}{a_{Si}} \times e^{-[\frac{\Delta G_1^O + \Delta G_{R\rightarrow H}}{RT}]}} \quad [4.10]$$

For chromium oxide reduction:

$$3C + Cr_2O_3 = 2Cr + 3CO(g) \quad [4.11]$$

$$K = \frac{\gamma_{Cr}^2 \times P_{CO}^3}{a_C^3 \times a_{Cr_2O_3}} = e^{-[\frac{\Delta G_1^O + \Delta G_{R\rightarrow H}}{RT}]}$$

Combining equations 4.9 – 4.11 gives:

$$P_{CO} = \sqrt[3]{\frac{\gamma_C^3 \times a_{Cr_2O_3}}{a_{Cr}^2} \times e^{-[\frac{\Delta G_1^O + \Delta G_{R\rightarrow H}}{RT}]}} \quad [4.12]$$

Carbon oxidation by gaseous oxygen:

$$2C + O_2 = 2CO \quad [4.13]$$

$$K = \frac{P_{CO}^2}{a_C^2 \times P_{O_2}} = e^{-[\frac{\Delta G_1^O + \Delta G_{R\rightarrow H}}{RT}]}$$

The partial pressure of CO gas is then given by:

$$P_{CO} = \sqrt{a_C^2 \times P_{O_2} \times e^{-[\frac{\Delta G_1^O + \Delta G_{R\rightarrow H}}{RT}]}} \quad [4.14]$$

From the values that will be obtained for the partial pressure of oxygen will determine the order of oxidation of Cr, Si and C in the metal bath. For the oxidation reactions (of Si, C and Cr) to be in mutual equilibrium with each other, the calculated values of the partial pressures of oxygen will have to be the same or close in comparison (Heikkinen et al, 2011). The calculated oxygen partial pressures were compared for higher and lower carbon contents as discussed by Heikkinen et al (2011) who stated that the partial pressure for oxygen increases as the carbon content in the metal bath decreases.

4.3 Rate equations in the converter decarburization process

As discussed in sections 2.5.8.1 and 2.5.8.2 of the literature review, oxidation of carbon by Cr_2O_3 at higher carbon contents is determined by the rate of oxygen being blown into the metal bath and by the liquid mass transfer of carbon to the bubble surface at lower carbon levels (Fruehan, 1976). As a result of this, there are two distinct regimes of carbon oxidation in the AOD for higher and lower carbon contents in the metal bath (Wei and Zhu, 2002).

4.3.1 Rate equations at high carbon contents

According to Wei and Zhu (2002), at high carbon contents in the metal bath, the average losses of the different components (Silicon, Carbon and Chromium in this case) can be modelled separately according to the rate equations below. For the purpose of this study, the terms high carbon and low carbon levels were taken as defined as C ≥ 2 wt. % and < 2 wt. %, respectively. In this case, the equations derived by Wei and Zhu (2002) were utilized to determine the rate of oxidation of C, Cr and Si at high carbon contents:

$$\frac{d[\%C]}{dt} = -\frac{2\eta Q_O}{22400} \times x_C \times \frac{100*M_C}{W_m} \quad [4.15]$$

$$\frac{d[\%Cr]}{dt} = -\frac{2\eta Q_O}{22400} \times x_{Cr} \times \frac{100*M_{Cr}}{1.5*W_m} \quad [4.16]$$

$$\frac{d[\%Si]}{dt} = -\frac{2\eta Q_O}{22400} \times x_{Si} \times \frac{100*M_{Si}}{2*W_m} \quad [4.17]$$

Where;

η is the utilization ratio.

Q_O is the flow rate of oxygen cm^3s^{-1}

M_i is molar mass of substance (i) expressed in $gmol^{-1}$

W_m is the mass of the liquid metal bath in grams.

X_i is the distribution ratio of oxygen within each component (i) in the liquid metal bath.

The distribution ratios of blown oxygen among the elements (X_i) are proportional to the Gibbs free energies of their oxidation reactions at the interface (Wei and Zhu, 2002). The equations proposed by Wei and Zhu (2002) were also applied to the data collected from the plant.

$$x_C = \frac{\Delta G_C}{\Delta G_C + {}^{\Delta G_{Cr}}/_3 + {}^{\Delta G_{Si}}/_2} \quad [4.18]$$

$$x_{Cr} = \frac{{}^{\Delta G_{Cr}}/_3}{\Delta G_C + {}^{\Delta G_{Cr}}/_3 + {}^{\Delta G_{Si}}/_2} \quad [4.19]$$

$$x_{Si} = \frac{{}^{\Delta G_{Si}}/_2}{\Delta G_C + {}^{\Delta G_{Cr}}/_3 + {}^{\Delta G_{Si}}/_2} \quad [4.20]$$

Where;

ΔG_i : is the Gibbs free energy for oxidation reactions of element (i) in Jg^{-1}.

x_i : is the distribution ratio of blown oxygen for element (i).

4.3.2 Rate equations for low carbon levels

The rate equation at low carbon content was derived from the work done by Wei and Zhu (2002) as shown in equations 4.21 – 4.24. For the purpose of this study, low carbon contents were defined as carbon ≤ 2 wt. % and this in accordance with the definition of low carbon content used in the process under study.

Wei and Zhu (2002) stated that in the refining process, oxidation of elements in the metal bath or reduction of oxides occur at the bubble surface and hence the area of the interfacial reaction (A_{rea}) is the approximate total area of the bubbles in the bath. The estimation of the area of interfacial reaction (A_{rea}) was defined as the approximate total surface area of the bubbles that is available for oxidation or reduction of elements during refining (Wei & Zhu, 2002). Using the expression proposed by Diaz et al (1997), the estimation for the total number of bubbles becomes:

$$n_b = 6QH_b/(\pi d_b^3 \mu_b) \quad [4.21]$$

Where:

n_b The total number of bubbles

Q Total gas flow rate cm^3s^{-1}

H_b Rising height of bubble

d_b Average diameter of bubble.

μ_b Velocity of bubble cms^{-1}.

The velocity of the bubbles in this case is then expressed as shown in equation 4.22 (Davies and Taylor, 1950; Wei and Zhu, 2002).

$$\mu_b = 1.02(\frac{gd_b}{2})^{1/2} \quad [4.22]$$

Based on the relationship shown in equation 4.21 and 4.22, the estimation of the area of reaction interface can be derived as (Wei and Zhu, 2002):

$$A_{rea} = 6QH_b/(d_b\mu_b) \quad [4.23]$$

The numerical value of H_b used in the present study was adopted from work by Wei and Zhu (2002), where it was calculated to be 95cm. At low carbon content, the liquid mass transfer of carbon in the bath becomes rate limiting (Wei and Zhu, 2002; Turkdogan and Fruehan, 1999; Fruehan, 1976). The mass transfer coefficient of carbon in the liquid bath (k_c) (Baird and Davidson, 1962) was calculated as shown;

$$k_C = 0.8 r_{eq}^{-1/4} D_C^{1/2} g^{1/4} \quad [4.24]$$

Turkdogan (1980) stated that at a sufficiently high gas stream velocity, the bubble sizes are generally uniform. From the work done from the water modelling work done by Wei at el (1999), D_c and d_b were adopted from the figures utilized by Wei and Zhu (2002) and being 7.46 cm^2/s and 2.5 cm, respectively as applied.

4.3.3 Equilibrium concentration of carbon

The typical reactions taking place during the refining process involves the oxidation of Cr and C, and being exothermic reactions, the temperature of the bath is consequently raised (Wei and Zhu). The equation below was then appropriately approved:

$$(Cr_2O_3) + 3[C] = 2[Cr] + 3\{CO\} \quad [4.25]$$

The equilibrium concentration of carbon at the interface was obtained by the formula shown below:

$$[\%C]_e = \frac{P_{CO}}{\gamma_C} \sqrt[3]{\frac{a_{[Cr]}^2}{a_{Cr_2O_3} \times K_{Cr-C}}} \quad [4.26]$$

The partial pressure used in the above equation was obtained from each of the 30 plant data samples collected at the second stage of the blowing process. The results were then tabulated so that they could be compared to the values obtained from plant measurements to determine if the model followed same trend as plant data.

4.4 Mass and energy balance for the AOD process

The input data for the model was tabulated as shown in appendices. The blowing time for each of the blowing intervals was also specified for each stage, and was manipulated to find optimum time per specific flow rate to achieve the desired carbon level.

The model took into account all the materials charged into the AOD, that is, burnt lime, burnt dolomite, FeSi and the molten alloy from the EAF. Each of the materials was analysed compositional consistency in order to calculate the input moles of the respective elements and oxides into the process.

The initial temperature of the bath was also measured, as this is critical in thermodynamic calculations of changes in the Gibbs free energy of reactions (ΔG). The thermodynamic calculations were conducted based on the thermodynamic data obtained from HSC version 7.0 (H-enthalpy, S-entropy, C-heat capacity) thermodynamic software.

The molar fractions and energy contributions to the process were calculated for the input materials. The elemental constituents of the alloy were analysed using the Spectromaxx Optical Emission Spectroscopy Analyser®, while the burnt lime and dolomite were analysed using the X Ray Fluorescence (XRF) analysis method. As the burnt lime, dolomite and FeSi were being fed into the AOD from the feed bunkers, initial temperature of 25^{o}C was assumed for the material.. The initial analysis and temperature in this model was selected randomly to form the basis for calculations.

The initial alloy content was added as one of the inputs. To determine decarburization extent, the initial carbon content had to be obtained. For the purposes of the model derivation, the analysis used for calculations was randomly chosen. The weight was also recorded to assist in determination of the contributions of each element and the temperature to calculate Gibbs free energies for each element in the metal bath.

Burnt lime and dolomite analysis was also taken into account. Though in this case, the CaO content for burnt lime was taken to be 100 wt. %, the model allows for adjustments according to analysis and specification of raw materials to be used. The initial temperature for these raw

materials was taken as 25^{o}C as the material charged into the AOD came from storage bunkers at room temperature.

The ratio of addition of lime: dolomite of 1.5 was used. Dolomite is added in the decarburization process to enhance the kinetics when the process goes to the reduction phase. The other advantage of dolomite addition is that the MgO in the slag reacts with silica (SiO_2), forming an intermediate phase of CaMg silicate and these phases are low melting thus making the slag quite fluid, and eliminating need for fluorspar enhancing mass transfer processes due to reduced viscosity, and consequently improve chromium recovery from slag (Nunnington, 2002). The model also catered for ferrosilicon addition for chromium recovery from slag.

On the inputs spreadsheet the input data was used to calculate the mass (in kg and kmols) of the individual elements and oxides. The detailed calculations are shown in the methodology chapter. Thermodynamic considerations were used to calculate predicted output and contribution of each element or oxide to the overall mass and energy balance.

The process outputs were also calculated using the same formulae as for process inputs (as described in the methodology). In this case a carbon composition in the final product of 1.0 wt. % was targeted and fixed. The model however utilizes excel solver to iterate to a predicted metal and slag composition based on the calculations already described.

The slag quantity generated from the decarburization, was also calculated using the quadratic formalism. The CO produced was a function of the C oxidized from the liquid bath as shown in the calculations. Once completion of model was achieved, comparison with results obtained from Wei and Zhu's rate equations could be compared to the plant data collected. The values of activity coefficients and activities obtained from the mass and energy balance model were also obtained and tabulated (appendix 10, 11 12 and 13).

4.4.1 Mass and energy balance construction procedure

The energy and mass balance model was constructed for the current AOD process. The table 4.1 shows the input data that was used. The (model was based on the first law of thermodynamics) principle of energy in = energy out (also implying to mass), is the basic law of conservation of energy that was applied to the model. Use of thermodynamic principles and work done by researchers such as Heikkinen et al (2011), Fruehan (1976), Ban-Ya (1992) amongst others, was applied into derivation of thermodynamic behaviour of the process under study. Assumptions to

certain process parameters such as initial temperature and weight of molten alloy were done to allow for calculations to be carried out. The model however allowed for change of these parameters to calculate any different scenario presented. Table 4.1 shows analysis of the initial raw materials used.

Table 4.1: Analyses of Material inputs into the AOD

Lime			**Dolomite**			**FeSi**			**Metal**		
Lime / Dolomite	-	1.5									
Al2O3	Mass%	0	**Al_2O_3**	Mass%	0.00	**Al**	Mass%	0.00	Mass of Tap/t		7
CaO	Mass%	80	**CaO**	Mass%	20.00	**C**	Mass%	0.00	Analysis	%C	3
Cr2O3	Mass%	0	**Cr_2O_3**	Mass%	0.00	**Cr**	Mass%	0.00		%Cr	67
MgO	Mass%	2	**MgO**	Mass%	30.00	**Fe**	Mass%	66.27		%Si	0.30
FeO	Mass%	0	**FeO**	Mass%	0.00	**Si**	Mass%	33.73		%Fe	29.70
SiO2	Mass%	0	**SiO_2**	Mass%	0.00						
LOI (CO2)	Mass%	0	**LOI (CO_2)**	Mass%	50.00						

For the initial calculation, a single tap was taken and the inputs analysed as shown above. From this data, the kmols and overall energy were calculated as shown below;

4.4.1. Calculating the initial mass (moles) and energy of the metal bath in the converter

The initial mass, (in moles) and the energy of the metal bath were calculated based on equation 4.27:

$$Molar\ mass = Mass\ (initial\ liquid\ metal) \times \%Mass\ fraction\ of\ element\ in\ metal \quad [4.27]$$

In order to get the moles of each element (in kilo-moles), the relationship between the mass of each element and its molar mass was considered as shown:

$$Kmols_X = Mass\ of\ element\ i / Mr_i \quad [4.28]$$

All calculations were taken at 1600 ^oC and ΔH also taken at the same temperature. The energy for each element was then calculated as shown below:

$$E = kmols_i \times \Delta H_i(at\ 1600^oC) \quad [4.29]$$

The same calculation was done for the main elements in the molten metal, and tabulated as shown in table 4.2:

Table 4.2: Moles and Energy for metal @1600 °C

	%Mass	Mass/kg	kmol	%mole	MJ
C	3.0%	210	17.48	12%	565.72
Cr	67.0%	4690	90.20	62%	4911.85
Si	0.3%	21	0.75	1%	68.27
Fe	29.7%	2079	37.23	26%	2805.67
Total	100%	7000	145.66	100%	8351.51

4.4.2. Calculating the mass (kmols) and energy balance for lime and dolomite

The burnt lime and dolomite added into the converter, just after charging of the molten alloy, is for slag formation in the vessel. The targeted slag basicity is approximately 1.8 ((Cao + MgO)/SiO_2) and the chemistry is 40 wt. % CaO, 15 wt. % MgO and 30 wt. % SiO_2 as discussed in literature.

On calculating the kilomols and Energy for burnt lime and dolomite as added into the converter for slag formation, the calculations shown below were done;

$$Mass_{CaO} = \%Mass_{CaO} \times Total\ mass\ (lime) \quad [4.30]$$

But total lime is obtained as shown in equation 4.31 as shown:

$$Total\ lime = total\ dolomite \times \%Mass_{CaO}\ (in\ lime) \quad [4.31]$$

The total dolomite (requirement) was calculated as shown in equation:

$$Total\ dolomite = \frac{total\ MgO\ mass\ (in\ slag)}{\%Mass\ MgO\ (in\ dolomite)} \quad [4.32]$$

In order to calculate the total mass of MgO in slag, the activity of MgO in the slag had to be determined and then the total MgO in slag then determined by the expression shown in equation 4.33;

$$total\ MgO\ (in\ slag) = a_{MgO} \times total\ slag\ mass \quad [4.33]$$

The total slag mass was obtained as shown in equation 3.34. (XRAM Technologies, 2016):

$$\text{Mass}_{\text{Slag}} = \frac{\text{Mols(FeSi+Alloy)}_{\text{Cr}} - \frac{\%\text{Mass(Cr)}}{\%\text{Mass(Si)}} * \frac{\text{Mr(Si)}}{\text{Mr(Cr)}} \times \text{Mols(Alloy+FeSi)}_{\text{Si}}}{\left(\frac{2 \times \frac{a_{Cr_2O_3}}{Mr_{Cr_2O_3}} - Mr_{Si} \times a_{SiO_2} \times a_{Cr}}{Mr_{SiO_2} \times a_{Si} \times Mr_{Cr}}\right)} \quad [4.34]$$

$a_{Cr_2O_3}$ – Activity coefficient for Cr_2O_3

a_{SiO_2} – Activity coefficient for SiO_2

Mr_i – Molecular Weights for element i

a_{Si} – Activity for Si

a_{Cr} – Activity for Cr

The energy and mols for CaO also calculated with the same formulae as was done for the metal elements. The calculation for the activity coefficients was also done and will be shown later. Energy calculations were done using ΔH at 25^{o}C.

The same calculations, as done for lime, were implemented were implemented for dolomite. As shown on the burnt lime calculations, the mass of slag is calculated same way. Energy calculations were also done using ΔH at 25^{o}C.

$$Mass_{CaO} = \%Mass_{CaO} \times Total\ mass_{dolomite} \quad [4.35]$$

From equation 4.35, total Dolomite mass was calculated as;

$$Total\ mass_{dolomite} = \frac{Mass\ of\ MgO\ in\ slag}{\%\ Mass_{MgO}\ in\ dolomite} \quad [4.36]$$

From the equation 4.36 above, mass % of MgO in dolomite was calculated as shown in equation 4.37.

$$\%Mass_{MgO} = a_{MgO} \times Mass_{Slag} \quad [4.37]$$

4.4.3 Kmols and energy calculations for FeSi in the reduction stage

Calculations for moles, mass and energy were done for Cr, Fe and Si using the same calculations and equations as for the alloy. The difference is in the energy calculations as value of ΔH used was at 25^{o}C.

$$Molar\ mass = Mass\ (initial\ liquid\ metal) \times \%Mass\ fraction\ of\ element\ in\ FeSi \quad [4.38]$$

To obtain the moles of each element, the relationship between the mass of each element and its molar mass was considered as shown in equation 4.39:

$$Kmols_X = Mass\ of\ element\ i/Mr_i \quad [4.39]$$

All calculations were taken at 25 ^{o}C (ambient temperature at which FeSi was charged into the converter) and ΔH also taken at the same temperature. The energy for each element was then calculated as illustrated in equation 4.40:

$$E = kmols_i \times \Delta H_i(at\ 25^oC) \quad [4.40]$$

Calculations done for the FeSi were tabulated in table 4.3:

Table 4.3: Moles and Energy calculations for FeSi

FeSi					
	%Mass	**Mass/kg**	**kmol**	**%mole**	**MJ**
Fe	34%	84.34	3.00	50.31	0.00
Si	66%	165.66	2.97	49.69	0.00
	100%	250.00	5.97	100.00	0.00

4.4.4 Mass and energy balance calculations for AOD gases

For the process under study, argon was only used in the reduction phase of the process. In the model however, provision was made for Argon in case there would be change in process and Argon used in place of nitrogen. The gas flow ratios of oxygen and an inert gas for this model give allowance for either nitrogen or argon to be used in conjunction with blown oxygen. The gases used in the model are all pure gases, as are the gases used in the process under study.

4.4.4.1 Oxygen

The mass % of oxygen was taken as 100% because it was pure Oxygen. Therefore, the total mass of oxygen can then be calculated as shown in equation 4.41:

$$\text{Total Mass } O_2 = \frac{X-Y}{2\times Mr_{O_2}} \quad [4.41]$$

Where,

X is mols of oxygen in the oxides in slag and oxygen in the gas produced as a result of the oxidation reactions (namely CO) and is calculated as:

$$X = 3 \times (Mol_{Al_2O_3} + Mol_{Cr_2O_3})_{slag} + 2 \times ((Mols(slag) + Mols(gas))_{SiO_2}) + ((Mols_{CaO} + Mols_{FeO} + Mols_{MgO})_{slag} + Mols_{CO}(gas)) \quad [4.42]$$

And Y is the molar contribution of the oxygen from the slag formers (lime and dolomite) and is calculated as:

$$Y = 3 \times ((Mols_{Lime} + Mols_{Dolomite})_{Al_2O_3} + (Mols_{lime} + Mols_{dolomite})_{Cr_2O_3}) + 2 \times (Mols_{SiO_2} + (Mols_{SiO_2} + Mols_{CO})_{Dolomite}) + ((Mol_{CaO} + Mol_{FeO} + Mol_{MgO})_{lime} + (Mol_{CaO} + Mol_{FeO} + Mol_{MgO})_{Dolomite} \quad [4.43]$$

In summary, the oxygen mass supplied through blowing into the metal bath could be obtained by subtracting the total oxygen in the slag (in the form of oxides) and the oxygen supplied within the oxides in the inputs (lime and dolomite etc.). This model however assumes that all oxygen utilized in oxidation reactions and no free oxygen escapes from the bath unreacted. The model does not also take into account post combustion reactions. All reactions are assumed to occur and finish in the decarburization interval.

4.4.4.2 Argon

In the case where argon is blown in conjunction with oxygen, typical oxygen:argon gas ratios are basically 3:1 at higher carbon contents and 1:1 at lower carbon contents for oxygen and argon respectively, during the decarburization process. The argon used in the model is pure argon.

%Mass = 100 wt. %

%Mol = 100 wt. %

However equation 4.41 was used in case when crude argon would be used in the process.

$$Mass\ of\ Argon = \%Mass \times Total\ Mass\ of\ Argon \quad [4.44]$$

But

$$\text{Total mass (Ar)} = \frac{\text{Flow rate(Ar)}}{\text{flow rate } (O_2)} \times \text{ total Mol } (O_2) \times \text{ Mr(Ar)} \quad [4.45]$$

The total flow rate of Argon was then obtained as shown in equation 4.43;

$$\text{Total Flow rate (Ar)} = \frac{\text{flow rate}(O_2)}{O_2/_{Ar}\text{Ratio}} = \sum_{n=1}^{y} \frac{\text{flow rate } (O_2)}{O_2/_{Ar}\text{ratio}} \quad [4.46]$$

Where n = 1-y blowing stages

For these particular calculations, Argon was not blown during the decarburization stages.

Table 4.4: Moles and Energy calculations for Argon at 25 °C

Argon				
%Mass	**Mass/kg**	**Kmol**	**%mole**	**MJ**
100	0	0	100	0

4.4.4.3 Nitrogen

Nitrogen is the inert gas used in the process under study in the AOD converter. The other reason for the choice of nitrogen over argon is the fact that nitrogen is significantly cheaper than argon to purchase. The total nitrogen requirement is calculated as:

$$\text{Mass } N_2 = \%\text{Mass} \times \text{total } N_2\text{mass} \quad [4.47]$$

But the total N_2 mass is calculated by taking into account the gas flow ratios of nitrogen and oxygen and the molar masses of nitrogen and oxygen as shown in equation 4.48:

$$\text{Total } N_2 \text{mass} = \frac{N_2 \text{flow rate}}{O_2 \text{flow rate}} \times \text{total Mols}(O_2) \times \text{Mr}(N_2) \quad [4.48]$$

But the total flow rate is expressed as shown in equation 4.49.

$$\text{Total Flow rate } N_2 = \frac{\text{total flow for all stages } (O_2)}{\text{total } {}^{O_2}/_{N_2}} \quad [4.49]$$

$$\text{Total Flow rate } N_2 = \sum_{n=1}^{y} \frac{\text{flow } (O_2)_n}{{}^{O_2}/_{N_2} \text{ratio}_n} \quad n=1\text{-}y$$

Y is defined as the number of blowing stages in the decarburization process with differing gas flow ratios.

4.5 Thermodynamics and Equilibrium considerations in AOD refining process

Equations 2.9 – 2.15 as described in the literature show competing reactions occurring in the converter. The general equation for the oxidation of carbon is shown in equation 4.50.
Taking the following equations 2.9 – 2.11 from literature and applying a general metal reduction equation, equation 4.50 becomes:

$$pM_xO_y + zC = rCO + sM \quad [4.50]$$

At equilibrium, equation 4.50 can be expressed in terms of the equilibrium constant (K) as illustrated in equation 4.51.

$$K = \frac{a_M^s \times P_{CO}^r}{a_{M_xO_y}^p \times a_C^z} \quad [4.51]$$

Taking into account the Gibbs free energy, equation 4.51 can be further expressed as shown in equation 4.52 below:

$$K = \frac{a_M^s \times P_{CO}^r}{a_{M_xO_y}^p \times a_C^z} = e^{-\frac{\Delta G + \Delta G_{R \to H}}{RT}} \quad [4.52]$$

Where ΔG is the free energy of reaction

$\Delta G_{R\rightarrow H}$ free energy for change between Raoultian and Henrian

T is the temperature measured as K

R is the universal gas constant and has value of 8.314 J/mol

P_i partial pressure of the component

α_i is the activity of the components

But $\alpha_i = \gamma_i X_i$

$P_i = X_i P$

With the preferred use of nitrogen as the inert gas for the process under study, it is paramount to investigate nitrogen solubility in the metal bath during the decarburization process. Fruehan (1992) stated that nitrogen dissolution has significantly higher in ferrochromium alloys than any other steel. He further stated that an increase in chromium content increases nitrogen dissolution, whilst an increase in sulphur decreased nitrogen dissolution. From the investigation Fruehan (1992) carried out, he concluded that for the dissolution of nitrogen followed equation 4.53 below:

$$\frac{1}{2}N_{2_g} = N \qquad [4.53]$$

$$K = \frac{P_N}{P_{N_2}^{\frac{1}{2}}} = e^{-\frac{\Delta G + \Delta G_{R\rightarrow H}}{RT}}$$

4.6 Interaction coefficients in metal and slag in the refining process.

Wada and Saito (1951) described interaction parameters relating to energy of mixing, hence dependent on interaction energies between solute and solvent atoms or between the solute atoms themselves. The authors further stated that the interaction parameters also related to the energy of mixing. Interaction coefficients were calculated for both metal and slag phases. In determining and estimating activity coefficients in this model, certain assumptions were made based on the limits highlighted in the points below:

- The average temperature of the bath during the initial/starting stages of the refining process was taken to be 1600^{o}C. As a result, the interaction coefficients were calculated at 1600^{o}C. The assumption was that the variation of the interaction coefficient values was not significant with the temperature variation in this study.

- The interaction coefficients proposed by Sigworth and Elliot (1974) are for dilute solutions in liquid iron as solvent, and their applications to Fe-Cr-C melts is based on low Cr contents.
- With the Nitrogen solubility model, Kim et al (2009) developed it for FeCr with Cr 15-60% and partial pressure of N_2 between 0.04-0.97 atm. It should be noted that the Cr content in the Fe-Cr-C melts considered in the process under study was higher than the 15-60 wt. % highlighted, and could be as high as 73 wt. % in the metal.

4.5.1 Activity coefficient calculations in metal phase

As discussed in literature, the refining process of a Fe-Cr-C system and the co-existence of solute atoms in a liquid bath were investigated. An increase in chromium content will result in a decrease in carbon activity (Ohtani, 1956). The activity coefficients for the metal phase constituents were calculated according to studies by Pelton and Bale (1986), who derived the following expression to determine the individual activity coefficients:

$$\ln\gamma_{solvent} = -\frac{1}{2}\sum_{j=1}^{N}\sum_{k=1}^{N}\varepsilon_{jk}X_jX_k \qquad [4.54]$$

$$\ln\gamma_i = \ln\gamma_{Solvent} + \sum_{j=1}^{N}\varepsilon_{ij}X_j \qquad [4.55]$$

From the expressions shown in equations 4.54 and 4.55:
X – Molar fraction of the component i or j
ε_{ij} Is the interaction parameter for components i and j, and was obtained by the expression shown in equation 4.56 (Sigworth and Elliot, 1974):

$$\varepsilon_{ij} = 230 \times \frac{MW_i}{MW_1} \times \sigma_i^j + \frac{MW_1 - MW_j}{MW_1} \qquad [4.56]$$

MW_i is the molar weight of a component, i
MW_1 is the molar weight of the solvent
σ is the 1st order interaction parameter.

From equations 4.54 – 4.56, the activity coefficients for the different elements in the alloy bath were calculated and tabulated as shown in table 4.5:

Table 4.5: Activity Coefficients for each element i in the ferrochromium alloy.

	Mass %	Mole%	Activity Coeff.	Activity
Al	0.00%	0.00%	1.44	0.00
C	1.00%	3.93%	0.08	0.00
Cr	65.54%	59.43%	0.91	0.54
Fe	29.93%	25.27%	1.12	0.28
N(g)	3.23%	10.87%	0.02	0.00
Si	0.30%	0.50%	1.75	0.01

Table 4.6: First Order Interaction Coefficients for liquid iron (Sigworth and Elliot, 1974)

First order interaction coefficients in liquid iron					
Item	**Al**	**C**	**Cr**	**N**	**Si**
Al	0.0450	0.0910	-	- 0.058	0.0056
C	0.0043	0.1400	- 0.024	0.1100	0.0800
Cr	-	- 0.1200	- 0.0003	- 0.1900	- 0.0043
N	- 0.028	0.1300	- 0.047	-	0.0470
Si	0.0580	0.1800	-0.0003	0.0900	0.1100

According to Kim et al (2009), the nitrogen solubility in the metal bath can be expressed as shown in equation 4.57, and that was the model used to predict nitrogen solubility in the investigation;

$$\log\gamma = \left(-\frac{148}{T} + 0.033\right) \times X_{Cr} + \left(\frac{1.56}{T} - 0.00053\right) \times X_{Cr}^2 \qquad [4.57]$$

X_{Cr} is the %mass of Cr.

T is the operating temp i.

The %mass of Cr was taken from the final product.

4.5.2 Activity coefficient calculations in the Slag Phase

From the work done by Ban-Ya (1992), it was concluded that by taking a component (i) in a multi component slag, the activity coefficient of this component can be expressed in terms of the quadratic formalism. The author went on to state that even for liquid silicate melts that are not strictly regular solutions, the same quadratic formalism could be used as if these solutions were

regular solutions. For slag phase components, the model by Ban-Ya (1993) was used. The model is illustrated in equation 4.58 as shown below:

$$RT\ln\gamma_i = \sum_{j=i+1}^{N} a_{ij}X_j^2 + \sum_{j=i+1}^{N}\sum_{k=j+1}^{N}(a_{ij} + a_{ik} - a_{jk})X_jX_k \quad [4.58]$$

Where α is activity of an oxide j,i,k

R – Universal gas constant 8.314J/mol

T Temp measured in degrees Kelvin

ΔG – Gibbs free energy of reaction –J/mol

$\Delta G_{R->H}$ – Gibbs free energy for change between Raoultian and Henrian standard states

The calculations for mole fractions for the oxides in the slag were calculated, in order to determine the activity coefficients above. Equation 4.59 illustrates the molar fraction calculation for CaO:

$$\%Mass_{CaO} = \%Moles_{CaO}\frac{Mr_{CaO}}{\sum_{i=1}^{n}(Mr\times Moles)_i} \quad [4.59]$$

But the molar percentage of CaO in the slag is expressed as:

$$\%Moles_{CaO} = \%Moles_{SiO_2} \times \text{Molar Basicity}\frac{CaO}{SiO_2} \quad [4.60]$$

Where the molar basicity of slag is expressed as a ratio of CaO and SiO2 as shown in equation 4.61 below:

$$\text{Molar Basicity}\frac{CaO}{SiO_2} = \text{Required Basicity} \times \frac{A+B*C}{D+A+B\times(C+E)} \quad [4.61]$$

$$A = \frac{(\%Mass/_{Mr})_{CaO}}{\sum_{i=1}^{n}(\%Mass)_i}\text{for dolomite}$$

$$B = \frac{(\frac{Lime}{Dolo}ratio\times\sum_{i=1}^{n}\left(\frac{\%Mass}{Mr}\right)_i + \frac{Lime}{Dolo}ratio\times\left(1-\frac{(Total\ \%Mass)_{Lime}}{Mr_{CO_2}}\right))}{\sum_{t=1}^{n}(\frac{\%Mass}{Mr})_t + (1-\frac{\sum_{a=1}^{n}(\%mass)_a}{Mr_{CO_2}})}$$

$$C = \frac{\frac{lime}{dolo}ratio\times\%Mass_{CaO}}{\frac{Lime}{Dolo}ratio\times\sum_{p=1}^{n}(\frac{\%Mass}{Mr})_p}\text{in lime}$$

$$D = \frac{(\frac{\%Mass}{Mr})_{MgO}}{\sum_{z=1}^{n}(\frac{\%Mass}{Mr})_z}\text{in dolomite}$$

$$E = \frac{\frac{\text{Lime}}{\text{Dolo}}\text{ratio} \times (\frac{\%\text{Mass}}{\text{Mr}})_{\text{MgO}}}{\frac{\text{lime}}{\text{Dolo}}\text{ratio}\sum_{b=1}^{n}(\frac{\%\text{Mass}}{\text{Mr}})_{b}} \text{ in lime}$$

The same equations can be used for $\%\text{Moles}_{\text{MgO}}$ except for C which then becomes as shown in equation 4.62:

$$C = \frac{\text{lime}}{\text{dolo}}\text{ratio}\frac{\%\text{Mass}_{\text{MgO}}}{\text{Mr}_{\text{MgO}}}\text{ in dolomite} \qquad [4.62]$$

The table below shows values obtained from the calculations;

Table 4.7: Interaction coefficients for slag phase.

	Mass %	Mole%	Activity Coeff.	Activity
Al2O3	0.00	0.00	0.01	0.00
CaO	0.51	0.48	0.34	
Cr2O3	0.01	0.00	8.78	0.04
FeO	0.14	0.11	1.43	0.16
MgO	0.08	0.12	0.13	
SiO2	0.30	0.28	0.16	0.03

Summary

In this chapter, thermodynamic concepts such as interaction coefficients were determined for the creation of the mass and energy balance model for the decarburization process. Interaction parameters are a measure of the interaction of an element or a compound with neighbouring atoms or compounds. Determination of activities and activity coefficients for individual components in the alloy bath and for each of the components in the multi-component slag melt was done in order to construct the mass and energy balance model's mass balance. Rate equations were also modelled mainly based on work by Wei and Zhu (2002), amongst other researchers. Once the models were constructed, they were then used as analysis tools for plant data and predictive purposes. From the rate equations, it became possible to predict final carbon content for the two different blowing stages under study, namely high and lower carbon blowing conditions. Tabulated figures for parameters used in the calculations and results obtained in the mass and energy balance model for input and output summaries are found in appendices 2 – 16.

CHAPTER 5

5. RESULTS AND DISCUSSION

5.1 Introduction

The previous chapter 3 and 4 on methodology were based on process description and model constructions based on thermodynamic derivations and rate equations. In this chapter, the process plant data was applied to the research done to investigate the effect of individual process parameters on the process under study. Different relationships and effect on overall process performances were investigated as well to understand how these relationships also impacted on the decarburization process.

5.2 Carbon removal trend with decarburization for plant data

Plant data for 9 heats were randomly taken and the carbon measured based on the initial carbon content against the carbon content during the course of the oxygen blowing stage and at the end of the blow. The intervals of sampling were largely determined by the AOD operator, as well as the conditions experienced during the decarburization process.

In this context, the initial carbon content refers to the carbon in the alloy bath after tapping from the EAF and charged into the AOD for the decarburization process. The results showing the change in the carbon content as a function of time were then plotted in order to ascertain the changes in carbon content with time.. Generally the change in the carbon content of the bath followed a polynomial curve as shown in in Figure 5.1:

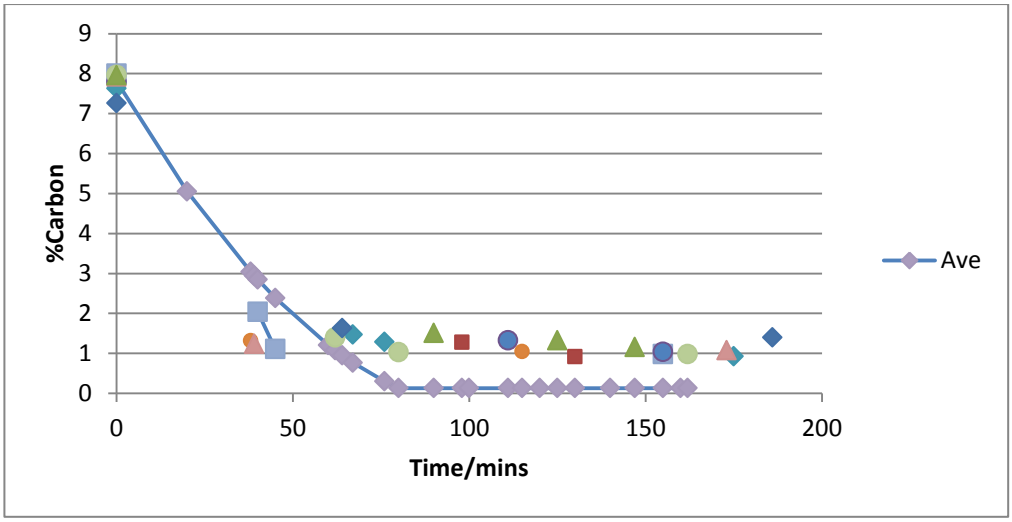


Figure 5.1: Change in carbon content of the bath as a function of blowing time for 9 random heats

As shown in Figure 5.1, the rate of decarburization was quite significant, as characterized by a steep decrease in carbon content from the initial 7.81 wt. % to 3.04 wt. % from the onset of blowing up to around 50 mins into the blow for the average trend. This is characterized by the steep decrease in carbon content observed on the graph above. According to Wei and Zhu (2002), the mass transfer of carbon to the reaction interface is not rate limiting at high carbon contents, and as a result, the overall rate of decarburization tends to be limited by the rate of oxygen blowing into the bath and/or the rate of mass transfer of oxygen to the reaction interface. In this regard, the observed carbon removal efficiency (CRE) also tends to high during the initial stages of the blow (Wei and Zhu, 2002; Turkdogan and Fruehan, 1999).

The observed in the carbon content tends to level off after 50 mins into the blow. In other words, rate of change in the carbon content drops significantly as the carbon levels approaches critical carbon content, after which the mass transfer of carbon to the reaction sites becomes rate limiting (Wei and Zhu, 2002; Turkdogan and Fruehan, 1999) At this stage, the rate of decarburization becomes significantly slower, and the observed trend on the graphs continue to level off towards the end of the blowing process. After the attainment of critical carbon content, the oxidation of chromium start to become significant, and as a result, chromium losses to slag are experienced (Wei and Zhu, 2002). Based on the AOD converting process of stainless steel, Visuri et al. (2013) estimated that the chromium oxide (Cr_2O_3) content of slags usually increases to about 30 to 40 wt. % at the end of the decarburization stage.

From the plant data, graphs showing the change in carbon content (ΔC), i.e. the difference between the initial and final carbon contents as a function of blowing time for both 1st and 2nd stage blows were constructed to evaluate if there was any relationship between the blowing time and the amount of carbon removal from the bath. The rate of change of carbon content (%ΔC) was further plotted as a function of time, and the results are shown in Figure 5.2.

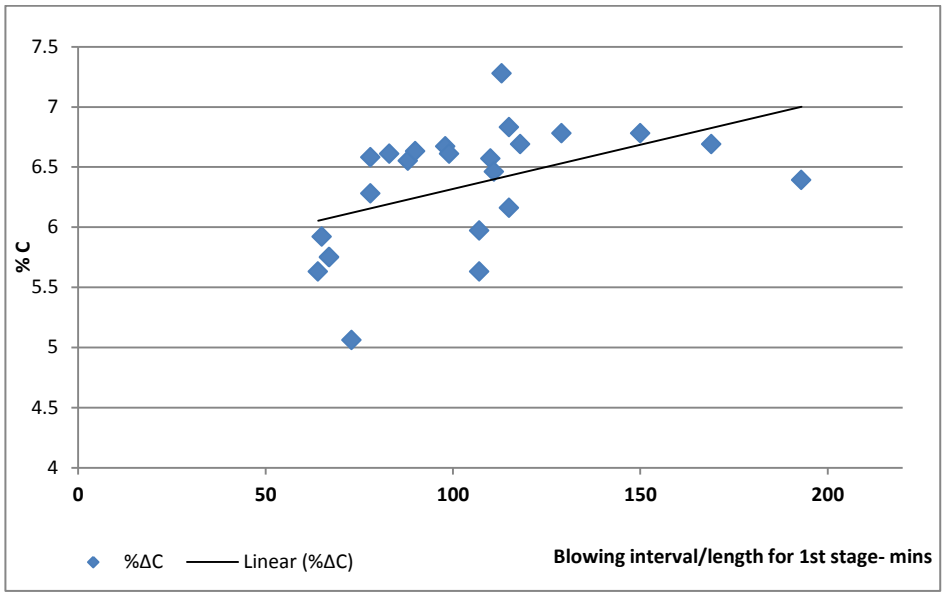


Figure 5.2: Drop in carbon content with blowing interval

It was observed for the longer time intervals resulted in a bigger drop in carbon composition during the first stage of the blow. This meant that the longer blowing cycles, the lower the residual carbon content of the bath due to more time available for mass transfer of carbon thus more carbon exposed for oxidation (Wei and Zhu, 2002; Fruehan, 1976).

The second blow stage showed an inverse trend. The longer the blow was, the lower the change in carbon in the bath. This is illustrated in the graph shown in Figure 5.3. The graph shows a plot of the second blow duration for each heat and the change in carbon (%ΔC) observed from the plant data.

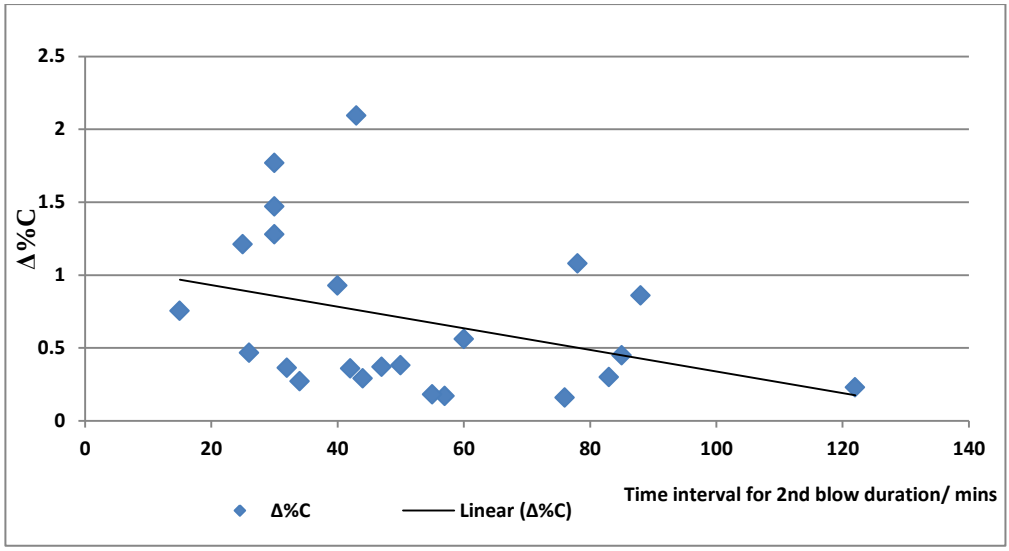


Figure 5.3: Change in carbon content (%ΔC) with blowing time

At lower carbon contents, decarburization becomes more difficult, particularly as the carbon content in the bath approaches the critical carbon range, and the loss of chromium due to oxidation becomes significant (Wei and Zhu, 2002; Turkdogan and Fruehan, 1999; Visuri et al., 2013). Furthermore, the chromium affinity for carbon also makes it difficult to decarburize at low carbon contents. As discussed in literature, chromium has affinity for carbon and mainly exists as chromium carbides in the high carbon ferrochromium alloy (Gasik, 2013; Ohtani, 1956; Venugopalan, 2005).

As a result, the affinity of chromium for carbon was investigated to evaluate if it had any impact on the decarburization process. The ratio of chromium to carbon (%Cr/%C) was plotted with the rate of decarburization for the first stage of the blow at higher carbon content, and for the second stage blow at lower carbon content in the metal bath. It was observed that for both the first and second stages of the decarburization process, the ratio of %Cr/%C generally increased as the rate of decarburization decreased, implying that it became more difficult to remove the carbon as the chromium content increased and as the carbon content decreased (as shown in figures 5.4 and 5.5).

The Cr/C ratio is lower for the first decarburization stage than for the second stage due to the higher carbon composition in the first stage of decarburization. From the figures 5.4 and 5.5, the higher the %Cr/%C the lower the %ΔC hence the lower the carbon content removed from the alloy melts. As the carbon content in the alloy decreases, the %Cr/%C ratio increases, as

illustrated by the difference in %Cr/%C values between figures 5.4 and 5.5. The second stage blow (as represented by figure 5.5) is usually characterized with the region of critical carbon where carbon removal becomes more difficult and hence an increase in the chromium losses. This can also be attributed to the chromium affinity to carbon and as the carbon depletes in the bath, the chromium affinity for oxygen becomes significant (Gasik, 2013; Wei and Zhu, 2002). The figure 5.4 below shows the relationship between Cr/C ratio and %ΔC and the trend shows that a decrease in the Cr/C ratio results in a higher carbon removal.

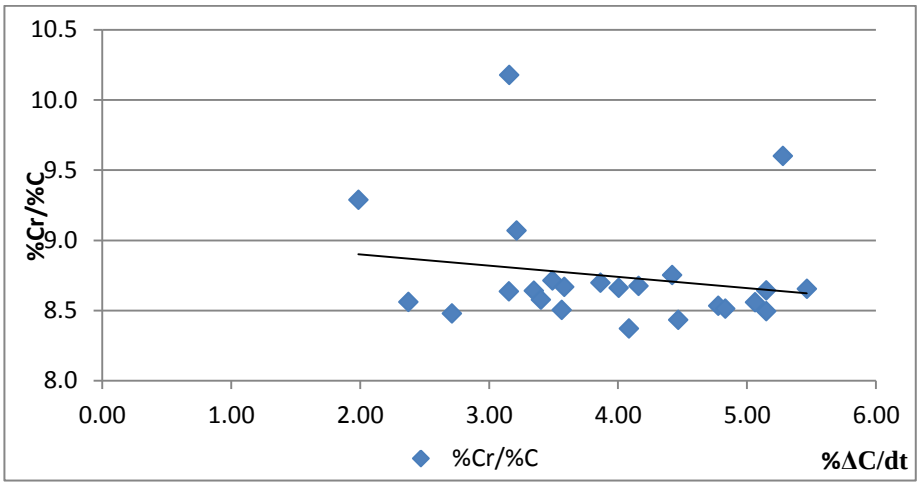


Figure 5.4: Relationship between the %Cr/%C ratio and rate of decarburization during the first stage of blow

Figure 5.5 at lower carbon contents as is characteristic of the second blowing stage, also shows the same trend as figure 5.4.

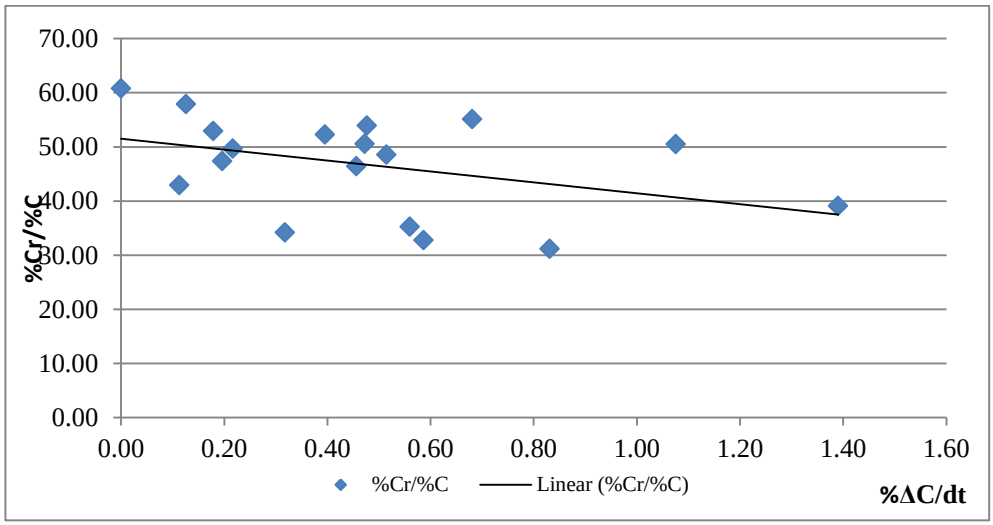


Figure 5.5: Relationship between Cr/C ratio and rate of decarburization during the second stage of the blow

5.3 Mass balance for AOD refining stage

In summary, the mass and energy balance was constructed as an analysis and predictive tool to analyse medium carbon ferrochromium production in the AOD. Thermodynamic principles were used as basis to predict behaviour of elements and oxides in the AOD bath. This included determination of Gibbs free energy of the elements at different temperatures and calculation of activities and activity coefficients. The rate equations as discussed in chapter 4, were also used to determine decarburization rates in the first and second stages of blowing corresponding to higher and lower carbon contents respectively. The performance of both models (mass and energy balance and rate equation models) was then compared against the achieved process plant data to measure the effectiveness of each model as a predictive tool.

Table 5.1 shows a summary of the principles used in the calculation of the energy and mass balance model for the AOD process under study. Quadratic formalism by Ban-Ya et al (1993) was used in conjunction with slag analysis obtained from samples taken during the blows, and the data was used to calculate the activities of the oxides in the slag. The models proposed by Pelton and Bale (1966) on unified quadratic formalism, and by Sigworth and Elliot (1974) on the thermodynamics of liquid dilute iron alloys, were used to calculate the activity coefficients the individual elements in the alloy.

Table 5.1: Summary of models used in the calculations of mass balance in the AOD

Temp				Temperatures were measured with a dip thermocouple during decarburization
Activities of SiO_2 & Cr_2O_3	a_{SiO_2}		$a_{Cr_2O_3}$	Quadratic formalism (Ban-Ya et al) with measured slag analysis from the process
Activity coefficients of Cr, Si & C	γ_{Si}	γ_C	γ_{Cr}	(Pelton & Bale (1966) & Henrian standard states for different metal analyses obtained from samples taken throughout the process
X_i	X_{Si}	X_C	X_{Cr}	Masses and metal sample analyses taken during the blowing down of carbon
ΔG_i^o	ΔG_{Si}^o	ΔG_C^o	ΔG_{Cr}^o	Calculated from HSC simulation software
				Signifies change from standard to Raoultian conditions. Obtained from the equation $RTln\gamma_i$
P_{CO}				Signifies the calculated estimate of ferro-static pressure in the AOD

5.3.1 Decarburization process at high carbon content during the first stage of the blow

On completion of the two models, it became possible to compare their performance according to the plant data obtained. The models' applicability was ascertained by keeping conditions the same and comparing output to the plant data.

5.3.1.1 Carbon removal comparison between models and plant data

The results from the models done, one using the Wei and Zhu (2002) rate equations at higher carbon and the other model formulated from heat and energy balance, were tabulated and shown in Figure 5.6.

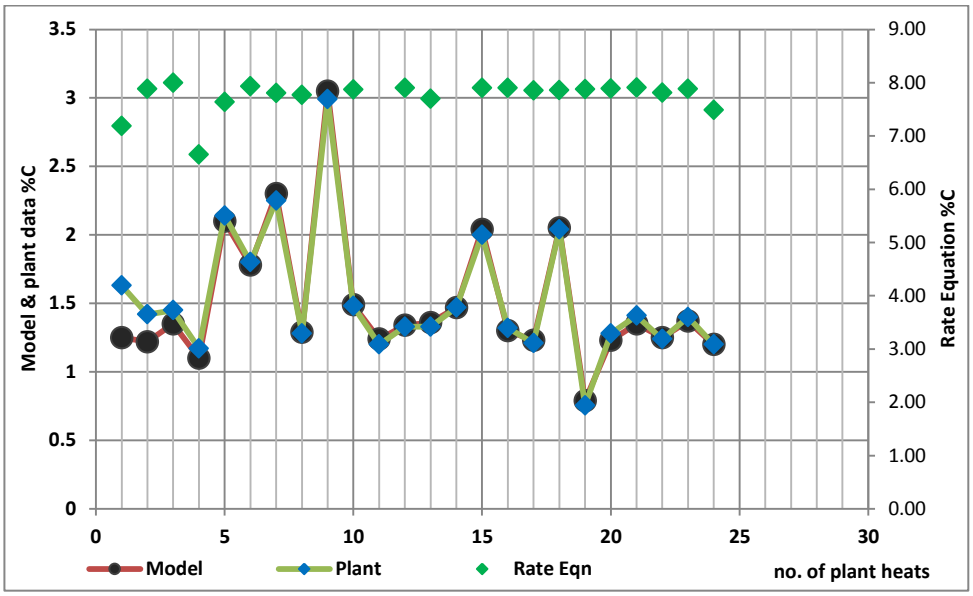


Figure 5.6: Comparison of model results vs. plant data for the first stage of the blow

The model constructed was used to predict the conditions of flow that would lead to the attainment of the same carbon level obtained in the plant under the same time intervals. By taking the time interval taken for each stage of the blowing process, initial temperature and metal analyses the same as in the process plant data collected, the gas flow rates (for oxygen and nitrogen) were varied until their values produced same carbon level output as observed in the plant data. It was also observed that the shorter the time interval, the higher the gas flow rates that are required to oxidize the carbon content down to the desired final composition.

A ratio of 2:1 for oxygen and nitrogen, respectively, was used for the first blowing stage. The basis of this assumption was based on work by Fruehan (1976) and Wei and Zhu (2002).

According to these researchers, the mass transfer of mass transfer to reactions sites is not rate determining at higher carbon levels, and hence the rate of decarburization is limited by the supply of oxygen to the reaction sites. As such, the rate of oxygen flow through the bath becomes rate determining (Fruehan, 1976; Wei and Zhu, 2002)). It was also noted that the rate equations proposed by Wei and Zhu (2002) at higher carbon content did not show any noticeable predicted change in the carbon composition at the same gas volumetric flows and time intervals.

In general, higher gas flow rates are required to take carbon to lower values, due to oxygen flow rate into the bath being rate limiting when carbon content is still high in the bath (Fruehan, 1976; Turkdogan and Fruehan, 1999; Wei and Zhu, 2002). The observed trend can be attributed to the fact that the rate equations for this model were designed for lower carbon contents in the range of carbon content of 2 wt. %, particularly pertinent in the refining process of stainless steels, and are significantly lower than the levels experienced in the context of this study (i.e., carbon content in the range 6.5 – 7.5 wt. %) In addition, the observed trend could also be attributed to the extent of oxygen utilization, as the determination of the oxygen utilization ratio still remains a very difficult parameter in the blowing process (Wei and Zhu, 2002).

The mass and energy balance model could be manipulated to check the conditions necessary to obtain the required carbon composition from the plant data, as the model has the advantage of predicting the conditions necessary to achieve a certain carbon composition. For the collected plant data, the mass and energy balance model and the manipulation of the gas flow rates while keeping other parameters constant, resulted in achievement of the same carbon contents in the final alloy bath obtained in the process plant data.

5.3.2 Comparison of the final chromium composition based on models and plant data

The chromium content predicted from the mass and energy balance model and rate equations were plotted against the actual plant data and results plotted in figure 5.7. At higher carbon levels, i.e. the first stage of the blow, the rate equation for chromium loss was also incorporated in the model proposed by Wei and Zhu (2002). In most cases for the first stage of the blow, the mass and energy balance model produced a better prediction than that obtained from the rate equation based on plant data which, for most parts of the blow had the lowest chromium predicted in the bath at the end of the first stage blow for the different heats.

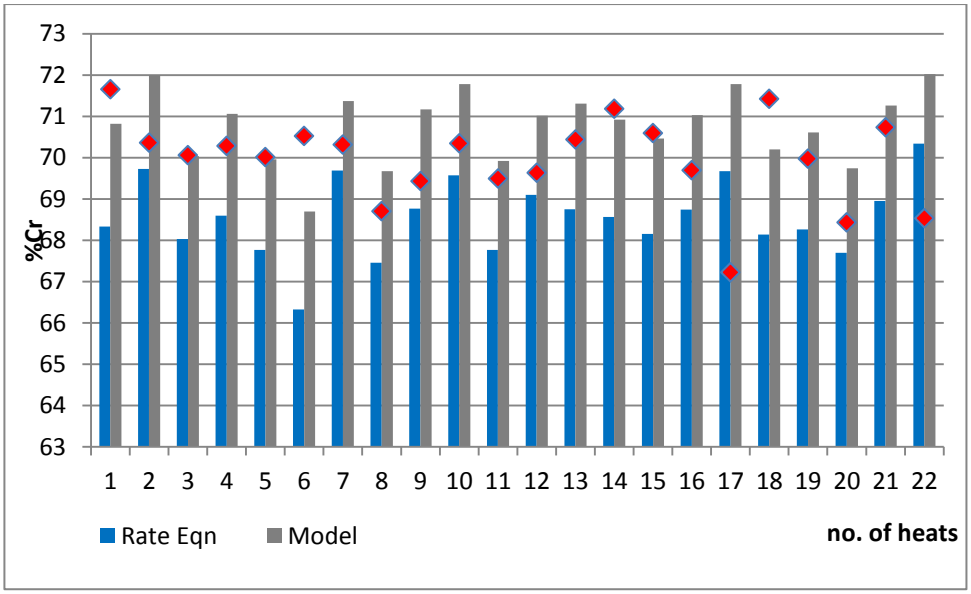


Figure 5.7: Comparison of final Cr in the alloy bath for the first stage of the blow at high carbon content

The chromium comparison was also done between the mass and energy balance and the process plant data for the second blowing stage and results shown in figure 5.8 below:

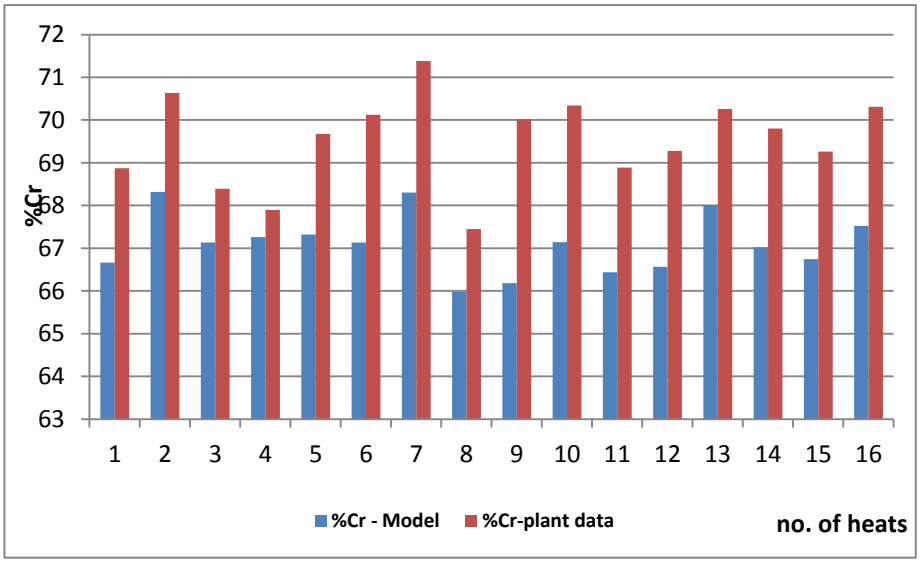


Figure 5.8: Comparison of final %Cr in the alloy bath predicted from rate equation model and plant data during the second stage of the blow

It is also important to note that the model predictions are based on equilibrium conditions being achieved in the bath (Heikkinen, 2011; Wei and Zhu, 2002). However, the attainment of equilibrium conditions may be difficult to during the whole duration of the blowing stages as there tend to be many variables changing at any given time, especially in a manual controlled

process where the operator's expertise has a significant impact on the process path (Heikkinen, 2011). Furthermore, the rate equation model proposed by Wei and Zhu (2002) was derived at lower chromium contents of approximately 18 wt. % Cr, whereas the application of the model in the present case is for bath composition with greater than 65wt. % Cr.

The discrepancy in terms of chromium composition of the bath will also have a bearing on the accuracy in prediction of the proposed rate equation model. The deviation from plant data and model was particularly evident in the second stage of the blow (as shown in figure 5.8), where the model predicted lower chromium contents than the actual plant data obtained. The deviation may be attributed to the model assumptions that all the oxygen blown into the AOD takes part in the oxidation reactions of silicon, chromium and carbon, which in reality may not be the case. The mass and energy balance model as well as the rate equations (in the first blowing stage) do not also take into account that oxygen has post combustion reactions in the converter, which might also contribute to the deviation between actual plant data and model predictions (Wei and Zhu, 2002).

5.3.3 Effect of initial temperature on the extent of decarburization

The mass and energy balance model was used to predict the effect of changing the initial bath temperatures on the extent of decarburization. The effect of initial temperature conditions were investigated by fixing the other parameters such gas flow rates, blow time interval, gas ratios, and initial composition of the alloy bath. The initial bath temperatures were varied between 1600°C and1780^{o}C, and results shown in Figure 5.9.

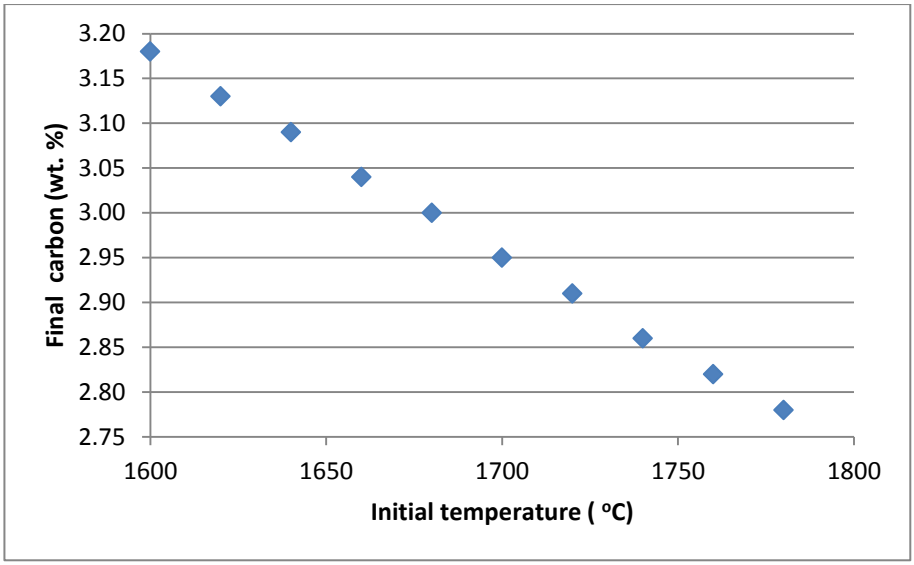


Figure 5.9: Effect of initial temperature on the extent of decarburization at high carbon content

As shown in Figure 5.9, an increase in the initial bath temperature would result in the attainment of lower final carbon content if all another critical parameters remain unchanged. The trend observed was supported by findings by Wei and Zhu (2011) based on the effects of the initial temperature on the decarburization in a combined-blown and top-blown AOD converter. Based on the heat studied, the end carbon after varying the initial temperature by +10K decreased from 0.035-0.034 wt. %, while that of %Cr increased from 17.9-17.92 wt. % in the metal bath (Wei and Zhu, 2002; Fruehan, 1976). With a decrease in of 10K, the end point carbon (carbon content at the end of the oxygen blowing process) increased to 0.036 wt. %, and the %Cr decreased to 17.88 wt. %.. The same analysis was done for lower carbon contents in the alloy bath (second blowing stage) and the results also showed a decrease in the final carbon achieved with an increase in initial temperature.

However, the thermodynamic feasibility as a result of the effect of initial temperature on the decarburization process, and hence the beneficial effects of high initial bath temperatures, do not take into account the need to control the starting temperatures in order to protect the refractory materials.. In the actual plant operation the changes in the process temperatures are constantly being monitored so as to avoid overheating of the AOD reactor, thereby mitigating the thermodynamic and kinetic benefits of operating at high initial bath temperatures.

In figure 5.10, the initial alloy bath temperature was also plotted against predicted final carbon content achievable. The same trend was also observed as in figure 5.9 and as discussed from the work by Wei and Zhu (2002).

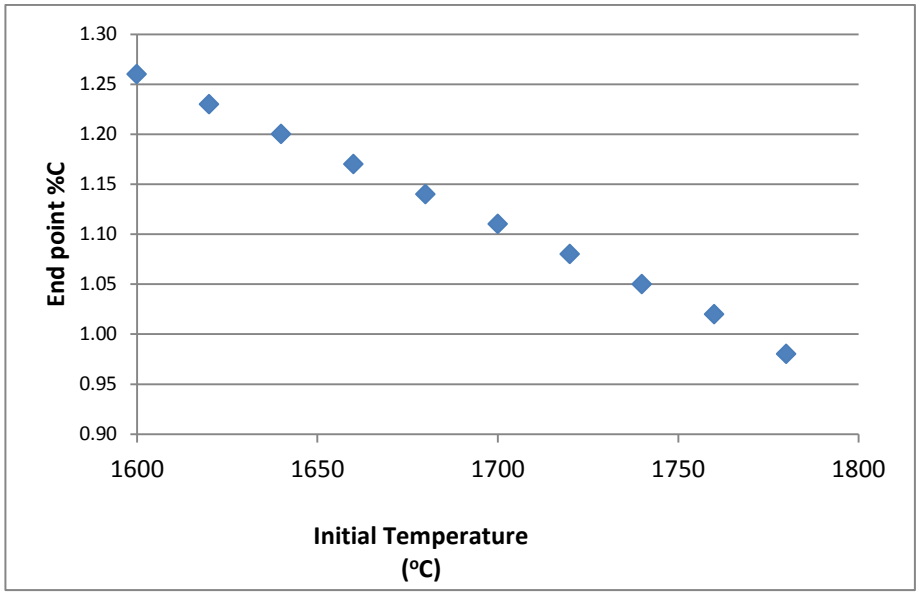


Figure 5.10: Effect of initial temperature on end point carbon at low carbon contents.

5.4 Effect of metal bath composition (Si, Cr and C) on the distribution ratio of oxygen

The distribution ratio of oxygen among elements in an alloy bath can be presumed to be proportional to the elements' Gibbs free energies of their oxidation reactions in the alloy bath. From the oxidation reactions of Cr, Si and C shown in literature, the distribution ratios of oxygen amongst these elements was used to derive the expressions to calculate how oxygen was distributed in the alloy bath elements (Wei and Zhu, 2002; Tohge et al, 1984).

The blown oxygen was seen to have different distribution ratios for Cr, C and Si when calculated. As the process progresses, these ratios will change with change in metal bath temperature and composition. The initial distribution ratios of blown oxygen for Cr, C and Si for the plant data are shown in the figure below. Carbon had the highest ratio of blown oxygen, which means that most of the blown oxygen went towards decarburization.

The distribution ratios for blown oxygen were then taken for carbon only and plotted on a graph versus initial temperature as shown in figure 5.11.

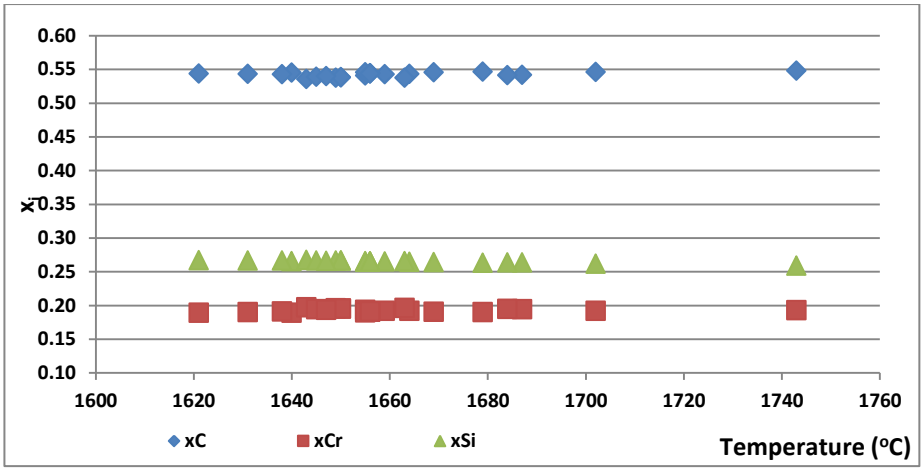


Figure 5.11: Relationship between initial temperature and distribution ratios of blown oxygen for Si, Cr and C

The trend showed that the distribution ratios increased with an increase in initial temperature. This is attributed to the fact that the Gibbs free energies were used for determining distribution ratios of blown oxygen, and they take into account temperature of the bath. Turkdogan and Fruehan (1999) stated that the Gibbs free energies were a function of temperature only, hence the trend observed in figure 5.11.

A plot of oxygen distribution ratio for carbon oxidation was constructed as shown in figure 5.12. The trend from the graph also showed that the distribution ratio of oxygen in the carbon oxidation also increased with increasing temperature.

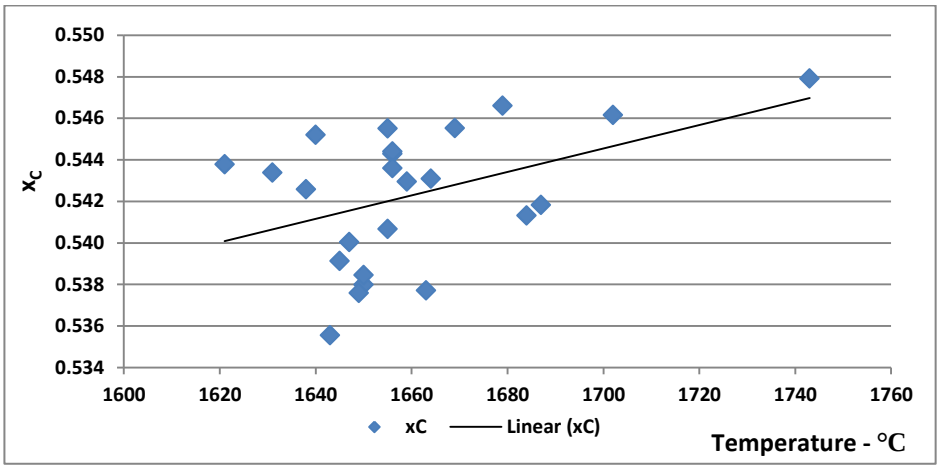


Figure 5.12: Effect of initial temperature on distribution ratios of blown oxygen for carbon

5.5 Effect of initial chromium content in the bath

The effect of initial chromium content (%Cr) on the extent of decarburization was also investigated based the mass and energy balance model. The basis of this investigation was to investigate the potential effect of the interaction between the Cr and the C in the metal bath. As discussed in section 5.3.2, chromium affinity for C can potentially impact the extent on the decarburization process. In this case, the effect of initial Cr content of the bath was investigated by fixing other parameters such as initial bath temp, initial metal analysis, gas flow rates and time interval for the blow. The results were plotted and the trend shown in the figure 5.13 below:

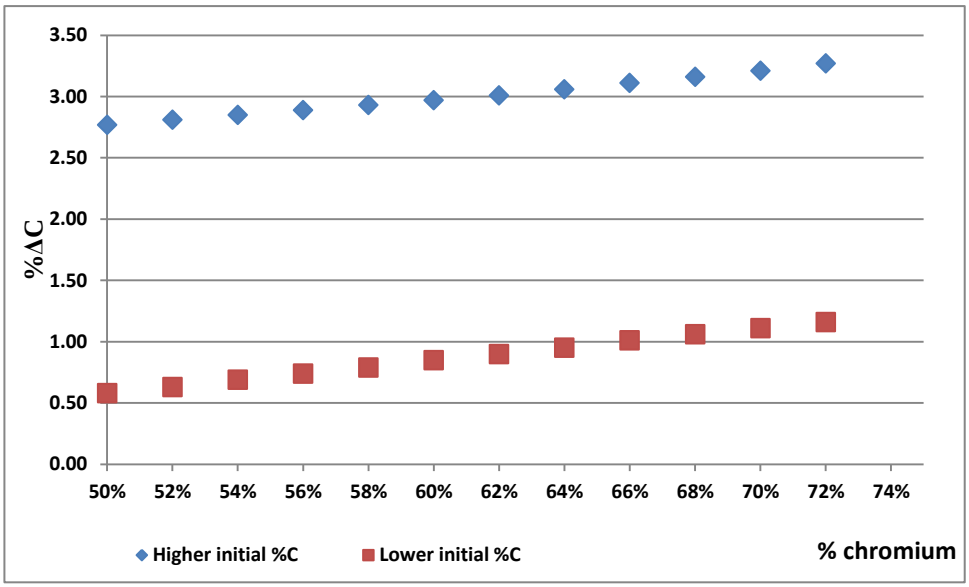


Figure 5.13: Effect of initial % chromium on decarburization

The Figure 5.13 shows that with an increase in initial chromium content, the end point carbon also increased and the relationship between the Cr and C follows an almost linear trend.

5.6 Effect of O_2 partial pressure on the extent of decarburization

The oxygen partial pressures calculation was shown in section 4.2.1. The average carbon for higher and lower carbon percent for the first and second stages, respectively, were obtained and compared as a function of the average partial pressure of oxygen gas. It was observed that for the carbon content of 7.87 wt. % the partial pressure of O_2 was about 4.51×10^{-13}, while a carbon content of 1.53 wt. % corresponded to O_2 partial pressure of 8.06×10^{-11}. The plant data showed that the partial pressure for oxygen was lower for the first stage of blowing than the partial pressure for oxygen at lower carbon levels in the second stage of blowing.

The calculated values are in agreement with the studies done by Heikkinen et al (2011), where the authors observed that the partial pressure of oxygen blown into the converter increased with decreasing carbon content and further increased with decarburization time. This phenomenon was well observed in the second stage of blowing as shown in Figure 5.14. With the decrease in silicon content due to oxidation into the slag, the SiO_2 activity in the slag increase and the oxidation of carbon becomes the main oxidation occurring in the bath, but once critical carbon is reached, there is an increase in chromium oxidation as well. Silicon will oxidize first, followed by carbon and chromium (as silicon and carbon get depleted in the alloy bath) (Heikkinen et al, 2011; Fruehan, 1976; Wei and Zhu, 2002).

According to Turkdogan and Fruehan (1999) as the carbon content becomes depleted and critical carbon is reached, the mass transfer of carbon to the reaction interface becomes slower and required partial pressure to oxidize carbon increases. This is illustrated in figure 5.14 which shows that an increase in carbon content in the alloy bath resulted in a decrease in the oxygen partial pressure required for carbon oxidation.

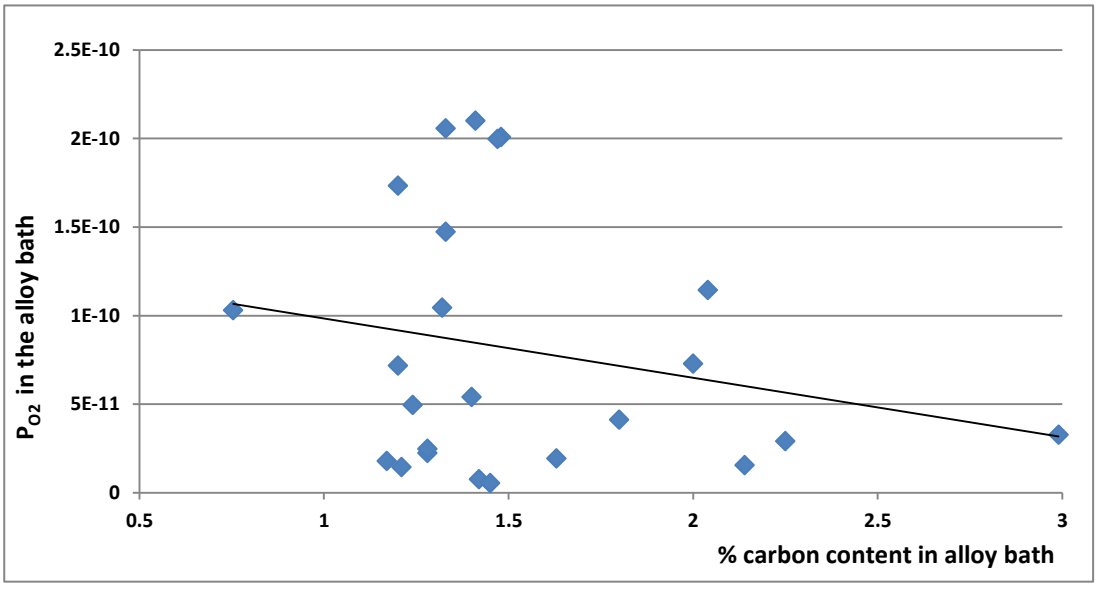


Figure 5.14: Relationship between carbon mass % vs P_{O2}

The relationship between temperature and the partial pressure of oxygen as shown in figures 5.15 and 5.16 for carbon oxidation were analysed for first and second stages of blowing respectively. It was observed that for both the first and second stages of decarburization, the

higher the temperature the higher the oxygen partial pressure. This was illustrated by Heikkinen et al (2011) when the authors plotted graphs of RT*ln(P_{O2}) against temperature in an attempt to study how temperature played a role on partial pressure of oxygen.

The figure 5.15 below shows the relationship between temperature and partial pressure of oxygen for the first blowing stage.

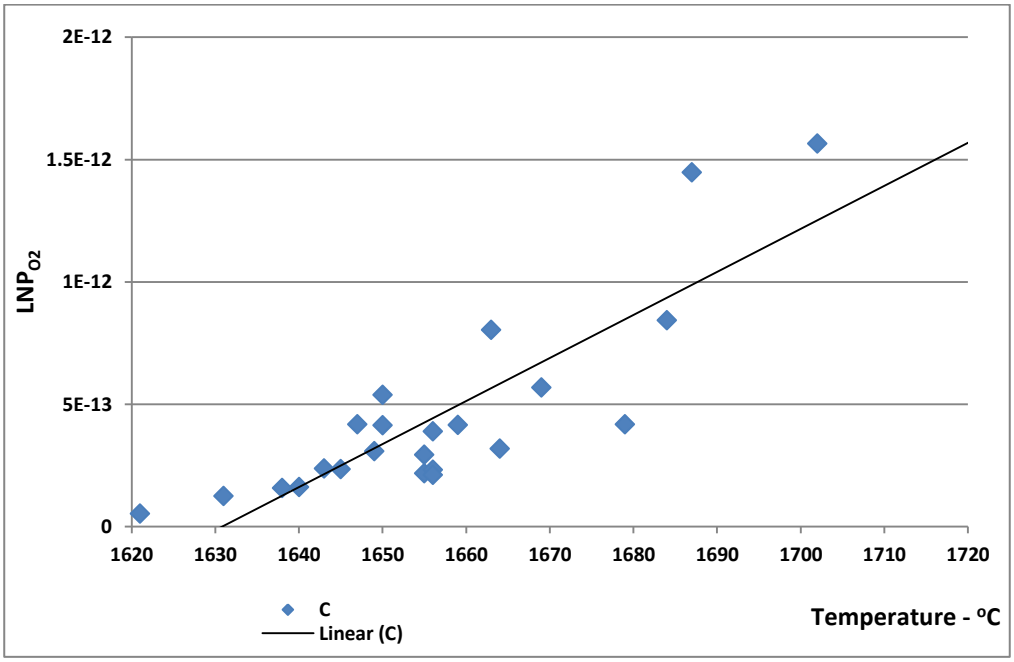


Figure 5.15: Relationship between temperature and partial pressure at higher carbon levels

Figure 5.16 illustrates the same relationship as figure 5.15, but for second blowing stage as discussed.

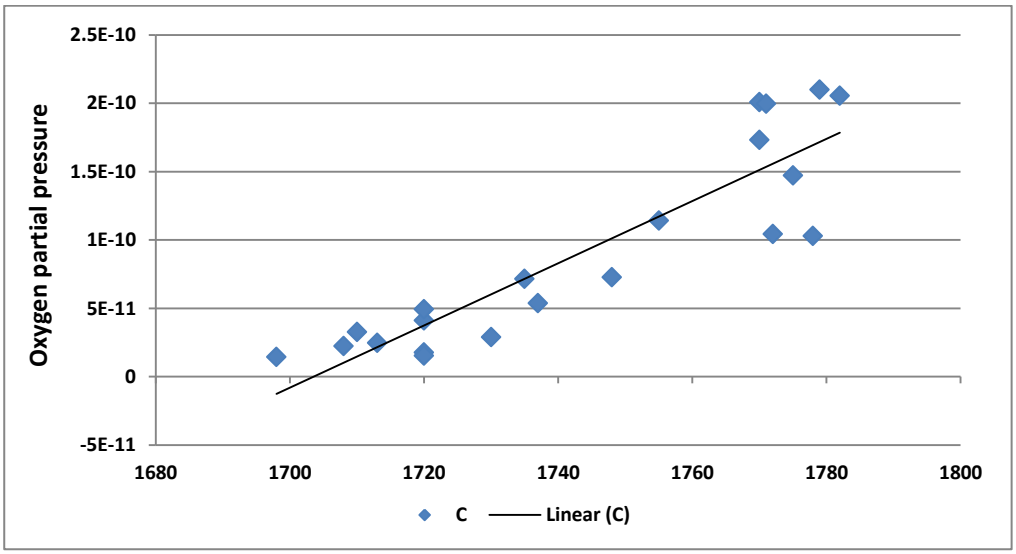


Figure 5.16: Relationship between temperature and oxygen partial pressure at lower carbon levels

5.7: Effect of CO partial pressure on the extent of decarburization

The relationship between the partial pressure of carbon monoxide (CO) required for the oxidation of carbon in the bath was investigated. It was observed that the partial pressure of CO increased with the increase in mole fraction of carbon in the bath for both the first and second stages of the blow. In general, the higher the carbon content in the bath, the more CO that will be generated during the decarburization process (Heikkinen et al, 2011). Figure 5.17 below illustrates the relationship between molar concentrations of carbon in the alloy bath with the partial pressure of carbon monoxide.

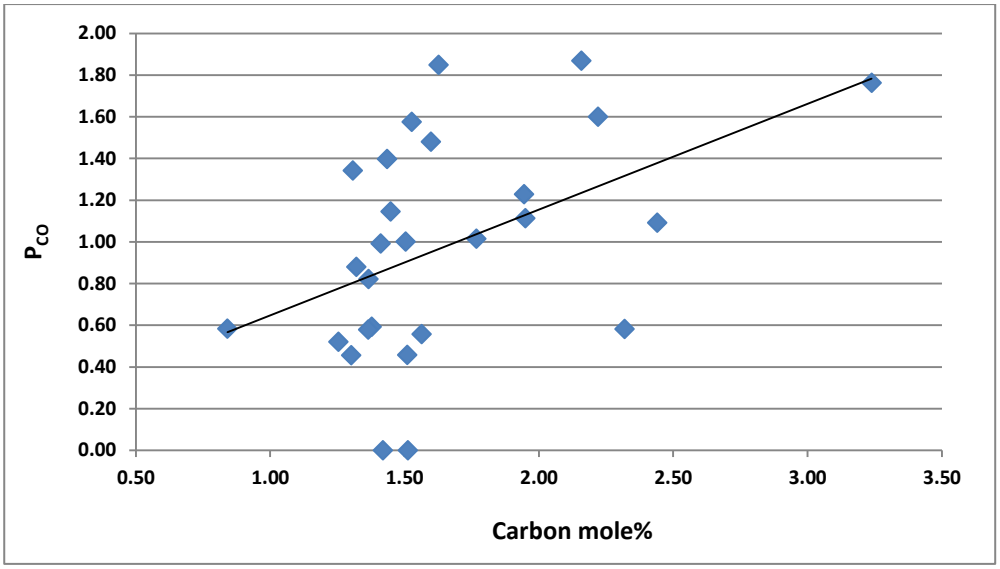


Figure 5.17: Calculated partial pressure of CO plotted as a function of mole fraction of carbon in the bath

5.8 Fitting of model and plant data at lower carbon levels

The second stage of blowing commenced once the first stage was completed (i.e. carbon content in the alloy bath was below 2.0 wt. %). In the second blowing stage, the oxygen and nitrogen ratio was adjusted to 1:1 respectively. Data collected from the plant process was used to model the rate equation by Wei and Zhu (for lower carbon content in the alloy bath) and the mass and energy balance model that was developed.

5.8.1 Comparison of modelled and plant data in terms of carbon removal

The energy and mass balance model as well as the rate equations as derived in chapter 4 and section 2.5.8.1 – 2.5.8.2, were utilized to investigate decarburization at lower carbon contents in the alloy bath. As already stated in chapter 3, lower carbon content referred to carbon contents that were below 2 wt. % in the process under study.

At lower carbon contents, the mass and energy balance model was also utilized to determine the gas flow rates necessary to achieve same plant data results. At this stage gas flow ratio for oxygen and nitrogen utilized in the converter for the second blowing stage was 1:1 respectively. The model was evaluated on the effectiveness of prediction of the outcome of the second blowing stage carbon compared to the plant data results.

The initial temperature, chemical analyses and time intervals for the duration of the second blowing stage as obtained from the process data were kept constant, with the exception of the gas flow rates that were then varied until the final carbon content compared closely to the plant data. The results of the comparison are shown in Figure 5.18.

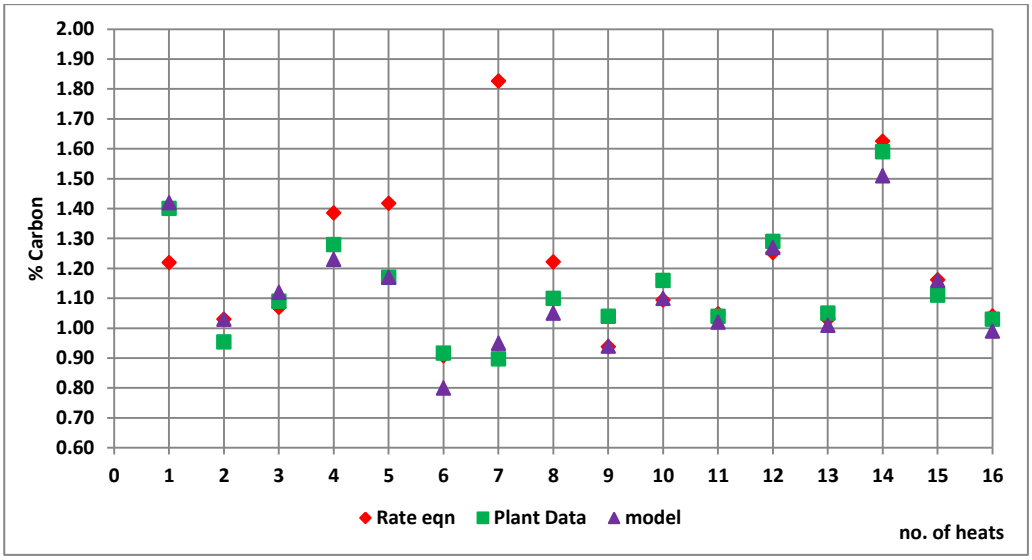


Figure 5.18: Comparison of the decarburization between modelled and plant data

As shown in Figure 5.18, there is a close prediction among the rate equation, (mass and energy balance and the rate equations) models, and the plant data. The two models under investigation showed accurate prediction of the final carbon compared to the final carbon content obtained from the plant data. For the same flow rates, chemical analyses and second stage blowing time, the extent of carbon removal in the two models accurately predicted the final carbon at the end of the second blowing stage, as observed in the comparison with actual plant results. This illustrated that both the mass and energy balance model and rate equations could accurately be utilized as predictive tools for the second blowing stage which involves lower carbon content.

5.9 Effect of gas flow rate on decarburization

The flow rate of oxygen directly influences the rate of decarburization, with extent of decarburization increasing with increase in oxygen flow rate when the amount of blown oxygen is still rate limiting (i.e. for higher carbon contents) (Turkdogan, 1980: Wei & Zhu, 2002). As discussed in Chapter 5.2, plant data was analyzed for the extent of carbon removal from the alloy bath (Δ%C) for the first and second blowing stages at different oxygen flow rates. The oxygen flow rates, in Nm^3, were correlated to the duration of each blow to determine the amount of

oxygen required to effect the carbon compositional change. The amount of oxygen used per interval was then plotted against the change in the carbon content during the different stages of blowing in the AOD heats, and the results are shown in Figures 5.19 – 5.20 for the first and second stages, respectively.

It was observed that an increase of the volume of oxygen blown into the AOD resulted in an increase in the amount of carbon removed from the alloy bath. This is due to an increase in the amount of dissolved oxygen (for carbon oxidation) per unit time resulting in increased moles of oxygen in the alloy bath that can react with carbon to form CO gas, consequently leading to an increase in the extent of carbon removal from the alloy bath (Turkdogan and Fruehan, 1999; Fruehan, 1976). However, a higher oxygen gas flow rate alone may not directly translate to a higher carbon removal in a real process plant scenario, as many variables can affect the amount and rate of carbon removal from the metal bath. Nevertheless, the mass and energy balance models and the rate equations developed in this study can be used to evaluate the impact of the volumetric flow rate of oxygen on decarburization after fixing all the other parameters.

The other important factor governing the maximum permissible volumetric flow rates of oxygen blown is the rise in temperature as a result of the exothermic reaction pertinent in the AOD refining process. As discussed in Chapter 2.5.2, excessively high temperatures presents operational challenges such as thermal degradation and the chemical dissolution by slag of the refractory lining materials. In general, typical refractory materials used in the AOD reactor often start to disintegrate at temperatures above 1750^{o}C (Schacht, 2004; Pretorius and Nunnington, 2002), and in this current operation, the permissible temperature increase is limited to 1780^{o}C. in the actual plant operation, the operator adjusts the volumetric gas flow rates by lowering the oxygen flow rate while simultaneous increasing the volumetric flow rate of nitrogen in an effort to manage the temperatures of the bath. Figure 5.19 shows the extent of decarburization with oxygen flow rate into the alloy bath for the first blowing stage.

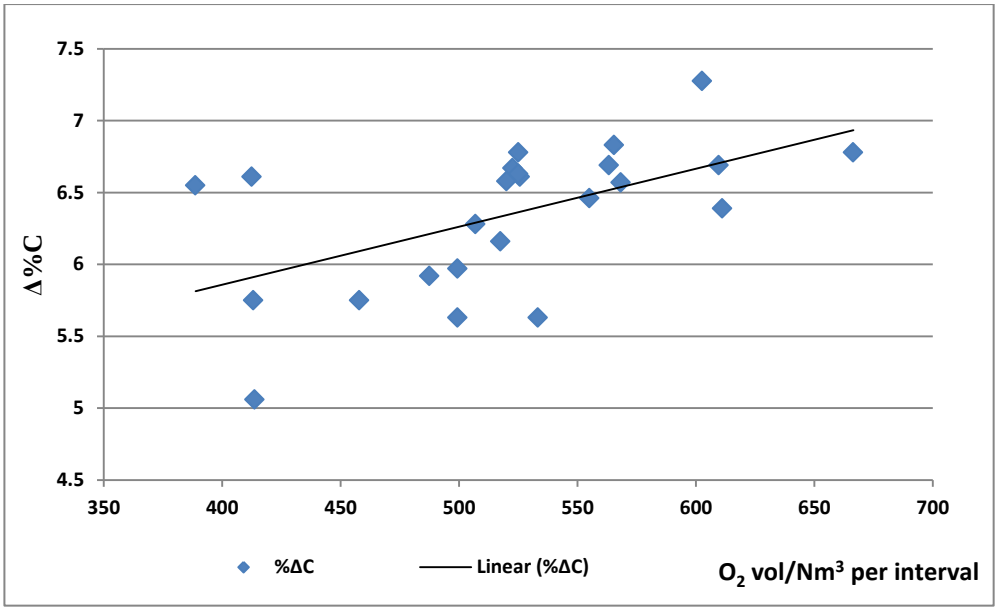


Figure 5.19: Effect of oxygen flow on decarburization in the first stage of blowing

The extent of decarburization with respect to oxygen flow rate was investigated and the results shown in figure 5.20 below:

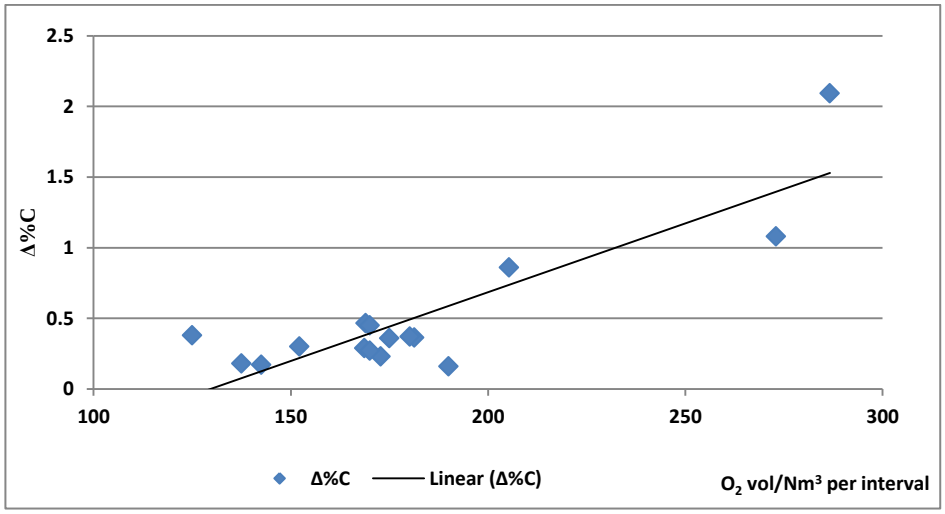


Figure 5.20: Effect of oxygen flow decarburization for the second stage of the blow

5.10 Relationship between Chromium content and Cr activity in the metal bath

The increase in molar concentration/content in the alloy bath results in an increase in the activity of chromium in the same alloy bath (Pelton and Bale, 1986; Fruehan, 1976; Turkdogan and Fruehan, 1999). This effect of chromium content in the alloy melt on the activity of chromium

was (as investigated by these researchers) was also investigated for the process plant data collected. The chromium contents measured in the alloy bath for different heats were used to calculate the activity of chromium to evaluate the existence of the relationship between the molar concentration of chromium and the activity of chromium in the alloy baths. Figure 5.21 shows the relationship between chromium content in the alloy bath and the activity of chromium.

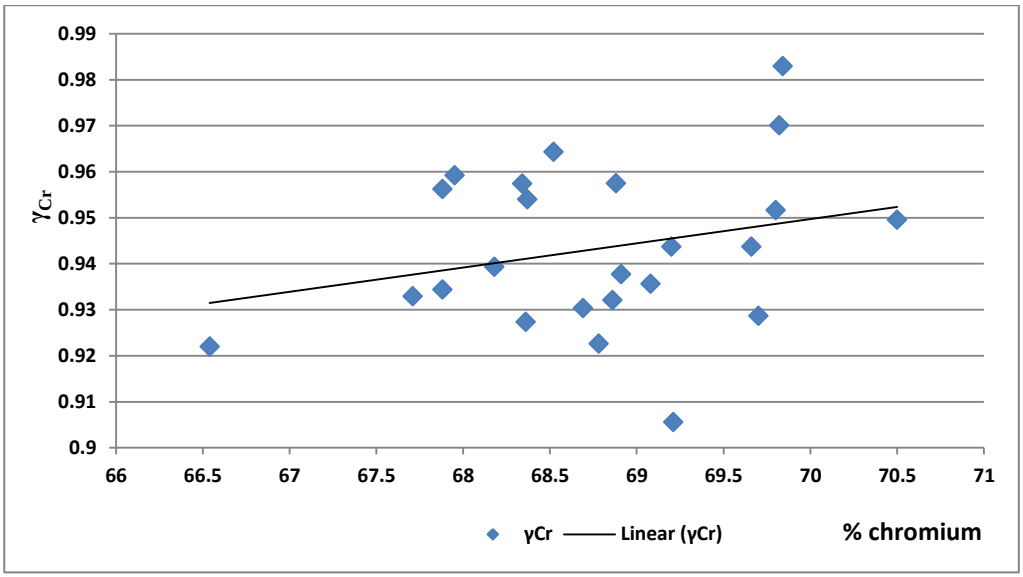


Figure 5.21: Relationship of chromium content and activity of chromium in the alloy bath

5.11 Effect of chromium on the activity of carbon in the alloy bath

Ohtani (1956) proposed that the chromium had an effect on the activity of activity in the bath, and that the addition of chromium to Fe-Cr-C baths lowered activity of carbon. The proposition by Ohtani (1956) was also supported by work done by Richardson and Dennis (1953). In the present study, the plant data was taken for both the first and second stages of the blow and plotted to evaluate if the chromium in the metal baths of the different heats had any effect on the activities of carbon in the respective baths. The calculated carbon activities were plotted against the various chromium contents, and the results are graphically depicted in Figures 5.22-5.23.

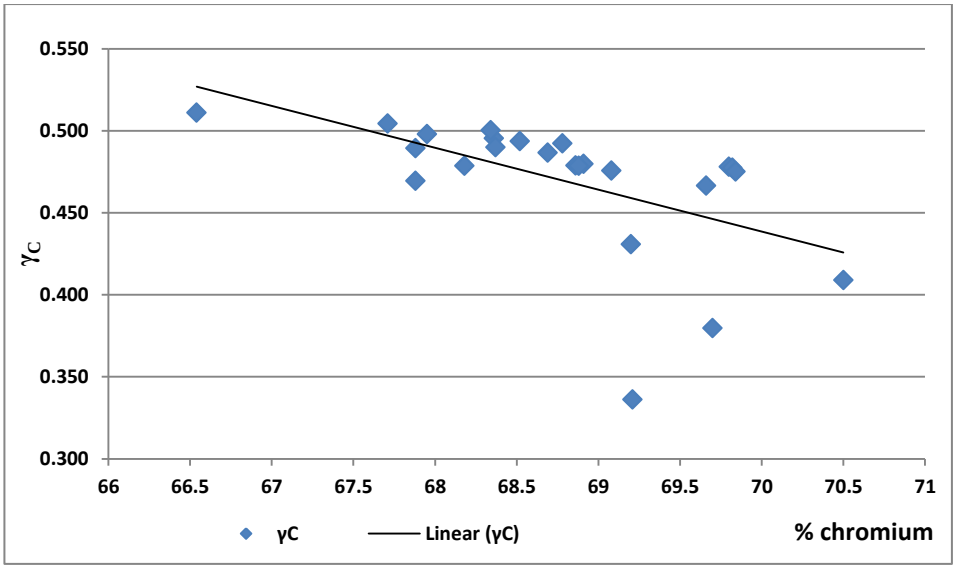


Figure 5.22: Effect of chromium on the activity of carbon at high carbon contents (first stage of blowing)

The effect of chromium on carbon activity was also illustrated in figure 5.23 for the second blowing stage as shown below.

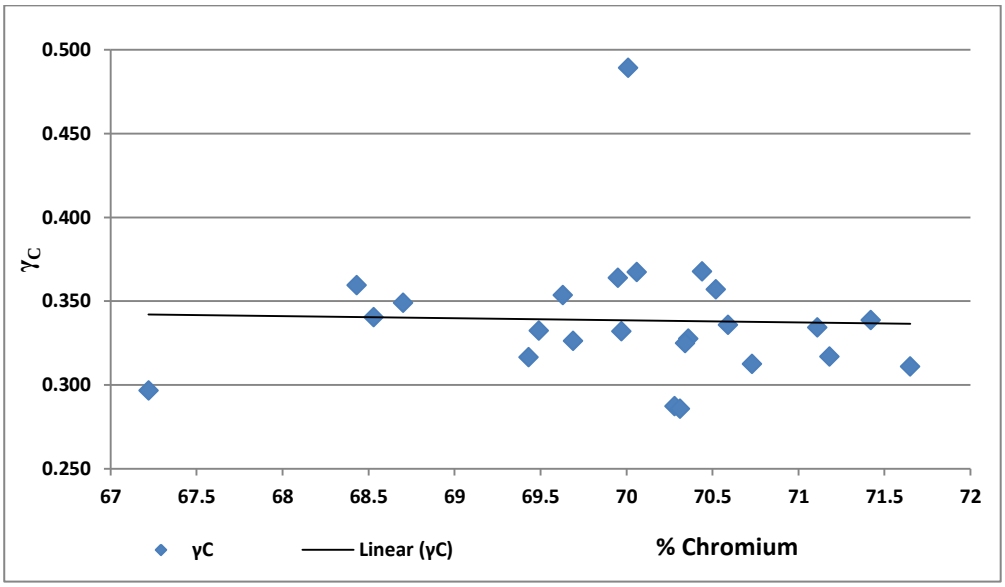


Figure 5.23: Effect of chromium content on activity of carbon at high carbon contents (second blowing stage)

As shown in Figures 5.22-5.23, the higher the chromium content of the metal bath, the lower the corresponding carbon activity. The observed trend is in agreement with the work done by Ohtani (1956). In addition, the decrease in the activity of carbon with increasing chromium is

significantly higher in the first stage of the blow with higher carbon content than in the second stage of the blow corresponding to lower carbon content.

According to Ohtani (1956), as decarburization continues the attractive energy between the chromium and the carbon which governs the affinity of Cr to C tends to increase due to the fact that the atoms of Cr and C lower each other's chemical potential. In addition, the temperature also plays an important role in lowering the activity of carbon in the same way as the increase of chromium in the bath (Ohtani, 1956). This will negatively impact on refining as it becomes increasingly difficult to decarburize as a result (Ohtani, 1956).

5.12 Relationship between Cr_2O_3 content and the activity of Cr_2O_3 in slag

Ban-Ya (1992) stated that in a multi-component slag, the activity coefficients could be described by the quadratic formalism for regular solution. Turkdogan and Fruehan (1999) went on to state that for typical AOD slags (for stainless steel production) slag basicity is high it translated to a higher silicon content in the steel and consequently a lower equilibrium slag/metal distribution of chromium resulting in a higher chromium recovery in slag.

From the plant data obtained, a graph was plotted to investigate this relationship between chromium oxides content in the slag and the corresponding activities of the chromium oxides. The mole fraction for Cr_2O_3 and the activities of Cr_2O_3were calculated as shown in Chapter 4.5.2 Figure 5.24 illustrates the relationship between the chromium oxides content is slag to the activities of the chromium oxides.

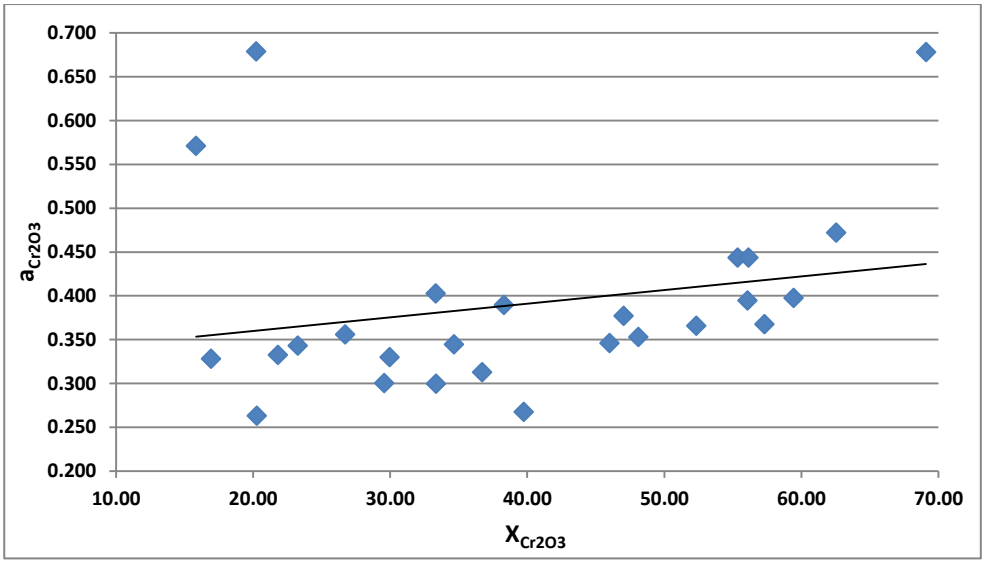


Figure 5.24: Relationship between chromium oxide and activity in slag

The chromium oxides tend exist both as Cr^{2+} and Cr^{3+} ions in slag (Ban-Ya, 1992; Gasik, 2013). However, the amount of Cr^{2+} ions in the slag depends on the total chromium oxide content in the slag (Gasik, 2013; Leuchtenmüller et al, 2016). This means that as the chromium oxide content in the slag increases, the amount of Cr^{2+} decreases and Cr^{3+} increases (Leuchtenmüller et al, 2016). As such, for the purposes of this study, it was also assumed that the predominant species was Cr_2O_3 (Cr^{3+} ions) due to the high Cr_2O_3 content in the slag (Pretorius and Nunnington, 2002). As shown in figure 5.24, the higher the mole fraction of Cr_2O_3 in the slag, the higher the activity of Cr_2O_3. A higher Cr_2O_3 content in slag results in the formation of spinels of MgO and FeO which have high melting points and make slag viscous leading to higher metallic chromium loss due to entrainment (Pretorius and Nunnington, 2002; Arh and Tehovnik, 2007).

The distribution of chromium oxides activity with differing temperatures of the melts for different heats was also investigated and the results are shown in Figure 5.25. Though no clear in the trend is observed for this particular set of data, studies done by Xiao and Holappa (1992) showed that the higher the bath temperature, the lower the activities of chrome oxides, albeit a small effect of temperature on the activities. This can be attributed to the fact that an increase in temperature of the bath will also increase the solubility of the chrome oxides in slag, thereby reducing the activities (Arh and Tehovnik, 2007). The reduction stage in the refining process with the addition of FeSi, recovers Cr_2O_3 that is in the slag phase. Visuri et al (2012) stated that FeSi is added as the reductant to reduce Cr_2O_3 and fluorspar added to reduce slag viscosity.



Figure 5.25: Relationship between temperature and chrome oxide activity

The activities of chromium oxides in slag are also strongly influenced by the basicity (CaO/SiO_2 ratio) of slag (Holappa and Xiao, 1992; Sano, 2004; Arh and Tehovnik, 2007). From the results plotted in Figure 5.26, an increase in activity of chrome oxides in slag was observed with an increase in the basicity of slag. Holappa and Xiao (1992) attributed this behavior to the fact at low basicity there is only a few oxygen ions, and this result in chromium oxides having lower activities due to a strong complexation with SiO_2.

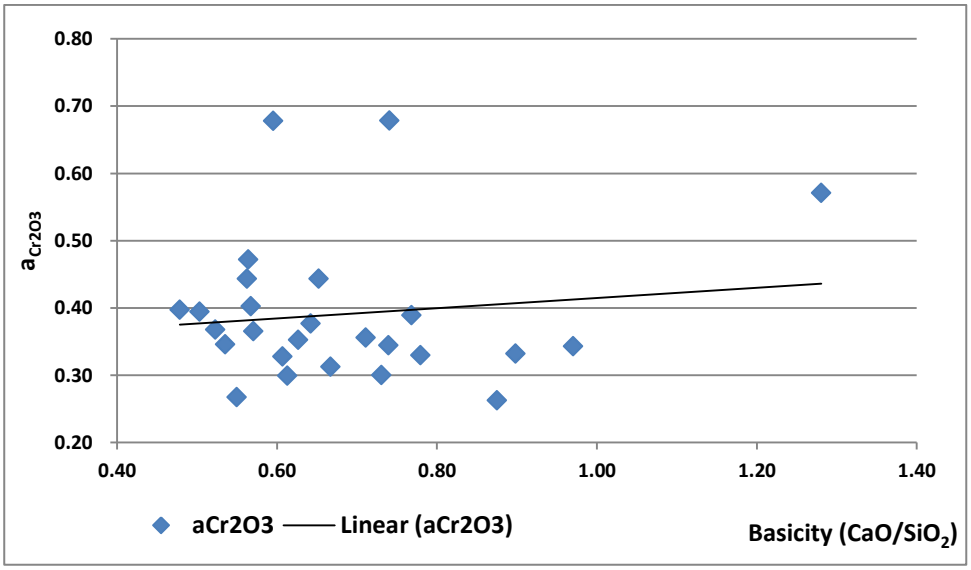


Figure 5.26: Effect of slag basicity on activities of chrome oxides

5.12 Nitrogen solubility in the alloy bath during decarburization

In the process under study, nitrogen was used as the inert gas in the AOD converter. However, nitrogen control in the alloy bath is critical to avoid precipitation of titanium nitride (TiN) and for the production of low nitrogen bearing alloys especially for high chromium steels (Kim et al, 2009). This is attributed to nitrogen solubility which increases with increase in chromium content and will tend to decrease with increase in sulphur content (Turkdogan and Fruehan, 1999; Fruehan, 1992; Kim et al, 2009).

In this study, alloy samples were analysed for dissolved nitrogen, and the results showed an average of 1.2 wt. % nitrogen in the alloy after the reduction stage. A plot of chromium content against the logarithm of the activity of nitrogen (the logarithm function utilized to produce a linear trend) as shown in figure 5.27 showed a correlation with the research by Kim et al (2009). The graph shows a general increase in the solubility of nitrogen with increasing chromium content. This shows that the relationship between %Cr by mass and $\lg f_N^{Cr}$ was independent of the partial pressure values of nitrogen. This agrees with the work done by Kim et al (2009) who proved that nitrogen partial pressure does not have a significant impact on nitrogen solubility. The increase in chromium content in the metal bath results in an increase in nitrogen solubility in the metal.

The dissolution of nitrogen is governed by Sievert's law, which states that solubility of any diatomic gas in a metal or alloy is proportional to the square root of that gas's partial pressure and the results obtained are in agreement with the work done by Kim et al (2009) based on samples containing up to 30 wt. %Cr. Furthermore, Kim et al. (2009) proposed that in Fe-Cr alloys with up to 30% Cr by mass, the Sievert's law of nitrogen dissolution holds.

Fruehan (1992) proposed that nitrogen dissolution in alloy bath could be reduced through degassing, blowing/purging the bath with an inert gas (such as argon) and use of special slags (containing CaO, BaO, Al_2O_3 and TiO_2). The company under study has resorted to purging with argon during reduction stage (recovery of chromium oxide in slag with FeSi as the reductant) as a technique of reducing nitrogen in alloy bath. But the high chromium content in the alloy bath poses a challenge as it promotes nitrogen dissolution thus the extent of nitrogen removal. The basic slags favour desulphurization so the effect of sulphur content on nitrogen removal as discussed by Fruehan (1992) is not realized (< 0.03 wt. % sulphur).

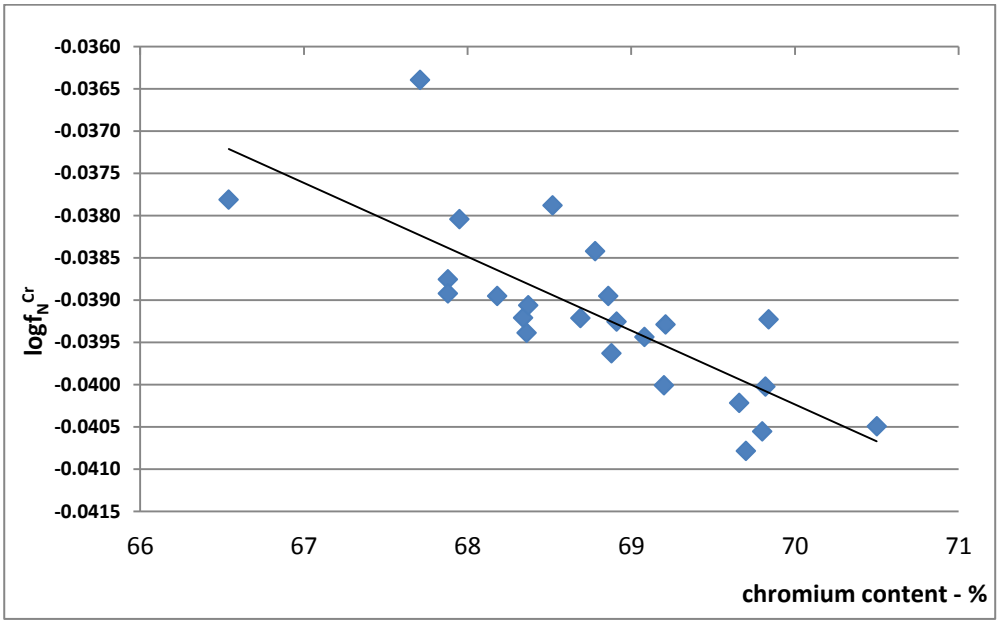


Figure 5.27: Relationship between %Chromium and nitrogen activity

5.13 Financial modelling of the AOD refining process

A financial model was constructed to determine the net smelter returns for the process under study. Cost model involved costs incurred from the EAF as this had bearing on the overall costs of the refining process as well. Costs such as raw material costs (high carbon ferrochromium alloy fines at 95 USc/lb., burnt lime and dolomite) and consumables such as electrodes ($2 525/ton of electrodes) and refractories were included. The costs were expressed in $USc/lb. of chromium to equate to the market trend of buying and selling of ferrochromium alloys (as they are sold according to units of chromium in the metal). Electricity was also observed to be another big cost driver for the re-melting of high carbon ferrochromium alloy fines, ranging between R0.85 – R2.00/kWh according to off peak and peak rate respectively according to Eskom rates at the time of the study.

The AOD costs included the cost of gases blown into the converter as well as the refractory lining and material utilized. The main cost drivers remained linings and cost of gases blown into the converter Argon cost R7.83/kg, nitrogen R1.08/kg, oxygen R1.07/kg and Liquid petroleum gas (LPG) utilized for heating ladles cost R7.62/kg. From this financial model, it can be calculated per heat to investigate whether a process is economical or not. The longer the AOD process takes, the more gases consumed and consequently the higher the cost of production. The

selling price of the final product at the time of the study was USD$1.75/lb. and average costs amounted to USD$1.35, leaving a margin of approximately USD$0.40/lb. The model was created to augment the mass and energy balance model which can optimize the blowing process. The financial model is then used to evaluate on whether the optimization done are cost effective financially, thereby creating a tool not only for technically and scientifically evaluating a process, but also financially evaluating the economic feasibility of these technical innovations in process optimization. Appendix 17 illustrates the template constructed for cost modeling.

Summary

The mass and energy balance and rate equation models were used as predictive tools for decarburization in the production of medium carbon ferrochromium alloy for the process under study. Upon investigation, it was observed that at higher carbon contents, the mass and energy balanced model results correlated to the carbon contents obtained in the plant data for the different heats. The rate equations at high carbon contents however were significantly different from the plant data and this was attributed to the development of the rate equations which were constructed for lower carbon contents in stainless steel production which are significantly lower than the carbon contents under study (Wei and Zhu, 2002). For lower carbon contents, both the mass and energy balance models and rate equations predictions for final carbon content were significantly accurate with respect to plant data results.

Upon analysis of activities of carbon for different heats, it was observed that the activity of carbon decreased with increasing chromium content in the alloy bath. Moreover, the activity of chromium oxide in the slag decreased with increasing in bath temperature due to increased solubility of chromium oxide. The same chromium oxide activity was also observed to increase with increase in slag basicity (Holappa and Xiao, 1992).

The extent of decarburization was related to the rate of oxygen flow and significant at higher carbon levels (defined as carbon content > 2.0 wt. %) compared to lower carbon contents ($\leq$ 2.0 wt. %). This was attributed to oxygen flow rate being rate limiting at higher carbon contents and at lower carbon contents, carbon mass transfer becomes rate determining (Fruehan, 1976; Wei and Zhu, 2002). Nitrogen dissolution in the alloy bath was also investigated as the process under study uses nitrogen in place of argon as the inert gas. The results showed an increase in nitrogen solubility with an increase in chromium content. This was in alignment with the research done

by Fruehan (1992) and Kim et al (2009) that attributed nitrogen solubility to increase in chromium and decrease in sulphur contents in the alloy bath.

CONCLUSION

Understanding the different roles of each parameter enables the understanding of decarburization in the AOD. By first understanding the thermodynamic relationships between different elements and oxides and their behaviour at high temperatures helps model and predict outcomes of complex reactions per particular interval. The broad objective of this study was to evaluate the practicability of thermodynamic and parametric modeling in the refining of high carbon ferrochromium alloy for the process under study. The secondary objectives were to formulate a mass and energy balance model and rate equations as predictive tools for the decarburization process. By assessing the current process being employed by the company under study, the objective of optimizing performance economically through understanding the process performance and methods of improving chromium recoveries was also investigated.

Oxygen is the main oxidant in the AOD and the elements in the molten metal (Si, C and Cr) are all oxidised during decarburization. It was also observed that the higher the oxygen flow rate, the more moles of oxygen in the bath at a particular time interval, hence the higher the decarburization rate. At higher carbon, it was observed that the oxygen flow rate required for carbon oxidation.

Activities of oxides in the slag could be analysed using quadratic formalism (Ban-Ya, 1993) and it was shown from the plant data that an increase in Cr_2O_3 in the slag results in an increased Cr_2O_3 activity. Basicity of the slag also had the same effect on chromium oxides activity resulting in an increase in chromium oxides as the slag basicity increased. For the process data, it was also observed that an increase in chromium content in the metal bath resulted in a decreased carbon activity, resulting in reduced decarburization. The effect was not as pronounced on the first stage of the blowing cycle due to the higher carbon content that it was on the second blowing stage.

The initial bath temperature was investigated and observed to be quite significant on the decarburization process. The effect was more pronounced when other parameters were kept constant and initial temperature varied over a wide range. The higher the initial temperature, the lower the carbon end point for a fixed time interval. This was modelled and agreed with work done by Wei & Zhu (2002) who also varied initial bath temperature with +/- 10K and observed

that an increase in initial temperature by 10K resulted in a decrease in the carbon end point, and the inverse also showed same result.

The rate equations proposed by Wei and Zhu (2002) were adapted to predict extent of decarburization (as well as other oxidation reactions occurring in the refining process) and how these rate equations compare to the actual plant data obtained for the different heats under study. However, the rate equations for higher carbon content did not produce results close to the achieved plant data since the original model was designed for lower carbon contents than those experienced in the present study. Furthermore at lower carbon contents both rate equation proposed by Wei and Zhu (2002) and the mass and energy models developed specifically for this study could be used to predict with a higher level of accuracy the final carbon content at the stipulated process parameters.

The initial temperature of the alloy has an impact on the end point of carbon in the process due to improved carbon removal efficiency with increase in temperature (Heikkinen, 2013; Turkdogan and Fruehan, 1999). However, there is only a limited increase on initial temperature permissible in practice in order for refractory material to last for longer as the refractory bricks start disintegrating and dissolving into the bath at bath temperatures in the excess of $1800^{o}C$ (Arh and Tehovnik, 2007; Schacht, 2004).

The oxygen flow rate will also impact on the rate of decarburization. The higher the flow rates the faster the carbon removal and the more the moles of oxygen available to oxidize a larger carbon percentage in the metal bath. The effect of chromium content on carbon activity becomes more pronounced the lower the carbon content in the bath. This is as a result of the affinity of chromium on carbon which becomes more pronounced at lower carbon contents hence negatively impacting on decarburization and increasing chromium loss to slag (Fruehan, 1976; Ohtani, 1956). At lower carbon contents below critical carbon content, the oxidation of chromium becomes more pronounced as the rate of decarburization is now determined by mass transfer of carbon to reaction interfaces and not on oxygen flow rate (Wei and Zhu, 2002; Turkdogan and Fruehan, 1999; Fruehan, 1976; Arh and Tehovnik, 2007).

The parametric modelling of parameters involved in decarburization of high carbon ferrochrome melt to produce medium carbon ferrochrome is feasible, hence leading to a better control on the

process and better predictability of the process. Through thorough understanding of thermodynamic principles, it is possible to model behaviour of the slag and alloy baths in the converter to predict the overall outcome of the extent of decarburization for the refining process.

RECOMMENDATIONS

The study involved the investigation of thermodynamic and parametric modeling in the refining of high carbon ferrochromium alloys. This was essential in understanding the effect of different parameters (such as gas flow rates and ratios amongst other parameters) in the refining process in order to attain the desired final product through the optimal control of these parameters and their influence on refining. The areas discussed below are points that require further study and work to ensure better understanding of the decarburization process in the making of medium carbon ferrochrome alloy.

The study that was done for this particular process and plant data had its own shortcomings. There is a need for further investigation (on the interaction between the different elements in the alloy bath under controlled conditions to investigate accuracy of the model in ideal conditions that can be obtained in a lab set up.

The physical modeling of AOD is an area for further investigation. For the purpose of this study, the physical values proposed by Wei and Zhu (2002) were used in the modeling with rate equations and may only be accurate under the conditions investigated by the researchers. Parameters such as converter size, bath depth, tuyere size and orientation all have impact on the extent and rate of decarburization. The determination of oxygen utilization potential is contentious in literature with very few researchers having investigated this concept. Dimensionless constants and parameters such as bubble sizes were assumed from the work done by Wei and Zhu (2002) and not from calculated values for the process under study. The determination of these constants still needs to be done for refining of high carbon ferrochrome as most the researchers investigated systems for stainless steel production and very little work was done for refining of high carbon ferrochromium alloys.

The models used for the mass and energy balance model had limits as to the composition of the Fe-C-Cr system being investigated. The model used for nitrogen solubility in alloy bath used by Kim et al (2009) was for a Fe-C system with chromium content 15 – 60 wt. % and the process under study had chromium contents of between 65 – 70 wt. %. This was further compounded by the use of the interaction coefficients published by Sigworth and Elliot (1974) which were investigated for dilute solutions in liquid iron, with iron as the solvent and only accurate for Fe-Cr solutions with low chromium concentrations. The process under study has chromium

concentrations of > 65 wt. % and as chromium is the main element in the alloy bath, determination of interaction parameters might need to further investigate the practicability of Fe-C-Cr systems with chromium as the solvent. The interaction coefficients were also calculated at 1600^{o}C though there were temperature variations in the process under study.

Further model development based on these issues raised is required. The areas discussed below are points that require further study and work to ensure better understanding of the decarburization process in the making of medium carbon ferrochrome alloy.

1. The determination of interaction coefficients specific to high carbon ferrochromium alloys. As already discussed, the interaction coefficients used in this study were published by Sigworth and Elliot (1974). However, such interaction coefficients were investigated for dilute solutions that have iron as the solvent, thereby making them only suitable and accurate for solutions of Fe-Cr melts containing lower concentrations of Cr. A further study to determine the interaction parameters by taking into account the high chromium content in HCFeCr melts requires determination of interaction parameters taking into account Cr as the solvent.
2. The investigation of nitrogen solubility done in the scope of this study was based on a model developed by Kim et al (2009). This model was designed for evaluating stainless steel systems for chromium content up to 30 wt. % and partial pressures for nitrogen 0.04-0.97 atm. The chromium contents involved in this study exceed the range, and hence could potentially affect accuracy of the models. Therefore investigations into nitrogen solubility at chromium contents exceeding 60 wt. % as the increase in chromium content in the alloy bath increases nitrogen solubility (Fruehan, 1992).
3. The chromium contents predicted by the mass and energy balance model showed difference between the actual and the predicted final compositions for chromium and silicon This can be attributed to the models adopted that were initially created to evaluate Fe-Cr-C systems containing up to 30 wt. % (most models in literature developed for stainless steels) chromium. As a result, there is need to investigate further the effects of higher Cr content on the decarburization process of Fe-Cr-C melts, particularly the potential effect of taking chromium as the matrix instead of iron as is commonly used in dilute Fe-Cr-C systems.
4. Physical modeling was not done in this study. The dimensionless constants used were based on work done by the researchers such as Wei and Zhu (2002) but were applicable

for stainless steels. There is need for further study to determine parameters such as bubble sizes and tuyere configurations applicable for the current set up of the process under study.

REFERENCES

1. Wei, J.H. and De-Ping Zhu, D.P (2002). Mathematical modelling of the argon-oxygen decarburization refining process of stainless steel: Part 1. Mathematical model of the process. Metallurgical & Materials Transactions 33B: 111-119.
2. Richardson, F.D. and Dennis, W.E. (1953). Effect of chromium on the thermodynamic activity of carbon in liquid iron- chromium-carbon metals. Journal of Iron Steel Institute: 257-263.
3. Heikkinen, H.P. and Fabritius, T. (2012). Modeling of the Refining Processes in the Production of Ferrochrome & Stainless Steel. Recent Researches in Metallurgical Engineering - From Extraction to Forming. Intech publishers, Shanghai. Available at http://www.intechopen.com/books/recent-researches-in-metallurgical-engineering-from-extraction-to-forming/modelling-of-the-refining-processes-in-the-production-of-ferrochrome-and-stainless-steel. Date accessed: 6/11/2016.: 65-88
4. Pretorius, E.B. and Nunnington, R.C (2002). Stainless steel slag fundamentals: from furnace to Tundish, Iron and Steel making. Journal vol. 29 (2): 133 – 139.
5. Heikkinen, E.P. (2013). On the Role of Computational Thermodynamics in Research and Development of AOD and processes. Available at http://cc.oulu.fi/~kamahei/z/tkt/HeikkinenEP-vk.pdf, date accessed: 6/11/2016.
6. Heikkinen, E.P., Ikäheimonen, T., Mattila, O. and Fabritius, T. (2011). A thermodynamic study on the oxidation of silicon, carbon and chromium in the ferrochrome converter. The 6th European Oxygen Steelmaking Conference, Stockholm: 229 – 238.
7. Chuang, H.C., Hwang, W.S., and Liu, S.H. (2009). Effects of Basicity and FeO Content on the Softening and Melting Temperatures of the CaO-SiO2-MgO-Al2O3 Slag System. Materials Transactions, Journal Vol. 50, No. 6: 1448 -1456.
8. Goldstein, M. (1978). Diffusion modeling of the Carburization Process. Metallurgical Transactions Journal Vol. 9A: 1515 - 1525
9. Arh B. and Tehovnik F. (2007). The oxidation and reduction of chromium of stainless steels in an electric arc furnace. Institute of Metals and Technology Journal Vol. 41(5): 203 – 211.
10. Bhardwaj B.P. (2014). The complete book of Ferroalloys. Niir Consultancy Services, New Delhi, India p185 – 200.

11. P.J. Bhonde, A.M. Ghodgaonkar and R.D. Angal (2007). Various Techniques to Produce Low Carbon Ferrochrome. Proceedings of the 2007 International Ferroalloys Congress, New Dehlie, India: 86 – 90.
12. Taylor C.R. and Custer C.C. (1985). Electric Furnace Steelmaking. Iron and Steel Society of AIME: p 124.
13. Product data sheet, 304/304L stainless steel. Available at www.aksteel.com/pdf/markets_products/.../304_304l_data_sheet.pdf. Date accessed: 5 March 2016.
14. Gasik M. (2013). Handbook of ferroalloys 1st Edition. Butterworth-Heinemann: p 268 – 314.
15. Schacht A. C. (2004). Refractories Handbook. Marcel Dekker Inc. Pittsburgh, Pennsylvania, U.S.A.: p109 – 128.
16. Chakraborty D., Ranganathan S. and Sinha S.N., August (2005). Investigations on the carbothermic reduction of chromite ores. Metallurgical and Materials Transactions Journal Vol. 16 (4): 437 – 444.
17. Ugwuegbu C., (2012). Technology innovations in the smelting of chromite ore. Innovative Systems Design and Engineering Vol.3 (12): 48 -54.
18. Infomine/commoditymine. Available at http://www.infomine.com/commodities/chromium-mining. Accessed at 6 March 2016.
19. Mac Rae D. R. (1992). Plasma-arc technology for ferroalloys, Part II. Proceedings of the 6th International Ferroalloys Congress, Cape Town. Journal Vol 1: 21-35.
20. Beskow K., Van Der Linde J-A and Rick C-J, (2010). Steam as process gas brings economic benefits to Columbus Stainless. Steel Times International. Available at http://www.uht.se/app/uploads/2015/06/2010-Steam-as-Process-Gas-Brings-Economic-Benefits-to-Columbus-Stainless-0-f6def6a8-f356-4f53-bd3e-f47d9236d2b0.pdf .Accessed at 10 March 2016.
21. Wei J.H, Cao Y., Zhu H.L. and Chi H.B. (2010). Mathematical Modeling Study on Combined Side and Top Blowing AOD Refining Process of Stainless Steel. ISIJ International, Journal Vol. 51(3): 365-374.
22. Turkdogan E.T. and Fruehan R. (1999). Fundamentals of Iron and Steelmaking. Steelmaking and Refining Volume, the AISE Steel Foundation, Pittsburgh, PA. p37 – 86.

23. Wei J-H and Zhu D-P. (2002). Mathematical Modeling of the Argon-Oxygen Decarburization Refining Process of Stainless Steel: Part II. Application of the model to Industrial Practice. Metallurgical and Materials Transactions Vol. 33B: 121 – 127.
24. Elyutin V.P. (1957). Production of ferroalloys and electrometallurgy 2nd edition. The State Scientific and Technical Publishing House, Moscow. p190 - 196
25. Fruehan R.J. (1976). Ironmaking and Steelmaking, Journal Vol. 3: p153-158.
26. Wei J.H. and Zhu D.P. (2002). Mathematical modeling of the Argon-Oxygen Decarburization refining process of stainless steel: Part 1.Mathematical Model of the Process. Metallurgical & Materials Transactions Vol. 33B: 111-119.
27. Jacques Belyveld (2016). Private Communication. XRAM Technologies, 2016.
28. Sigworth G.K. and Elliot J.F. (1974). The thermodynamics of liquid dilute iron alloys. Metal Science Vol. 8(1): .298–310.
29. Ban-Ya S. (1993) Mathematical Expression of Slag-Metal Reaction in Steel making process by Quadratic Formalism on the Regular Solution Model, ISIJ International, Vol 33(1): 2-11.
30. Kim W., Lee C., Wook C. and Pak J. (2009). Effect of Chromium on Nitrogen Solubility in Liquid Fe-Cr Alloys containing 30 mass% Cr. ISIJ International Vol.49 (11): 1668-1672.
31. Heikkinen E-P, Ikaheimonen T, Mattila O, Fabritius T and Visuri, V-V (2011). Behaviour of Silicon, Carbon & Chromium in the Ferrochrome Converter – A comparison between CTD and process samples. The 6th European Oxygen Steelmaking Conference – Stockholm: 229 – 238.
32. Xiao Y. and Holappa L., 1993. Determination of Activities in Slags containing Chromium Oxides Met and Material Transactions Vol 33B: 66 - 74.
33. Sigworth G.K. and Elliott J.F., 1974. The thermodynamics of liquid dilute iron alloys. Metal Science Vol 8 (9): 298-310.
34. Bale C.W., Pelton A.D., Thompson W.T., Eriksson G, Hack K, Chartrand P, Decterov S, Melancon J and Petersen S (2007). Factsage, Thermfact & GTT-Technologies, 2007
35. Bale C.W. and Pelton A.D. (1990). The unified interaction parameter formalism: Thermodynamic consistency and Applications. Metallurgical Transactions Vol. 21A: 1997 – 2002.
36. Castle T.A. (1979). Thesis title: A computer-simulation model for AOD process control, Lehigh University, Pennsylvania. Available at

http://preserve.lehigh.edu/cgi/viewcontent.cgi?article=2833&context=etd. Accessed 29/05/2017

37. Diaz M.C., Komarov S.V. and Sano M. (1997). Bubble behaviour and absorption rate in gas injection through rotary lances. Iron and Steel Institute of Japan International Vol. 37(1): p. 1-8
38. Baird M.H.I. and Davidson J.F. (1962). Gas absorption by large rising particles. Chemical Engineering Science Vol. 17: 87-93.
39. Turkdogan E.T. (1980). Physical Chemistry of High Temperature Technology. Academic Press, New York. p.359.
40. Ghose S., Nanda J.K. and Patel B.B. (1983). Duplex process for production of low carbon ferrochrome. Available at http://eprints.nmlindia.org/6027/1/215-217.PDF Accessed 15/08/2016: 215 – 217.
41. Yu H.C., Wang H.J., Chu S.J. and XU Z.B. (2015). Evaluation on heat and material balance of CO_2 involved in converter process for M-LCFeCr production. Proceedings of the 14th International Congress Ferroalloys Congress. Kiev, Ukraine: 58 – 64.
42. Leuchtenmüller, M., Roesler, G and Antrekowitsch, J. (2016). Recovery of chromium from stainless steel slags. MicroCAD International Multidisciplinary Scientific Conference, Hungary. Available at http://.www.uni-miskolc.hu/~microcad/publikaciok/2016/B_3_Manuel_Leuchtenmueller.pdf Accessed on 15/08/2016
43. Cramer, L. A., Basson J. and Nelson L.R. (2004). The impact of platinum production from UG2 ore on ferrochrome production in South Africa, Proceedings, Tenth International Ferro Alloys Congress, Cape Town:517 – 527.
44. Slatter D., Barcza N.A., Curr T.R., Maske K.U. and McRae L.B. (1986).Technology for the production of new grades and types of ferroalloys using thermal plasma. Proceedings of the 4th International Ferroalloys Congress, Rio De Jenaro 1986: 191 – 204.
45. Davies R.M. and Taylor G.T. (1950). The Mechanics of Large Bubbles Rising Through Liquids and Through Liquids in Tubes. Proc. R. Soc. London, Ser. A200, p 375.
46. Xiao Y., Holappa L. (1992). Determination of activities in slag containing chromium oxides. ISIJ International Vol. 33(1): 66-74.
47. Visuri V.V., Jarvinen M., Sulasalmi P., Heikkinen E.P., Savolainen J. and Fabritius T. (2012). A mathematical model for the reduction stage of the AOD process. Part I: Derivation of the model. ISIJ International Vol. 53(4): 603 – 612.

48. Visuri V-V., Jarvinen M., Sulasalmi P., Heikkinen E-P., Savolainen J. and Fabritius T. (2012). A mathematical model for the reduction stage of the AOD process. Part II: Model validation and results. ISIJ International Vol. 53(4): 613 – 621.

49. Spinola C., Galvez-Fernandez C.J., Munoz-Perez J., Jerrer J., Bonelo J.M., and Visozo J. (2006). An empirical model of the decarburization process in stainless steel production. IEEE International Conference, Mumbai: 1794 -1799.

50. Wang H., Teng L. and Seetharaman S. (2012). Investigation of the oxidation kinetics of Fe-Cr and Fe-Cr-C melts under controlled oxygen partial pressures. Metallurgical and Materials Transactions Vol 43B(6):1476 – 1487

51. Hockaday S.A.C. and Bisaka K. (2010). Some aspects of the production of ferrochrome alloys in pilot DC arc furnaces at Mintek. Proceedings of the 12th International Ferroalloys Congress, Helsinki:368 – 376.

52. Bhonde P.J., Ghodgaonkar A.M. and Angal R.D. (2007). Various techniques to produce Low Carbon Ferrochrome. Proceedings of the 11th International Ferroalloys Congress XI, Mumbai: 85 – 90.

53. Shoko N.R. and Chirasha J. (2004). Technological change yields beneficial process improvement for low carbon ferrochrome at Zimbabwe Alloys. Proceedings of the 10th International Ferroalloys Congress: 'Transformation through technology', Cape Town: 94 – 102.

54. Wang H.J., Yu H.C., Chu S.J. and Xu Z.B. (2015). Evaluation on heat and materials balance of CO_2 involved in converter process for M-LCFeCr production. Proceedings of the 14th International Ferroalloys Congress, Kiev:58 – 64.

55. Beskow K., Rick C.J. and Vesterberg P. (2015). Refining of Ferroalloys with the CLU process. The Proceedings of the 14th International Ferroalloys Congress, Kiev: 256 – 263.

56. Rick C-J. and Engholm M. (2011). Refining in AOD at high productivity with low environmental impact. The 6th European Oxygen Steelmaking Conference, Stockholm. Programme No. 3(07): 352 - 358.

57. Song H.S., Byun S.M., Min O.J., Yoon S.K. and Ahn S.Y. (1992). Optimization of the AOD Process at POSCO. Proceedings of the 1st International Ferroalloys Congress, Cape Town: 89-95.

58. Chuang H.C., Hwang W.S. and Liu S.H. (2009). Effects of basicity and FeO content on the softening and melting temperatures of the $CaO\text{-}SiO_2\text{-}MgO\text{-}Al_2O_3$ slag system. Material Transactions Journal Vol.50 (6): 1448 – 1456.

59. Seetharaman S., Jalkanen H., Holappa L., McLean A., Guthrie R. and Sridhar S. (2014). Treatise on process metallurgy, Industrial processes, Part A, Vol. 3. Elsevier Ltd., UK: p 223 – 271.
60. Gaskell D.R. (2013). Introduction to the Thermodynamics of Materials fourth edition. Taylor and Francis Group, New York, London.
61. Fuwa T. and Chipman J. (1959). Activity of Carbon in Liquid-Iron alloys. Transactions of the. Metallurgical Society of AIME, Vol 215: 708 – 716.
62. Wada H. and Saito T. (1951). Interaction parameters of alloying elements in molten iron. Transactions of the. Japan Institute of Materials Journal Vol. (2): 15 – 20.
63. Darken L.S. (1967). Thermodynamics of binary metallic solutions. Metallurgical Society of AIME Transactions Vol. 239: 80 – 89.
64. Chuang H.S., Hwang W.S. and Liu S.H. (2009). Effects of basicity and FeO content on the softening and melting temperatures of the CaO-SiO_2-MgO-Al_2O_3 slag system. Materials Transactions Vol. 50(6): 1448 – 1456.
65. MetalBulletin Available at: https://www.metalbulletin.com/Article/3441493/Samancor-stops-medium-and-low-carbon-ferro-chrome-production.html Accessed on 25/06/2016.

APPENDICES

	Implementation:21/04/2016 **AOD Logsheet** Document:FER/AODLS1REV3	**EAF T AOD**

AOD:		**Tap #:**		**Date:**		**Start AOD Time**	
Operator:				**Tap Mass:**		**End AOD Time**	
Operator:				**Ladle #**		**Total tap to tap**	

	Fines	Fines	Fines	Lime	Dolomite	FeSi	Start Time	Stop Time
1st charge								
2nd charge								
3rd charge								
4th charge								
Totals								

Time	**Temprerature**

	Oxygen	Nitrogen	Argon	LP Gas	Start Time	Stop Time
Blow 1						
Blow 2						
Blow 3						
Blow 4						
Blow 5						
Blow 6						
Blow 7						
Blow 8						
Blow 9						
Blow 10						
Totals						

Comments and Delays

Ladle tap temp:		
Time Started	Time Ended	Temp

Sample:	**% C**	**% Si**	**% Cr**	**% Fe**
Spark 1				
Spark 2				
Spark 3				

Refractories	
Lining heat number	
Lining Description	

Appendix 1: AOD logsheet used in process under study.

Item	Unit	Stage 1	Stage 2	Stage 3	Stage 3
Max Flow O_2	Nm^3/h			120.00	0.00%
Max Flow N_2	Nm^3/h			120.00	1.00%
Max Flow Ar	Nm^3/h				
Total Time	min	20.00	80.00	20.00	
O_2 / N_2	-	2.00	0.50	1.00	
O_2 / Ar	-	-	-	-	0.50%
O_2	Nm^3/h	120.00	60.00	120.00	
	Nm^3			194.80	
N_2	Nm^3/h	60.00	120.00	120.00	
	Nm^3			194.80	
Ar	Nm^3/h	-	-	-	
	Nm^3			-	

Appendix 2: Initial gas flows and gas ratios in model calculations

Item	Unit	Crude
Al	Mass%	0.00%
C	Mass%	3.00%
Cr	Mass%	67.40%
Fe	Mass%	29.25%
N(g)	Mass%	0.00%
Si	Mass%	0.35%
Weight	kg	7,000.00
Temperature	deg C	1,600.00

Appendix 3: Initial alloy bath analysis as charged into the AOD from the EAF

Lime / Dolomite	-	1.50
Al_2O_3	Mass%	0.00%
CaO	Mass%	100.00%
Cr_2O_3	Mass%	0.00%
MgO	Mass%	0.00%
FeO	Mass%	0.00%
SiO_2	Mass%	0.00%
LOI (CO_2)	Mass%	0.00%
Weight	kg	276.92
Temperature	deg C	25

Appendix 4: Lime analysis as added into the AOD

Al_2O_3	Mass%	0.00%
CaO	Mass%	20.00%
Cr_2O_3	Mass%	0.00%
MgO	Mass%	30.00%
FeO	Mass%	0.00%
SiO_2	Mass%	0.00%
LOI (CO_2)	Mass%	50.00%
Weight	kg	184.62
Temperature	deg C	25

Appendix 5: Dolomite analysis is added into the AOD

Al	Mass%	0.00%
C	Mass%	0.00%
Cr	Mass%	0.00%
Fe	Mass%	66.27%
Si	Mass%	33.73%
Weight	kg	264.37
Temperature	deg C	25

Appendix 6: FeSi analysis as added into the AOD

Appendix 7: Process input calculation summary

Item	Alloy						Lime					
	Mass %	Mole %	kg	kmol	deg C	MJ	Mass %	Mole %	kg	kmol	deg C	MJ
Al	0.00%	0.00%	-	-	-	-	0.00%	0.00%	-	-	-	-
C	3.00%	12.00%	210.00	17.48	1,600.00	565.72	0.00%	0.00%	-	-	-	-
Ca	0.00%	0.00%	-	-	-	-	0.00%	0.00%	-	-	-	-
Cr	67.40%	62.26%	4,718.28	90.74	1,600.00	4,941.47	0.00%	0.00%	-	-	-	-
Fe	29.25%	25.15%	2,047.22	36.66	1,600.00	2,762.78	0.00%	0.00%	-	-	-	-
Mg	0.00%	0.00%	-	-	-	-	0.00%	0.00%	-	-	-	-
N(g)	0.00%	0.00%	-	-	-	-	0.00%	0.00%	-	-	-	-
Si	0.35%	0.60%	24.50	0.87	1,600.00	79.65	0.00%	0.00%	-	-	-	-
Al_2O_3	0.00%	0.00%	-	-	-	-	0.00%	0.00%	-	-	-	-
CaO	0.00%	0.00%	-	-	-	-	100.00%	100.00%	276.92	4.94	25.00	-3,135.28
Cr_2O_3	0.00%	0.00%	-	-	-	-	0.00%	0.00%	-	-	-	-
FeO	0.00%	0.00%	-	-	-	-	0.00%	0.00%	-	-	-	-
MgO	0.00%	0.00%	-	-	-	-	0.00%	0.00%	-	-	-	-
SiO_2	0.00%	0.00%	-	-	-	-	0.00%	0.00%	-	-	-	-
Ar(g)	0.00%	0.00%	-	-	-	-	0.00%	0.00%	-	-	-	-
CO(g)	0.00%	0.00%	-	-	-	-	0.00%	0.00%	-	-	-	-
CO_2(g)	0.00%	0.00%	-	-	-	-	0.00%	0.00%	-	-	-	-
N_2(g)	0.00%	0.00%	-	-	-	-	0.00%	0.00%	-	-	-	-
O_2(g)	0.00%	0.00%	-	-	-	-	0.00%	0.00%	-	-	-	-
Total	100.00%	100.00%	7,000.00	145.76	1,600.00	8,349.62	100.00%	100.00%	276.92	4.94	25.00	-3,135.28

Item	Dolomite						FeSi					
	Mass %	Mole %	kg	kmol	deg C	MJ	Mass %	Mole %	kg	kmol	deg C	MJ
Al	0.00%	0.00%	-	-	-	-	0.00%	0.00%	-	-	-	-
C	0.00%	0.00%	-	-	-	-	0.00%	0.00%	-	-	-	-
Ca	0.00%	0.00%	-	-	-	-	0.00%	0.00%	-	-	-	-
Cr	0.00%	0.00%	-	-	-	-	0.00%	0.00%	-	-	-	-
Fe	0.00%	0.00%	-	-	-	-	66.27%	49.69%	175.18	3.14	25.00	- 0.00
Mg	0.00%	0.00%	-	-	-	-	0.00%	0.00%	-	-	-	-
N(g)	0.00%	0.00%	-	-	-	-	0.00%	0.00%	-	-	-	-
Si	0.00%	0.00%	-	-	-	-	33.73%	50.31%	89.18	3.18	25.00	-
Al_2O_3	0.00%	0.00%	-	-	-	-	0.00%	0.00%	-	-	-	-
CaO	20.00%	15.94%	36.92	0.66	25.00	- 418.04	0.00%	0.00%	-	-	-	-
Cr_2O_3	0.00%	0.00%	-	-	-	-	0.00%	0.00%	-	-	-	-
FeO	0.00%	0.00%	-	-	-	-	0.00%	0.00%	-	-	-	-
MgO	30.00%	33.27%	55.38	1.37	25.00	- 826.70	0.00%	0.00%	-	-	-	-
SiO_2	0.00%	0.00%	-	-	-	-	0.00%	0.00%	-	-	-	-
Ar(g)	0.00%	0.00%	-	-	-	-	0.00%	0.00%	-	-	-	-
CO(g)	0.00%	0.00%	-	-	-	-	0.00%	0.00%	-	-	-	-
CO_2(g)	50.00%	50.79%	92.31	2.10	25.00	- 825.35	0.00%	0.00%	-	-	-	-
N_2(g)	0.00%	0.00%	-	-	-	-	0.00%	0.00%	-	-	-	-
O_2(g)	0.00%	0.00%	-	-	-	-	0.00%	0.00%	-	-	-	-
Total	100.00%	100.00%	184.62	4.13	25.00	-2,070.09	100.00%	100.00%	264.37	6.31	25.00	- 0.00

Item	Oxygen						Nitrogen					
	Mass %	Mole %	kg	kmol	deg C	MJ	Mass %	Mole %	kg	kmol	deg C	MJ
Al	0.00%	0.00%	-	-	-	-	0.00%	0.00%	-	-	-	-
C	0.00%	0.00%	-	-	-	-	0.00%	0.00%	-	-	-	-
Ca	0.00%	0.00%	-	-	-	-	0.00%	0.00%	-	-	-	-
Cr	0.00%	0.00%	-	-	-	-	0.00%	0.00%	-	-	-	-
Fe	0.00%	0.00%	-	-	-	-	0.00%	0.00%	-	-	-	-
Mg	0.00%	0.00%	-	-	-	-	0.00%	0.00%	-	-	-	-
N(g)	0.00%	0.00%	-	-	-	-	0.00%	0.00%	-	-	-	-
Si	0.00%	0.00%	-	-	-	-	0.00%	0.00%	-	-	-	-
Al_2O_3	0.00%	0.00%	-	-	-	-	0.00%	0.00%	-	-	-	-
CaO	0.00%	0.00%	-	-	-	-	0.00%	0.00%	-	-	-	-
Cr_2O_3	0.00%	0.00%	-	-	-	-	0.00%	0.00%	-	-	-	-
FeO	0.00%	0.00%	-	-	-	-	0.00%	0.00%	-	-	-	-
MgO	0.00%	0.00%	-	-	-	-	0.00%	0.00%	-	-	-	-
SiO_2	0.00%	0.00%	-	-	-	-	0.00%	0.00%	-	-	-	-
Ar(g)	0.00%	0.00%	-	-	-	-	0.00%	0.00%	-	-	-	-
CO(g)	0.00%	0.00%	-	-	-	-	0.00%	0.00%	-	-	-	-
CO_2(g)	0.00%	0.00%	-	-	-	-	0.00%	0.00%	-	-	-	-
N_2(g)	0.00%	0.00%	-	-	-	-	100.00%	100.00%	243.51	8.69	25.00	0.00
O_2(g)	100.00%	100.00%	278.15	8.69	25.00	- 0.00	0.00%	0.00%	-	-	-	-
Total	100.00%	100.00%	278.15	8.69	25.00	- 0.00	100.00%	100.00%	243.51	8.69	25.00	0.00

Item	Argon					
	Mass %	Mole %	kg	kmol	deg C	MJ
Al	0.00%	0.00%	-	-	-	-
C	0.00%	0.00%	-	-	-	-
Ca	0.00%	0.00%	-	-	-	-
Cr	0.00%	0.00%	-	-	-	-
Fe	0.00%	0.00%	-	-	-	-
Mg	0.00%	0.00%	-	-	-	-
N(g)	0.00%	0.00%	-	-	-	-
Si	0.00%	0.00%	-	-	-	-
Al_2O_3	0.00%	0.00%	-	-	-	-
CaO	0.00%	0.00%	-	-	-	-
Cr_2O_3	0.00%	0.00%	-	-	-	-
FeO	0.00%	0.00%	-	-	-	-
MgO	0.00%	0.00%	-	-	-	-
SiO_2	0.00%	0.00%	-	-	-	-
Ar(g)	100.00%	100.00%	-	-	-	-
CO(g)	0.00%	0.00%	-	-	-	-
CO_2(g)	0.00%	0.00%	-	-	-	-
N_2(g)	0.00%	0.00%	-	-	-	-
O_2(g)	0.00%	0.00%	-	-	-	-
Total	100.00%	100.00%	-	-	25.00	-

Appendix 8: Process output summary for mass and energy balance model

	Alloy						Slag						Gas					
Item	Mass %	Mole %	kg	kmol	deg C	MJ	Mass %	Mole %	kg	kmol	deg C	MJ	Mass %	Mole %	kg	kmol	deg C	MJ
	Mass %	Mole %	kg	kmol	deg C	MJ	Mass %	Mole %	kg	kmol	deg C	MJ	Mass %	Mole %	kg	kmol	deg C	MJ
Al	0.00%	0.00%	-	-	-	-	0.00%	0.00%	-	-	-	-	0.00%	0.00%	-	-	-	-
C	1.00%	3.93%	71.90	5.99	1,720.00	211.63	0.00%	0.00%	-	-	-	-	0.00%	0.00%	-	-	-	-
Ca	0.00%	0.00%	-	-	-	-	0.00%	0.00%	-	-	-	-	0.00%	0.00%	-	-	-	-
Cr	65.54%	59.43%	4,712.64	90.63	1,720.00	5,508.11	0.00%	0.00%	-	-	-	-	0.00%	0.00%	-	-	-	-
Fe	29.93%	25.26%	2,151.87	38.53	1,720.00	3,116.71	0.00%	0.00%	-	-	-	-	0.00%	0.00%	-	-	-	-
Mg	0.00%	0.00%	-	-	-	-	0.00%	0.00%	-	-	-	-	0.00%	0.00%	-	-	-	-
N(g)	3.23%	10.88%	232.46	16.60	1,720.00	463.80	0.00%	0.00%	-	-	-	-	0.00%	0.00%	-	-	-	-
Si	0.30%	0.50%	21.57	0.77	1,720.00	72.63	0.00%	0.00%	-	-	-	-	0.00%	0.00%	-	-	-	-
Al_2O_3	0.00%	0.00%	-	-	-	-	0.00%	0.00%	0.00	0.00	1,720.00	- 0.00	0.00%	0.00%	-	-	-	-
CaO	0.00%	0.00%	-	-	-	-	47.18%	48.38%	313.85	5.60	1,720.00	- 3,064.13	0.00%	0.00%	-	-	-	-
Cr_2O_3	0.00%	0.00%	-	-	-	-	1.24%	0.47%	8.24	0.05	1,720.00	- 49.80	0.00%	0.00%	-	-	-	-
FeO	0.00%	0.00%	-	-	-	-	13.64%	10.92%	90.74	1.26	1,720.00	- 177.73	0.00%	0.00%	-	-	-	-
MgO	0.00%	0.00%	-	-	-	-	8.33%	11.88%	55.38	1.37	1,720.00	- 708.65	0.00%	0.00%	-	-	-	-
SiO_2	0.00%	0.00%	-	-	-	-	29.62%	28.35%	197.06	3.28	1,720.00	- 2,595.61	0.00%	0.00%	-	-	-	-
Ar(g)	0.00%	0.00%	-	-	-	-	0.00%	0.00%	-	-	-	-	0.00%	0.00%	-	-	-	-
CO(g)	0.00%	0.00%	-	-	-	-	0.00%	0.00%	-	-	-	-	97.18%	97.18%	380.80	13.59	1,720.00	- 734.74
CO_2(g)	0.00%	0.00%	-	-	-	-	0.00%	0.00%	-	-	-	-	0.00%	0.00%	-	-	-	-
N_2(g)	0.00%	0.00%	-	-	-	-	0.00%	0.00%	-	-	-	-	2.82%	2.82%	11.04	0.39	1,720.00	22.04
O_2(g)	0.00%	0.00%	-	-	-	-	0.00%	0.00%	-	-	-	-	0.00%	0.00%	-	-	-	-
Total	1	1	7190.4499	152.51738	1720	9372.885	100.00%	100.00%	665.274	11.567552	1720	-6595.924	100.00%	100.00%	391.8424	13.9891327	1720	-712.7

Item	Mass %	Mole %	Activity Coeff.	Activity
Al	0.000	0.000	1.440	0.000
C	0.010	0.039	0.078	0.003
Cr	0.655	0.594	0.915	0.544
Fe	0.299	0.253	1.117	0.282
N(g)	0.032	0.109	0.024	0.003
Si	0.003	0.005	1.751	0.009
Al_2O_3	0.000	0.000	0.009	0.000
CaO	0.460	0.472	0.335	
Cr_2O_3	0.012	0.005	8.335	0.041
FeO	0.147	0.118	1.450	0.156
MgO	0.085	0.122	0.141	
SiO_2	0.296	0.284	0.106	0.028

Appendix 9: Activity and activity coefficients calculations for mass and energy balance model

Item	Al	C	Cr	N	Si
Al	0.0450	0.0910	-	- 0.0580	0.0056
C	0.0430	0.1400	- 0.0240	0.1100	0.0800
Cr	-	- 0.1200	- 0.0003	- 0.1900	- 0.0043
N	- 0.0280	0.1300	- 0.0470	-	0.0470
Si	0.0580	0.1800	- 0.0003	0.0900	0.1100

Appendix 10: first order interaction coefficient in liquid iron

ε_{CC}	Al	C	Cr	N(g)	Si
Al	5.52	5.29	0.07	- 2.60	1.14
C	5.30	7.71	- 5.07	7.09	9.75
Cr	0.52	- 5.15	0.00	- 10.21	- 0.00
N	- 2.59	7.22	- 10.00	0.75	5.93
Si	6.96	9.69	0.00	5.94	13.22

Appendix 11: Calculated interaction coefficients for the energy and mass balance model

Item	Value
Al	0.029
C	0.57
Cr	1
Si	0.0013

Appendix 12: Activity coefficients at infinite solutions

Item	Fe^{2+}	Ca^{2+}	Cr^{3+}	Mg^{2+}	Si^{4+}	Al^{3+}
Fe^{2+}	-	- 31,380		33,470	- 41,840	- 41,000
Ca^{2+}	- 31,380	-	44,235	- 100,420	- 133,890	- 154,810
Cr^{3+}		44,235	-	28,085	- 48,975	- 46,210
Mg^{2+}	33,470	- 100,420	28,085	-	- 66,940	- 71,130
Si^{4+}	- 41,840	- 133,890	- 48,975	- 66,940	-	- 127,610
Al^{3+}	- 41,000	- 154,810	- 46,210	- 71,130	- 127,610	-

Appendix 13: Interaction energy between cations of major steel making slags

Item	MW	Unit
Al	26.98	g/mol
Al_2O_3	101.96	g/mol
Al_2O_3(l)	101.96	g/mol
Ar(g)	39.95	g/mol
C	12.01	g/mol
CO(g)	28.01	g/mol
CO_2(g)	44.01	g/mol
Ca	40.08	g/mol
CaO	56.08	g/mol
CaO(l)	56.08	g/mol
Cr	52.00	g/mol
Cr_2O_3	151.99	g/mol
Cr_2O_3(l)	151.99	g/mol
Fe	55.85	g/mol
FeO	71.85	g/mol
FeO(l)	71.85	g/mol
Mg	24.31	g/mol
MgO	40.30	g/mol
MgO(l)	40.30	g/mol
N(g)	14.01	g/mol
N_2(g)	28.01	g/mol
O_2(g)	32.00	g/mol
Si	28.09	g/mol
SiO_2	60.08	g/mol
SiO_2(l)	60.08	g/mol

Appendix 14: Molar weights for oxides and elements in the energy and mass balance model.

Appendix 15: Initial analysis of hot metal charged into the AOD for the process under study

TAP NO		Temp	Cr	C	Si	Fe	mins
91	7	1621	69.7	7.26	0.0812	22.9588	64
178	6.5	1702	68.52	8.03	0.114	23.336	83
194	7	1631	69.8	8.06	0.0831	22.0569	99
196	6.5	1664	69.21	6.8	0.115	26.5	107
195	6	1655	68.18	7.89	0.0954	23.8346	67
177	7	1687	68.78	8.08	0.111	26.78	78
98	7	1684	67.95	8	0.117	23.933	67
97	6.5	1663	66.54	7.95	0.0972	25.4128	98
96	7	1650	69.82	8.05	0.103	22.027	73
77-1	5	1743	67.71	8.03	0.0905	24.1695	88
81	8	1659	68.91	7.98	0.0813	23.0287	129
186	6.4	1640	69.66	7.96	0.0788	22.3012	90
185	7	1656	67.88	7.79	0.0971	24.2329	111
167	6.6	1638	69.2	7.63	0.0943	23.0757	115
165	7	1669	68.86	7.97	0.0759	23.0941	107
86	7.4	1656	68.69	8.01	0.0751	23.2249	118
85	6.7	1643	68.36	8.04	0.0753	23.5247	115
192	7	1645	68.88	7.96	0.104	23.056	65
191	6.5	1679	69.84	8.03	0.117	22.013	113
92	6	1649	68.34	8.06	0.108	23.492	150
172	6.5	1655	68.37	7.99	0.106	23.534	78
173	6.5	1650	67.88	7.93	0.117	24.073	169
189	7	1656	69.08	7.97	0.077	22.873	110
190	7	1647	70.5	7.59	0.0847	21.8253	193

Appendix 16: Second blowing stage initial data from the process under study

Tap	Temp	Cr	C	Si	Fe	mins
91	1721	69.95	1.63	0.143	28.277	122
178	1685	71.65	1.42	0.131	26.799	26
194	1682	70.36	1.45	0.133	28.057	42
196	1720	71.11	1.17	0.175	26.5	34
195	1720	70.06	2.14	0.155	27.645	88
177	1720	70.28	1.8	0.106	26.78	40
98	1730	70.01	2.25	0.148	27.592	78
97	1708	70.52	1.28	0.127	28.073	32
96	1710	70.31	2.99	0.113	26.587	43
76	1720	68.95	1.77	0.151	28.09	30
77-1	1770	68.7	1.48	0.11	29.71	50
81	1770	69.43	1.2	0.138	29.232	76
186	1782	70.34	1.33	0.193	28.137	57
185	1775	69.49	1.33	0.121	29.059	44
167	1771	69.63	1.47	0.127	28.773	55
166	1720	69.63	1.47	0.127	27.73	30
165	1748	70.44	2	0.148	27.412	60
86	1772	71.18	1.32	0.1	27.4	34
85	1698	70.59	1.21	0.113	28.087	25
192	1755	69.69	2.04	0.147	28.123	85
191	1778	67.22	0.754	0.149	31.877	15
92	1713	71.42	1.28	0.141	27.159	30
172	1779	69.97	1.41	0.151	28.469	83
189	1737	70.73	1.4	0.146	27.724	47

Appendix 17: Financial modeling of the AOD and EAF process

Item	Description	Units	Total Consumption t/t Alloy (Saleable Alloy)	Unit Cost Cost USD/ton	Unit Delivery Cost to Plant US$/ton	Total Cost US$/ton Alloy (Saleable Alloy)	% Of Total Cost	Total Cost USc/lb	Source (Pricing)
FURNACE PRODUCTION CAPACITY									
	Hot Metal	**tpa**	**14,864**						
	Energy Requyired for smelting	**kWh/t**	**921.7**	**(SER - 533)**					
VARIABLE OPERATING COSTS - EAF			**(Incl Losses)**						
1	**FEED MATERIALS**								
	Total Ore	t/t	**2.22**						
	Chromite	t/t	**2.22**	$220.00	$0.00	$488.40			
		t/t		$0.00	$0.00	$0.00			
	Total Reductant	t/t	**0.6281**						Used 110%
	Al	t/t	**0.6281**	$1,594.00	$0.00	$1,001.19			LME (Discount up to 800USD/t on scrap possible
	Total Fluxes	t/t	**0.0225**						
	Lime	t/t	**0.5**	$95.00	$0.00	$47.50			
	Dolomite	t/t	0.023	$95.00	$0.00	$2.14			
2	**REFRACTORIES**								
	Lining				$0.00	$0.00			
	Gunnite				$0.00	$0.00			
	Ramming				$0.00	$0.00			
	Patching				$0.00	$0.00			
	Leveling powder				$0.00	$0.00			
	Roof caster				$0.00	$0.00			
					$0.00	$0.00			
	Subtotal					**$1,539.23**	**83.66%**		
VARIABLE OPERATING COSTS - AOD			**(Incl Losses)**						
3	**Fluxes and reductants**	t/t	0.023						
	Lime	t/t	0.500	$95.00	$0.00	$47.50			
	FeSi				$0.00	$0.00			
	Flurspar				$0.00	$0.00			
	Dolomite	t/t	0.023	$95.00	$0.00	$2.14			
	Subtotal					**$49.64**	**2.70%**		
4	**REFRACTORIES**								
	Lining				$0.00	$0.00			
	Gunnite				$0.00	$0.00			
	Subtotal					**$0.00**	**0.00%**		
5	**GASES**								
5.1	LPG				$0.00	$0.00			
5.2	Oxygen				$0.00	$0.00			
5.3	Nitrogen				$0.00	$0.00			
5.4	Argon				$0.00	$0.00			
	Subtotal					**$0.00**	**0.00%**		
6	**DIESEL AND OIL**								
6.1	Diesel				$0.00	$0.00			
6.2	Oil				$0.00	$0.00			
	Subtotal					**$0.00**	**0.00%**		
7	**OTHER CONSUMABLES**								
7.1	Tuyeres				$0.00	$0.00			
7.2	Electrodes				$0.00	$0.00			
7.3	Thermocouples & Pipes				$0.00	$0.00			
7.4	Thermosamples				$0.00	$0.00			
	Subtotal					**$38.23**	**2.08%**		
8	**ENERGY**								
8.1	Electric Power	KWh/t	921.667	$0.080	$0.00	$73.73			
8.2	Auxillary Power (incl Final Product)	KWh/t	184.333	$0.080	$0.00	$14.75			
	Subtotal					**$88.48**	**4.81%**		
	TOTAL VARIABLE OPERATING COSTS					**$1,715.58**	**93.2%**		
	FIXED COSTS		**Unit**	**(USD$/yr)**					
9	**LABOUR**								
	Permanent Complement (Including Lea	$/yr		$598,578	$0.00	$0.00			
	Contracting Complement	$/yr			$0.00	$0.00			
10	**VEHICLES (Consumables)**								
	Maintenance & Depreciation					$0.00			
11	**MAINTENANCE**								
	Direct Maintenace (2% of Capital USD1	$/yr	1.0%	$10,000		$100.00			
	Major Repairs (1.5% of Capital)	$/yr	3.0%	$5,000		$150.00			
12	**Miscellaneous costs**								
	Handling Charges	$/yr		$0		$0.00			
	Administrative Expenses	$/yr		$0		$0.00			
	Interest & Financial Costs	$/yr		$0		$0.00			
	Marketing & Overheads Costs	$/yr		$0		$0.00			
	Subtotal	**$/yr**		$0		**$250.00**	**13.6%**		
13	**Environmental**								
	Monitoring (Water&Air)	$/yr		$1.00		**$1.00**			
	Rehabilitation provision	$/yr							
	Subtotal	**$/yr**		$0		**$1.00**	**0.1%**		
TOTAL FIXED OPERATING COSTS						**$251.00**	**13.6%**		
TOTAL SMELTER COST						**$1,539.23**	**83.7%**		
TOTALCONVERTER COST						**$49.64**	**2.7%**		
TOTAL PRODUCTION COST						**$1,839.87**		138.63	
SALES PRICE						**$2,514.00**		182.27	Metal Bulletin
MARGIN						**$674.13**		43.64	